DEVELOPMENT AND PRELIMINARY USE OF AN APPARATUS FOR PARTIAL PHOTOIONIZATION CROSS-SECTION MEASUREMENTS

by

J.M. Hutton B.Sc. (Hons.)
Department of Physics

A thesis
submitted for the degree of
Master of Science
at the
University of Adelaide

June, 1981

TABLE OF CONTENTS

Chapter 2. DESCRIPTION AND OPERATION OF THE APPARATUS

TABLE OF CONTENTS (Cont.)

This thesis describes the development and preliminary use of an apparatus designed to measure branching ratios and relative partial cross-sections for photoionizing processes as a function of wavelength by using the technique of photoelectron spectroscopy. Of particular interest was the ability of this apparatus to measure the strengths of transitions to vibrational states of the ion at autoionizing resonances. Such results could then be used to test theoretical descriptions of autoionization.

The choice of the analyser to take these measurements was important. The light source used was a Hinteregger lamp coupled to a 1 metre monochromator and because of the low intensity of this dispersed continuun light source, an analyser with a large collecting aperture was needed. It was also important to select an analyser which is highly stable over long data collecting periods as well as having an easily calibrated efficiency function. A hemispherical retarding grid analyser has these characteristics and so was used for this project. The resolution of the analyser was better than 100 meV (actually 30 meV at 5 eV or 45 meV at 9 eV) and so the vibrational levels of diatomic molecules were able to be separated.

Using this analyser, photoelectron spectra of Xenon, Argon and Krypton were recorded using radiation of wavelengths 58.4 and 73.6nm, Nitrogen at 58.4nm and Oxygen at 58.4nm and on the J autoionizing levels between 85 and 90nm.

To analyse these spectra, a curve-fitting program was written but it was not completely developed at the conclusion of the project. Instead, the results were analysed by hand; a method which showed the potential of the system.

Within the accuracy of the method, the results showed good agreement with other experimental data, where available. The preliminary analysis brought to light some improvements to the equipment which need to be made as well as modifications to overcome some difficulties experienced in using the curvefitting program.

PREFACE

This thesis contains no material which has been accepted for the award of any other degree or diploma in any University. To the best of the author's knowledge and belief it contains no material previously published or written by another person, except where due reference is made in the text.

J.M. Hutton,

June, 1981.

STATEMENT OF ORIGINALITY

The work described in this thesis was carried out in collaboration with W. Lindemans and Dr. A.J. Blake, who designed the photoelectron spectrometer. The author's principal contributions were to investigate the characteristics of the apparatus, to operate the equipment to obtain data at the J autoionizing levels of oxygen and to produce a preliminary analysis program.

ACKNOWLEDGEMENTS

The development of the equipment described in Chapter 2 was carried out in conjunction with W. Lindemans. The author would like to thank him for his co-operation during this work and for his invaluable help at all stages.

I gratefully acknowledge the guidance of Professor J.H. Carver who initiated the project and also of my other supervisor Dr. A.J. Blake, who was always willing to provide encouragement and useful advice whenever needed. For managing to cope with the rush at the end made even more difficult by the separation of student and supervisor by a distance of 1600 km during a time when Telecom was on strike, he has won my eternal gratitude.

For many hours of helpful, interesting and fruitful discussions, as well as for criticising the theory in Chapter 1, I would like to thank Dr. L. Torop, who almost managed to inspire me with an enthusiasm for autoionization.

I also acknowledge useful discussions with Dr. D.G. McCoy, Dr. T. Hobbs and Dr. B. Horton.

Thanks are due to S. Dowden, J. Wright and F. Smith of the Laboratory Technical Staff for their assistance.

To my friends, especially A. Davis, D. Gigney and J. Lean who helped me through times of crisis as well as providing companionship at all times, I would like to express my sincere thanks.

I would also like to thank F. Thompson for a magnificent typing effort and for coping so well with all the problems caused by my imminent overseas trip.

K. Smart was responsible for the fine draughting shown in the diagrams and M. Epstein helped with final preparation.

My special thanks are due both to my parents, who made it all possible, and to my parents-in-law, who took over my normal domestic duties to allow me to finish on time.

Finally I would like to express my gratitude to Richard who has persevered with me and my thesis for a long while and who has done all he can to enable me to produce this thesis.

CHAPTER 1 INTRODUCTION

1.1 PHOTOELECTRON SPECTROSCOPY

1.1.1 Photoionization

If, when an atom or molecule absorbs a photon an electron is ejected, it is said to have been been photoionized and it is left in an ionic state. In order to conserve momentum in the reaction, virtually all the kinetic energy is carried away by the less massive photoelectron and so the kinetic energy of the ion can be neglected. This then gives, by the conservation of energy, the relation

$$h\nu - I.P. = V \qquad \ldots(1)$$

where ν is the frequency of the incident photon, I.P. denotes the minimum energy required to remove the electron from a particular bound state (ie. the ionization potential), and the kinetic energy of the electron is V.

The study of the kinetic energy of these photoelectrons is known as photoelectron spectroscopy (PES). Work in this field was first described by VILESOV, KURBATOV and TERENIN (1961), who studied electron energies as a function of wavelength for organic compounds at wavelengths greater than 105nm. Independently TURNER and AL-JOBURY (1962) reported on measurements of photoelectrons of different gases at the HeI resonance line at 58.4nm.

1.1.2 Uses of Photoelectron Spectroscopy

From equation (1), it can be seen that the measurement of kinetic energies of the photoelectrons can be used to determine the ionization potentials of atomic or molecular states if the photon energy is known. Ionization potentials from threshold techniques such as the convergence of Rydberg series in absorption spectra are often difficult to obtain or are inaccurate because the spectra are complicated by overlap of vibronic structure, ionization to

vibrationally and rotationally excited states and by the presence of features due to autoionization. Measurements of ionization potentials by photoelectron spectroscopy are not hindered by these problems.

Ionization potentials can be thought of as the negative of the molecular orbital energies or eigenvalues. This assumption, is in essence, Koopman's theorem. Thus the technique of PES allows measurement of a quantity which is directly comparable with theory and so results in a better understanding of the molecule. PES is particularly important in the determination of information about inner orbitals, especially in polyatomic molecules, which is not available by conventional spectroscopy. Much PES work is carried out by chemists who use the technique as a tool in their understanding of atomic and molecular bonding, as well as in qualitative analysis. BAKER et al(1972), in their review book, present many examples of the application of PES particularly in chemistry.

Photoelectron spectroscopy has also been used in the measurement of partial photoionization cross-sections as a function of wavelength. BLAKE and CARVER (1967) were the first to use PES to distinguish between the various competing processes which occur when photoionization takes place in gases. More accurate work in the same department has since been done (eg. BAHR et al., 1972).

Of particular interest to the author is the use of PES to measure intensities of transitions from one electronic state to different vibrational levels of another electronic state (see, for example, a review article by NATALIS, 1976). PES is invaluable in being able to measure these vibrational intensities at various wavelengths, particularly those at which autoionization takes place. Comparison with theory can again add to our understanding of atoms and molecules.

From the brief description given here, it can be seen

that PES is very important in the investigation of the interaction of electromagnetic radiation with matter as well as the internal structure of molecules and atoms. A more detailed description of the principles and uses of PES is given in a review article by BAHR (1973) as well as other general papers and books (eg. BAKER and BETTERIDGE, 1972; EASTMAN and NATHAN, 1975; ELAND, 1974; FROST, 1974; SEVIER, 1972).

Finally, some comments about the wavelength of the radiation used is necessary. PES has been developed through two main branches depending on the wavelength of the radiation used to produce the photoelectrons. D. W. Turner is considered to be the pioneer of work with U.V. photons whereas K. Siegbahn has used mainly x-rays. Both have written books which provide detailed reviews in their fields (TURNER et al, 1970; SIEGBAHN et al, 1969).

1.2 MOLECULAR SPECTROSCOPY

1.2.1 Introduction

In addition to transitions between electronic states, molecular spectra are made more complex by transitions between various vibrational and rotational states. Of main interest to this thesis are transitions from the lowest vibrational level of the ground electronic state of diatomic molecules to different vibrational levels of highly excited electronic states and the decay of these states by autoionization. This section of the thesis will thus look briefly at the theory of vibrational spectra of diatomic molecules and provide theoretical factors which can be compared directly with experimental results.

1.2.2 Quantum mechanics and Spectroscopy

Spectra of atoms and molecules can be used to experimentally test theoretical descriptions of their structure. Any theory must at the very least be able to predict the wavelengths, and hence energy, of photons emitted by or absorbed by atoms or molecules. Classical theory was not able to explain the discrete line spectra shown by atoms and the Bohr model of the atom was inadequate to describe the spectra of atoms other than hydrogen. Quantum mechanics or wave mechanics, in which a wave motion is associated with an atomic or molecular system, is now the accepted theory.

The fundamental equation of motion of quantum mechanics is the Schroedinger equation. For the motion of a single mass point of mass m the equation is

$$\frac{\partial^2\psi}{\partial x^2} + \frac{\partial^2\psi}{\partial y^2} + \frac{\partial^2\psi}{\partial z^2} + \frac{8\pi^2 m}{h^2}(E - V) = 0 \qquad \ldots(2a)$$

where ψ is the amplitude of the wave motion

V is the potential energy of the mass point

$E = h\nu$ is the total energy of the mass point

ν is the frequency of the wave motion.

This equation is, in general, only soluble for certain definite values of E known as eigenvalues. These values of E agree with experimental results if suitable potential energy values are used. Another way of writing equation (2a) is

$$H\,\psi(r) = E\,\psi(r) \qquad \ldots(2b)$$

where $H = \frac{h^2 \nabla^2}{8\pi^2 m} + V(r)$

and H is known as the Hamiltonian or energy operator.

1.2.3 The Born-Oppenheimer Approximation

The Schroedinger equation for a diatomic molecule can be written:

$$\frac{1}{m}\Sigma \nabla_i^2 \psi + \Sigma \frac{1}{m_j} \nabla^2 \psi + \frac{8\pi^2}{h^2}(E - V) = 0 \qquad \ldots(3)$$

where $\nabla_i^2 = \frac{\partial^2}{\partial x_i^2} + \frac{\partial^2}{\partial y_i^2} + \frac{\partial^2}{\partial z_i^2}$

m = mass of electrons

x_i, y_i, z_i = co-ordinates of electrons

m_j = mass of nucleus j

x_j, y_j, z_j = co-ordinates of nucleus j

BORN and OPPENHEIMER (1927) have shown that for most cases ψ can be resolved as

$$\psi = \psi_e(\ldots x_i, y_i, z_i)\ \psi_n(\ldots x_j, y_j, z_j \ldots) \qquad \ldots(4)$$

Where ψ_e and ψ_n are solutions to the equations

$$\frac{1}{m}\Sigma_i \nabla_i^2 \psi_e + \frac{8\pi^2}{h^2}(E_{el} - V)\psi_e = 0 \qquad \ldots(5)$$

and

$$\Sigma \frac{1}{m_j} \nabla_j^2 \psi_n + \frac{8\pi^2}{h^2}(E - E_{el} - V_n)\psi_n = 0 \qquad \ldots(6)$$

Equation (5) represents the Schoedinger equation for the electrons moving in the field of the fixed nuclei with potential energy V_e and as R, the internuclear distance, varies, V_e and therefore the eigenfunction ψ_e and the eigenvalues E_{el} also vary. Equation (6) is the Schroedinger equation for the nuclei moving under the potential $(V_n + E_{el})$ where V_n is the Coulomb potential of the nuclei.

Born and Oppenheimer have shown that the Schroedinger equation for the whole molecule is satisfied only if

$$\sum_j \left(\frac{z}{m_j} \frac{\partial \psi_e}{\partial x_j} \frac{\partial \psi_n}{\partial x_j} + \frac{\partial \psi_e}{\partial y_j} \frac{\partial \psi_n}{\partial y_j} + \frac{\partial \psi_e}{\partial z_j} \frac{\partial \psi_n}{\partial z_j} + \psi_n \nabla_j^2 \psi_e \right)$$

can be neglected.

This will hold if the variation of ψ_e with internuclear distance R is sufficiently slow so that terms such as $\frac{\partial \psi_e}{\partial x_j}$ and higher order derivatives can be ignored. It can be assumed that these can be ignored because the period of electronic motion is approximately 100 times faster than the period for the vibration of the nucleus. Thus the use of $(E_{el} + V_n)$ as the potential energy for the motion of the nuclei is justified and equation (4) is valid in the above approximation. In other words, the electronic and nuclear motions can be treated separately due to the large difference between the electronic and nuclear masses.

The nuclear motion, that of a vibrating rotator in a potential well of the energy (potential and kinetic) of the electrons and the Coulomb energy of the nucleus, may be further separated to a good approximation, into its vibrational and rotational components. Hence the total energy E of the molecule may be considered as

$$E = E_e + E_v + E_r$$

where E_e represents the electronic energy

E_v represents the vibrational energy

E_r represents the rotational energy

The difference between successive 1) E_e values is of the order of 1 eV 2) E_v values is approximately 0.1 eV and 3) E_r values about 0.001 eV. In photoelectron spectroscopy rotational motion is beyond the resolution of most photoelectron spectrometers.

1.2.4 The Franck-Condon Principle

As mentioned earlier, photoelectron spectroscopy can be used to measure the relative intensities of transitions between the ground state of the molecule and various vibrational states of the ion. Quantum mechanics can be used to derive these intensities theoretically and hence a direct comparison can be made between theory and experiment.

To determine these intensities, use is made of the Franck-Condon principle which states that "an electronic transition takes place so rapidly that a vibrating molecule does not change its internuclear distance and nuclear velocities appreciably during the transition". Classically, the most intense vibrational transitions will be the ones represented by vertical lines on a potential energy curve of a molecule. Figure 1.1 shows an example of this idea.

The quantum mechanical derivation of the most intense transition is a little more complex.

Using time-dependent perturbation theory, it can be shown (eg. PAULING and WILSON, 1935) that the intensity of a transition, caused by electromagnetic radiation, between states n and m depends on the square of the magnitude of the vector quantities $\vec{R}^{nm}$. These $\vec{R}^{nm}$ are the matrix elements of the electric dipole

$$\vec{R}^{nm} = \int \psi_n^{*\prime} \vec{M} \psi_m \, d^3R \qquad \ldots(7)$$

where the integrals are to be taken over the whole configuration space of the 3N co-ordinates and

$$\vec{M} = \sum_i Q_i \vec{r}_i \qquad \ldots(8)$$

where Q_i is the charge on the i^{th} particle whose position is $\vec{r}_i$.

If the matrix element $\vec{R}^{nm}$ is different from zero for two states n and m, the states combine with each other with a certain probability of emission or absorption of radiation; if it is zero, the transition is forbidden as a dipole transition.

Using the Born-Oppenheimer approximation, the wave function of a molecule can be written as a product of the electronic, vibrational and rotational wave functions. For such a molecule, the dipole moment can be factorized to obtain the expression

$$\vec{R} = \int \psi_{v'} \vec{R}_e(R) \psi_{v''} dR \int \psi_{r'} D(\Omega) \psi_{r''} d\Omega \qquad \ldots(9)$$

where ψ_v is the vibrational wave function

ψ_r is the rotational wave function

$\vec{R}_e(R)$ is the electronic dipole transition moment in the molecular frame.

R represents the nuclear separation

$D(\Omega)$ is a tensor transforming the electronic dipole moment from the molecular frame to the laboratory frame.

$\vec{R}_e$ can be replaced by $\overline{\vec{R}_e}$ an average value over R for a given transition. Thus equation (9) becomes

$$\vec{R} = \vec{R}_e \int \psi_{v'}^* \psi_{v''} dR \int \psi_{r'}^* D(\Omega) \psi_{r''} d\Omega \qquad \ldots(10)$$

The part $\int \psi_{r'}^* D(\Omega) \psi_{r''} d\Omega$ is related to rotational transitions and is of no relevance in photoelectron spectroscopy.

The interesting part $\int \psi_{v'} \psi_{v''} dR$ is known as the overlap integral or Franck-Condon amplitude and the square of this overlap integral is known as the Franck-Condon factor $q_{v'v''}$ for the transition between vibrational levels v' and v". Thus

$$q_{v'v''} = \left(\int \psi_{v'}^* \psi_{v''} dR \right)^2 \qquad \ldots(11)$$

It can then be seen from equation (10) and remembering that the intensity of a transition depends on the square of $\vec{R}$, that the intensity for the transition between vibrational levels v' and v" is directly proportional to $q_{v'v''}$. Thus, using the assumption

that $\vec{R}_e$ varies slowly with R, the final expression for the intensity of a vibrational transition is

$$I \propto q_{v'v''} \quad \text{or} \quad I \propto \left(\int \psi_{v'}^{*} \psi_{v''} dR\right)^2 \qquad \ldots(12)$$

Hence the most probable transition is the one which corresponds to two states whose eigenfunctions have maximum overlap.

As well as this factor, the actual observed intensity distribution will obviously depend on the population of the molecules in the initial state. For vibrational levels, this is given by the expression

$$N(E) \propto \exp(-E/kT) \qquad \ldots(13)$$

where N(E) is the number of molecules of energy E

k is Boltzman's constant

T is the temperature of the molecules

At room temperature, kT is the order of 3×10^{-2} eV and the energy of the first vibrational level is of the order of 10^{-1} eV. Thus it can be seen that most of the molecules are in the v" = 0 state at room temperature.

To compare the predictions of the quantum mechanical theory with that of classical mechanics, consider the case shown in Fig. 1.1. Classical mechancis predicts that the vertical transition, i.e. from v" = 0 to v' = 6, is expected to be the most intense. The eigenfunction of the v" = 0 state has its maximum value at the nuclear separation corresponding to the potential minimum and the eigenfunctions for the higher vibrational levels have maximum values near the classical turning point. The overlap integral will hence be greatest for the v" = 0 to v' = 6 transition which agrees qualitatively with the classical prediction.

1.2.5 Potential energy curves

To calculate the Franck-Condon factors for various transitions it is necessary to known the wave functions for the

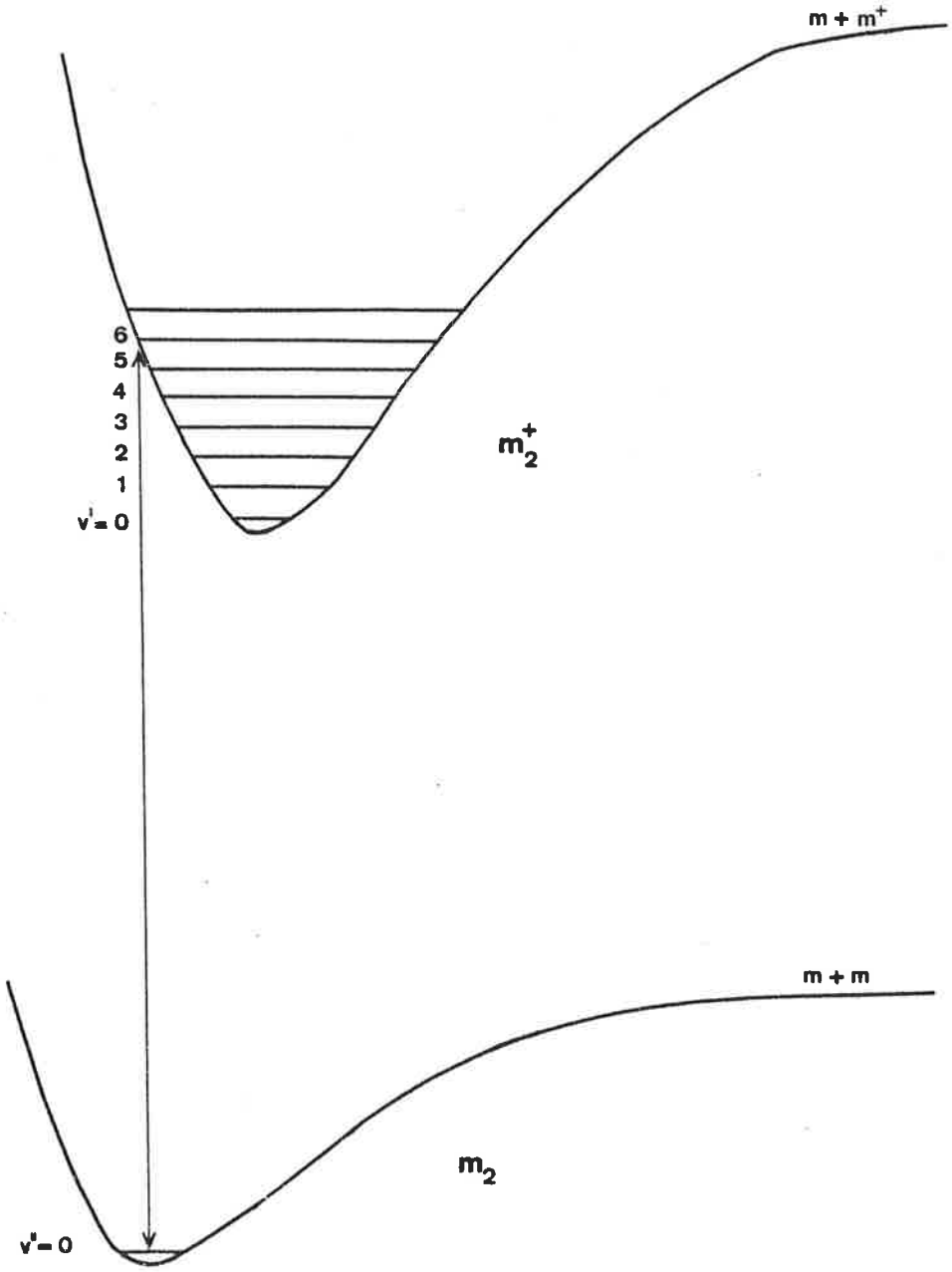

Fig.1.1. Potential well diagram showing the most intense vibrational transition.

vibrational levels of the various electronic states of the molecule and ion. Before the wave functions can be calculated, the potential energy curves of the electronic states must be known in order to solve equations (5) and (6).

One method of obtaining these potentials curves is to assume the validity of some empirical curve such as given by the Morse (MORSE, 1929), the Hulbert-Hirschfelder (HULBERT and HIRSCHFELDER, 1941) or the Lippincott (LIPPINCOTT, 1953) functions and obtain the parameters for the curve from spectroscopic data. STEELE, LIPPINCOTT and VANDERSLICE (1962) gave a comparative study of these empirical internuclear potential functions as well as a brief description of and comparison with the Dunham (DUNHAM, 1932) and RKR (RYDBERG 1931, 1933; KLEIN, 1932; REES, 1947) methods of determining potentials. Either of these methods can be used when spectroscopic data is available over a wide range of energy levels.

In his method of obtaining potential energy curves for the bound states of diatomic molecules, Dunham used the WKB method to show that the energy levels have the form

$$E_{v,j} = \sum_l \sum_m Y_{lm} (v + \tfrac{1}{2})^l J^m (J + 1)^m \qquad \ldots(14)$$

where l and m are summation indices and v and J are the vibrational and rotational quantum numbers respectively and where the Y_{lm} are coefficents which can be determined from the experimental rotational and vibrational levels. If the potential is assumed to be of the form

$$V = a_o\left(\frac{\Delta r}{r_e}\right)^2\left[1 + a_1\left(\frac{\Delta r}{r_e}\right) + a_2\left(\frac{\Delta r}{r_e}\right) + \ldots\right] + B_e J(J+1)\left[1 - 2\frac{\Delta r}{r_e} + 3\left(\frac{\Delta r}{r_e}\right)^2 - 4\left(\frac{\Delta r}{r_e}\right)^3 + \ldots\right] \qquad \ldots(15)$$

where $\Delta r = r - r_e$, then the a_i's can be related to the Y_{lm}'s. Since the Y_{lm}'s are determined from the experimental data, the potential energy function based on this data can be calculated from equation (15). The most serious drawback of the Dunham method is that it diverges as the energy approaches the dissociation limit and hence must be used with care at higher vibrational levels.

Perhaps the most satisfactory method for generating potential energy curves from the experimental data is the RKR method. This method is based on a first order WKB approximation and involves the solution of the two Klein integral equations:-

$$f(U) = d\int\{U - E(I,K)\}^{-\frac{1}{2}}dI \qquad \ldots(16)$$

$$g(U) = d\int\{(\frac{\partial E}{\partial K})(U - E(I,K)^{-\frac{1}{2}}\}dI \qquad \ldots(17)$$

where U is the potential energy for which the turning points are required (Note:- U = U(r))

$d = 1/\ 2\Pi(2\mu)^{\frac{1}{2}}$

μ = reduced mass of the molecule

$I = h(v + \frac{1}{2})$

v = vibrational quantum number

I' = value of I when V = E ie. value of I for which integrand vanishes

E(I,K) = vibrational - rotational energy levels

$K = \frac{h^2}{8\Pi^2\mu} J(J + 1)$

J = rotational quantum number

For the rotationless state of the molecule (J =0), a change of variable I to the vibrational quantum number v gives:-

$$f_v = c_1\int\{G(v) - G(v')\}^{-\frac{1}{2}}dv' \qquad \ldots(18)$$

$$g_v = 1/c_1\int\{B(v')(G(v) - G(v')\}^{-\frac{1}{2}}dv' \qquad \ldots(19)$$

where $C_1 = (h/8\ \Pi^2 c\mu)^{\frac{1}{2}}$

G(v) and B(v) are the conventional expressions for the vibrational energy and the rotational constant (COXON, 1971; TELLINGHUISEN, 1972). The turning points of the motion r_{max}, r_{min} can then be obtained from

$$r_{\substack{max\\min}} = (f/g + f^2)^{\frac{1}{2}} \pm f \qquad \ldots(20)$$

Rydberg had previously solved similar equations by graphical methods. Klein solved these equations numerically but the process was fairly laborious and considerable care had to be taken

to obtain accurate results.

Rees pointed out that equations (16), (17) and (20) can be readily solved for f and g if $E(I,K)$ can be expressed as a quadratic in $I=h(v + \frac{1}{2})$;

$$E(I,K) = \omega_e(v + \tfrac{1}{2}) - \omega_e x_e(v + \tfrac{1}{2})^2 - \alpha_e(v + \tfrac{1}{2})J(J + 1) + B_e J(J + 1) + DJ^2(J + 1)^2 + \ldots \quad \ldots(21)$$

where $(\omega_e, \omega_e x_e, \alpha, \ldots)$ etc. are constants. Usually $E(I,K)$ cannot be expressed over the whole experimental range by such an expression, but it can be expressed as a quadratic over different regions so that the entire range can be covered by a series of quadratics. Rees also considered the case where $E(I,K)$ can be expressed as a cubic in I but the calculations are much more difficult and laborious. The success of this method depends on the accuracy of the second anharmonicity constant $\omega_e y_e$ and these values are usually not very reliable.

VANDERSLICE, MASON, MAISCH and LIPPINCOTT (1959) compared the Rydberg-Klein graphical/numerical procedure with the Rees analytical modification. They found that for H_2 the Rees modification of the Rydberg-Klein method generates results which agree within the limits of accuracy of the latter.

Since the RKR method is a semi-classical one, the possibility exists that the results for the lower vibrational levels could be unreliable. VANDERSLICE et al (1959) calculated the potential curve of H_2 in the vicinity of the minimum by the Dunham method which is known to be accurate in this region. The results were in good agreement with those calculated by the RKR method. In fact, JARMAIN (1960) and HURLEY (1962) have shown that the two methods are equivalent for the lower vibrational energy levels. Both methods are WKB methods and hence semi-classical and so it is surprising that either describes the potential energy curve successfully at the minimum. The fact that both methods do give good

results there may be explained by the fact that, in this region, the curve is very similar to the potential energy curve of an harmonic oscillator. The energy levels of the harmonic oscillator as calculated using the WKB approximation are exactly the same as those given by quantum mechanics and therein lies the success of the two methods at low vibrational energies.

It is worth considering the relative merits of the RKR and Dunham methods. The Dunham method assumes a polynomial representation of the potential energy curve around the minimum. Since such an expansion cannot converge at very large values of R(internuclear separation), this method must fail for the higher vibrational levels even though it is accurate for the lower levels. Thus this method has basically the same disadvantage as all the other methods which assume an algebraic form for the potential energy curve.

The main disadvantage of the RKR method is that the potential energy curve can be constructed only in the region for which sufficient spectroscopic data exists and its accuracy depends on the accuracy of the experimental results.

Many different methods have been derived for evaluating the Klein equations. With the increase in the use of computers, the integrations do not present the problems they did in the past. Nevertheless, much work has been done to devise methods which get around the problems involved when the integrand is zero as well as attempts to simplify the calculations (SINGH and JAIN (1962); WEISSMAN, VANDERSLICE and BATTINO, (1963); RICHARDS and BARROW, (1964); ZARE, (1964); GILMORE, (1965); SPINDLER, (1965); ZELESNIK, (1965); COXON, (1971)).

1.2.6 Comparison of Calculated Franck-Condon Factors

For this thesis, an available computer program (GARDNER, 1970) was used to calculate Franck-Condon factors for transitions in O_2 from RKR potentials. This program used the method of WEISSMAN et al (1963) to evaluate the potential energy curve for energy levels for which $v \leq 3$ and the method of RICHARDS and BARROW (1964) for the higher vibrational levels. The spectroscopic data (G(v) and B(v) values) used were those compiled by WALLACE (1962). Gardner used the subroutine of ZARE and CASHION (1963) based on the method of COOLEY (1961) to solve the Schroedinger equation and hence to find the Franck-Condon factors for ionizing transitions in N_2, NO, O_2, CO and H_2.

The Franck-Condon factors of greatest interest to this thesis are those for the transitions $O_2 X^3\Sigma_g^-(v'' = 0) \rightarrow O_2^+ X^2\Pi_g$ $(v' = 0,1,2,\ldots)$ as well as from the J series of autoionizing levels to $O_2^+ X^2\Pi_g (v' = 0,1,2,\ldots)$.

Table 1.1 shows the variation in Franck-Condon factors using different potential energy curves for the former transitions. It can be seen that the maximum difference between RKR (GARDNER) and RKR (ALBRITTON) is about 7%. The experimental errors at these higher vibrational levels could be at least as big, and so it does not seem critical as to which potential energy curve is used. In fact the Morse potential is quite adequate for most purposes. For work in this thesis, it was decided to use the Franck-Condon factors of ALBRITTON et al from KRUPENIE (1972).

TABLE 1.1

Comparison of calculated Franck-Condon Factors for Transitions

$O_2\ X\ ^3\Sigma_g^-(v''=0)$ to $O_2^+\ X\ ^2\Sigma_g\ (v'=0, 1....)$

i)

v'	RKR[a)]	RKR[b)]	RKR[c)]	Morse[b)]
0	0.1819	0.1826	0.1884	0.1832
1	0.3613	0.3613	0.3645	0.3592
2	0.2936	0.2936	0.2901	0.2925
3	0.1268	0.1266	0.1227	0.1278
4	0.0315	0.0312	0.0298	0.0323
5	0.0045	0.0044	0.0042	0.0047
6	0.0004	0.0003	0.0003	0.0004

ii) % difference when compared to RKR[c)]

v'	RKR[a)]	RKR[b)]	Morse[b)]
0	3.5 %	3.1 %	2.8 %
1	0.9 %	0.9 %	1.5 %
2	1.2 %	1.2 %	0.8 %
3	3.3 %	3.2 %	4.2 %
4	5.7 %	4.7 %	8.4 %
5	7.1 %	4.8 %	11.9 %
6	not enough significant figures ⟶		

a) GARDNER (1970)

b) ASUNDI and RAMACHANDARAO (1969)

c) ALBRITTON et al from KRUPENIE (1972)

1.3 AUTOIONIZATION

1.3.1 Introduction

Excitation of an electron other than the most loosely bound one, or simultaneous excitation of two electrons, may result in a set of discrete states which extend above the normal ionization threshold. Thus two different "states" of the atom or molecule (one of which is a continuum state) may have the same energy. A mixing of the eigenfunctions of the two states will occur and so the true state is an hybrid. Part of the time the system is in the discrete state, part of the time it is in the continuum state. However, once the system enters the continuum state, ionization occurs and the system cannot return to the discrete state. Thus a radiationless transition occurs from the discrete state into the continuum state. This process is known as autoionization.

Electronic states of atoms and molecules are usually classified as belonging to various configurations, according to the independent particle approximation. One such approximation is the central field approximation, which assumes that each of the electrons moves in a spherically symmetric potential energy that is produced by the nucleus and the average effect of all the other electrons (see eg. SCHIFF, 1955). Each electron is then classified by its quantum numbers n and l and the configuration of the atom or molecule is given by the listing of the quantum numbers of all the electrons.

When other terms in the Hamiltonian (see equation (2b)) thatare disregarded in the independent particle approximation are now included, the actual stationary states may be represented as superpositions of states which are "mixed" by the "configuration interaction". The mixing of a configuration belonging to a discrete spectrum with continuum configuration gives rise to the pheromenon of auto-ionization.

In the central-field approximation, if an inner electron is excited to a state which lies above the ionization threshold for a more loosely bound electron, the atom or molecule remains in this configuration. With the introduction of other terms in the Hamiltonian due to eg. the instantaneous interelectronic interaction, this state then becomes a mixture of the discrete state and the continuum. The discrete state is no longer stable but exists for a short time before decaying by emission of an electron accompanied by an internal rearrangement of the system leaving behind an ion. This process is known as autoionization.

1.3.2 An example of Autoionization

To illustrate the above description of auto-ionization, it is convenient to use the Helium atom as an example. Using the central field approximation, for such a two electron system there will be a set of configurations

$$\left.\begin{array}{l}(1s)^2,\ (1s)\ (2s),\ (1s)\ (3s),\ \ldots.(1s)(E_c s)\\ \qquad (1s)\ (2p),\ (1s)\ (3p),\ \ldots.(1s)(E_c p)\end{array}\right\}\ \text{1snl...I states}$$

in which one electron is always in the ground (1s) orbital and $(E_c s)$, $(E_c p)$ ...denote continuum orbitals of positive energy E_c and orbital angular momentum numbers 0, 1.....

In addition to this set, there will be others in which both electrons are excited. For example, there is the set based on 2s

$$\left.\begin{array}{l}(2s)^2,\ (2s)\ (3s),\ \ldots.(2s)\ (E_c s),\\ \qquad (2s)\ (2p),\ \ldots.(2s)\ (E_c p),\end{array}\right\}\ \ldots\text{IIs}$$

and on 2p

$$\left.\begin{array}{l}(2p)^2,\ (2p)\ (3p),\ \ldots.(2p)\ (E_c p)\\ \qquad (2p)\ (3s),\ \ldots.(2p)\ (E_c s)\end{array}\right\}\ \ldots\text{IIp}$$

and so on.

The actual situation in Helium is illustrated in Fig. 1.2. Corresponding to each single electron orbital (nl) there exists a Rydberg series of states converging to a limit. Above this limit the series becomes a continuum.

The important point for present purposes is that the energy of any of the doubly excited configurations will coincide with that of a member of the singly excited set in which the excited orbital (E_1) is one of the continuum. For example, the state $(2s)^2$ resides in the continuum of the series of states 1snl. Thus the energy of the $(2s)^2$ state is the same as that of the system of a helium ion (He^+ + (1s)) with a free electron of particular energy.

If the effect of inter-electronic repulsion is now considered, the $(2s)^2$ state is no longer stable i.e. it is not an eigenfunction of the total Hamiltonian $H = H_0 + H'$, where H_0 is the Hamiltonian due to the central field approximation and H' is the Hamiltonian due to the perterbation of the states by interelectronic repulsion. The state will thus decay with a certain lifetime into the continuum. This lifetime is determined by the strength of the interaction of the discrete state with the continuum of overlapping energy.

1.3.3 Theories of Autoionization

The problem that the auto-ionization theoreticians face is producing a theory which deals with the effects of configuration interaction on intensities and which finds the correct linear combination of the discrete state and the continuum at the energy of interest to give the true eigenstate of the total Hamiltonian.

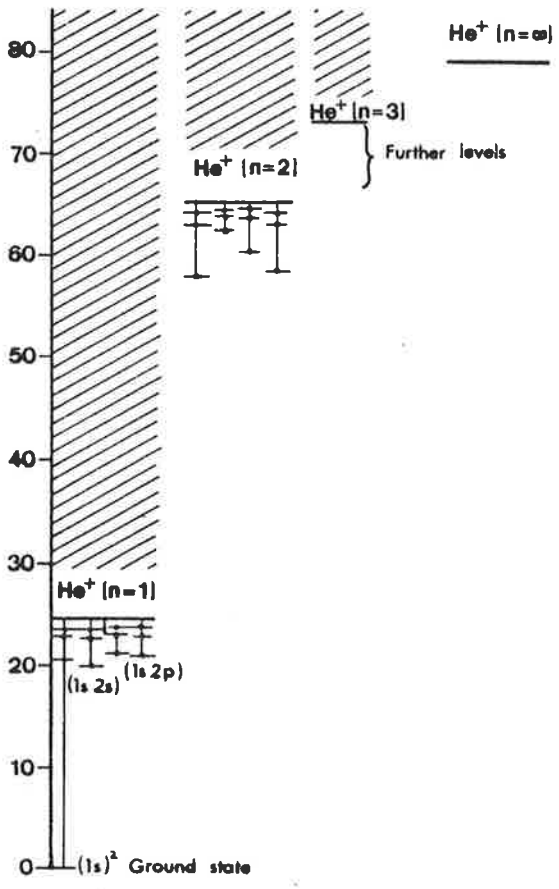

Fig. 1.2. Energy diagram for neutral He atoms (modified from MASSEY AND BURHOP, 1969, Fig. 9.1).

The main types of theory are:

a) R - matrix theory (BURKE and TAYLOR, 1974)

b) Feschbach's projection theory (FESCHBACH, 1967)

c) Quantum defect theory (DILL, CHANG and FANO, 1973)

d) Fano - Mies theory (FANO, 1961 and FANO & COOPER, 1965; MIES, 1968)

The Fano-Mies theory has the least complex physical meaning and so is the one chosen for this thesis. TOROP (unpublished) and BARDSLEY (1968) have extended this theory to cover autoionization in molecules.

The simplest case of autoionization is the configuration interaction between one discrete state and more than one overlapping continuum for an atomic state. Fano and Cooper found that the total photoabsorption cross-section over a resonance can be given by

$$\sigma(\varepsilon) = \sigma_a\{(q + \varepsilon)^2/(1 + \varepsilon)^2\} + \sigma_b \qquad \ldots(22)$$

where $\varepsilon = (E - E_r)/\frac{1}{2}T$

E = photon energy

E_r = unperturbed energy of the discrete state

h/T = mean lifetime of the level with respect to autoionization

q = "line - profile index" and is a function of the eigenfunctions of the discrete state and the continuum states

$\sigma(\varepsilon)$ = absorption cross-section of photons of energy E

σ_a = absorption cross-section corresponding to states of the continuum which do interact with the discrete autoionizing level

σ_b = absorption cross-section corresponding to states of the continuum which do not interact with the discrete autoionizing state.

For partial cross-sections in molecules, similar types of equations have been put forward (HUTTON and TOROP, unpublished; BARDSLEY, 1968; SMITH, 1970a, b). For the case of one vibrational

autoionizing level and making the assumptions that i) the Born - Oppenheimer approximation holds i.e. the wavefunction varies only slightly with change in internuclear distance and ii) the widths of the autoionizing states are much less than the separation between successive states, for a single resonance ν which does not overlap with any other resonance the partial cross-section to the vibrational level α of the ion is

$$\sigma_\alpha = \sigma_c(F_\alpha^c + F_{\alpha,\nu}F_\nu^b\{\frac{q - i}{\varepsilon + i}\})^2 \quad \ldots(23)$$

where σ^c = total absorption cross-section to all states of the continuum

F_α^c = Franck-Condon amplitude for the transition from the initial state of the molecule to the vibrational state α of the ion

$F_{\alpha,\nu}$ = Franck-Condon amplitude for the transition from the autoionizing level ν to the vibrational level α of the ion

F_ν^b = Franck-Condon amplitude for the transition from the initial state to the autoionizing level ν

q and ε as defined in equation (22)

1.3.4 Experimental Evidence for Autoionization

BEUTLER (1935), while examining the photon absorption spectra of rare gases found unusually broad, asymmetrical lines between the $^2P_{3/2}$ and $^2P_{1/2}$ limits. FANO (1935) interpreted these lines in terms of the excited levels of the atom convergent on the $^2P_{1/2}$ level of the ion and which decay into the ion in its $^2P_{3/2}$ state plus a free electron. Many other such lines have been observed in photon absorption spectra and electron scattering experiments since then by many different workers.

Autoionization observed in photoelectron spectra is

more recent. In 1965, DOOLITTLE and SCHOEN (1965) were investigating the photoelectron spectra of hydrogen using a monochromator at wavelengths of 77.2nm, 78.0nm and 79.0nm. They found that at the different wavelengths, the height of the curve at zero retarding potential, which should be proportional to the ionization cross-section is larger at 78nm than at 77.2nm or 79nm. They also found that the v = 1 state of the H_2^+ ion was strongly enhanced at 78nm. It was assumed that the v = 1 state at 78nm was largely excited through autoionization.

COLLIN and NATALIS (1968) and PRICE (1968) investigated the effects of autoionization on the vibrational distribution of the molecules oxygen, nitrogen, carbon monoxide and nitric oxide by comparing photoelectron spectra obtained using the 58.4nm HeI resonance line with those obtained using the Ne doublet at 73.6 - 74.4nm and the Ar doublet at 104.8 - 106.7nm. Collin and Natalis found, for example, that at 58.4nm only four vibrational levels of O_2^+ in the $X^2\Pi_g$ state were observed but at the Ne discharge lines, the vibrational sequence of O_2^+ in the first excited state extended up to v' = 20. Note that this technique depends on the chance of finding an autoionizing state which nearly coincides with the lines of the lamp spectra.

BERKOWITZ and CHUPKA (1969) studied the photoelectron spectra at autoionizing resonances in molecular hydrogen and nitrogen with dispersed radiation. BAHR et al (1971a, b) recorded spectra at a number of well-defined autoionization resonances in NO, N_2, CO and O_2 using the radiation from the Hopfield continuum of a He discharge lamp dispersed by a 1 metre monochromator. Considerable differences between the resonance spectra and those recorded at nearby off-resonance wavelengths were observed.

In a previous paper, BLAKE et al (1970) had discussed the theory that the photoelectron spectra resulting from autoion-

ization can be described by the distribution of Franck-Condon factors for the transition from the autoionizing state to the vibrational states of the ion. This would explain the change in intensities of the vibrational levels on resonance, for example in the spectra of Collin and Natalis previously mentioned.

To verify this hypothesis, RKR potentials (see section 1.2.5) were calculated for the low-lying neutral and ionic states. As no rotational data were available for the autoionizing states, RKR curves could not be computed and so Morse potential energy curves were calculated for the auto-ionizing states. The Franck-Condon factors for the decay of the autoionizing state to the ionization continuum and the Franck-Condon factors from the ground state of the molecule to the first ionic state were computed from the wavefunctions calculated from the potential energy curves.

The contribution to the resonance spectra was estimated from the values of the photoionization coefficients on resonance and at a nearby off-resonance wavelength. The vibrational distribution due to the resonance alone was found by subtracting the 58.4nm spectrum from the resonance spectrum, in proportion to the continuum contribution. The results were then compared with the calculated Franck-Condon factors.

The authors concluded that the nature of the photo-electron spectrum at resonance is determined by the Franck-Condon factors linking the autoionizing state with the ion and their experimental results agreed with theoretical predictions at least qualitatively.

KLEIMENOV, CHIZHOV and VILESOV (1971) studied autoionization processes in nitric oxide in the wavelength region 128 to 90nm. As there was not much information about the potential energy curves of the autoionizing states, a comparison with calculated Franck-Condon factors was not given but they suggested that the

Franck-Condon principle may not hold in autoionization.

TANAKA and TANAKA (1973) on the basis of their photoelectron spectra at some autoionizing states of oxygen near the ionization threshold concluded that the vibrational distributions of photoelectron spectra from autoionizing states were clearly different from those of calculated Franck-Condon factors for the direct ionizing transition. The classification of the autoionizing states in this region was incomplete at that time which caused problems in comparisons of their calculated Franck-Condon factors for the autoionizing transitions and their experimental results. Since then, KATAYAMA, HUFFMAN and TANAKA (1973), have reported re-measurements of the absorption spectrum of oxygen in the wavelength range 65nm to 110nm which have clarified this problem.

An interesting paper which compares experimental results with Smith's (SMITH, 1970 (a), (b)) theory was published by KINSINGER and TAYLOR (1973). The photoelectron spectra of oxygen between 80 and 85nm were recorded and from this data, a quite successful comparison between experimental and calculated results was made.

The assumption that the 58.4nm photoelectron spectrum of oxygen can be used as a off-resonance position to estimate the continuum contribution to the cross-section has been refuted by work of GARDNER and SAMSON (1974b). They compared calculated Franck-Condon factors (KRUPENIE, 1972) with experimental values at 58.4nm and 30.4nm. For the transitions to $O_2^+ \times {}^2\Pi_g$ and $B^4\Sigma_g^-$ the experimental intensities from the 30.4nm spectrum agreed more closely with the calculated FCF than those at 58.4nm suggesting that some of the 58.4nm distribution comes from autoionization.

1.4 ANGULAR DISTRIBUTION OF PHOTOELECTRONS

The angular distribution of photoelectrons emitted from a randomly oriented set of atoms or molecules is dependent on the polarization and direction of propagation of the incident photon beam and it also depends on the initial kinetic energy of the photoelectrons and the energy level from which the photoelectrons are ejected. Thus great care must be taken in the measurement of relative transition probabilities with a photo-electron spectrometer to overcome or allow for this angular dependence.

COOPER and ZARE (1968) have shown that, if unpolarized radiation is used to produce photo-electrons, the differential cross-section for electrons emitted in a dipole transition in a direction θ to the radiation beam direction is given by

$$\frac{d\sigma}{d\omega} = \frac{\sigma_{total}}{4\pi}\{1 - \beta P_2(\cos\theta)\} \qquad \ldots(24)$$

where β is an asymmetry parameter. For $\theta = 54^0\ 44'$ the relation between the differential cross-section and the total cross-section is independent of β.

More recent work (LINDEMANS et al, 1979) has suggested that for a finite beam source and finite electron aperture the electron count rate is found by integrating equation (24) over the source volume and the cone of acceptance into the analyser. The expression found is

$$I(\phi) = A(\phi) + \beta B(\phi) \qquad \ldots(25)$$

The value of ϕ for which $B(\phi) = 0$ making the electron count rate proportional to the cross-section σ_{total} depends on the geometry of the system.

The original aim of this thesis was to fit experimental autoionization data from oxygen to the Fano-Mies configuration interaction theory of autoionization. As was described in Section 1.3.4, only KINSINGER and TAYLOR (1973) have attempted to do this. BAHR et al (1971) and BERKOWITZ and CHUPKA (1969) were using a simplified version of the theory when they assumed that the distribution of electron energy amongst the vibrational states of the ion was determined by the Franck-Condon factors between the autoionizing state and the vibrational states of the ion. They did not take into account that, because there are two paths to the final state of the ion, namely direct ionization and ionization via the autoionizing state, interference will occur as shown by Fano.

In order to make this comparison, a suitable spectrometer with good energy resolution and high count rate was needed. Much time was spent developing this system and then taking high quality autoionization data. A program to analyse this data was developed but unfortunately no time was left to compare this data to the theory. The spectra should yield Franck-Condon amplitudes for the transition from the autoionizing state to the vibrational states of the ion and hopefully theoretical physicists will use these in the future.

The next chapter deals with the features of the apparatus and the reasons why it is a valuable instrument to use to investigate autoionization in molecules.

CHAPTER 2 DESCRIPTION and OPERATION OF THE APPARATUS

INTRODUCTION

In order to measure the intensities of vibrational transitions as a function of wavelength by the method of photo-electron spectroscopy, an experimental arrangement of four basic units is required. These are

1. a lamp producing radiation with a continuous range of wavelengths in the extreme ultra-violet region
2. a monochromator to disperse this radiation
3. a chamber where this radiation can interact with the gases being studied and
4. a spectrometer to analyse the energy of the electrons emitted during this interaction.

Fig. 2.1 shows a general view of the apparatus used to measure photoionization processes, including the units mentioned above.

This chapter contains a description of these units, the features of the apparatus which make it particularly suitable for measurements of vibrational intensities and the steps taken to produce optimal results. Of special importance is the discussion on choice, operation and performance of the spectrometer as much time and effort was spent on optimising the conditions necessary to produce high quality data.

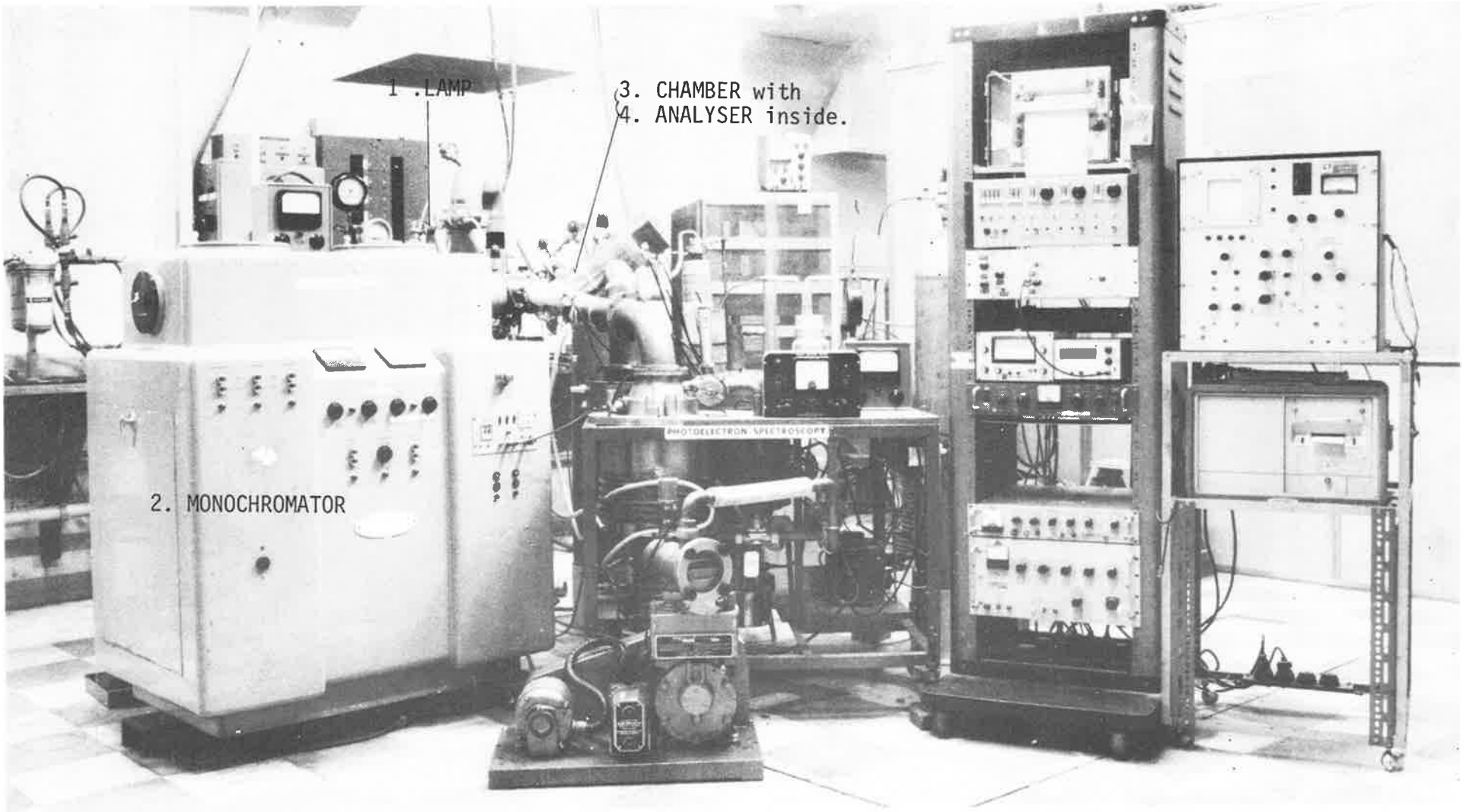

Fig 2.1 General view of the apparatus used to measure photoionization processes.

2.1 THE LAMP

Ultraviolet radiation was produced in a water-cooled pyrex discharge tube (Fig. 2.2). In the wavelength range 100 to 60nm, emissions of the Hopfield continuum, corresponding to transitions of excited He_2 molecules back to their repulsive ground state, were excited by a thyrotron triggered discharge from a 5kV D.C. supply, (HUFFMAN et al, 1965). An A.C. voltage of 15kV was used to produce the resonance lines of Helium (58.4nm) and Neon (73.6nm and 74.4nm).

The pressure in the lamp for the resonance lines was about 0.5 Torr (mm Hg) but for the Hopfield continuum a pressure of aprroximately 25 Torr (mm Hg) was needed. This required differential pumping between the lamp and the monochromator. This pumping system consisted of a Rootes Blower and backing pump for the first stage and an oil booster pump and backing pump as the second stage.

Using this system and with 100 μ entrance slits on the monochromator and 25Torr gas pressure in the lamp, the pressure in the monochromator was kept below 10^{-4} Torr.

Industrial grade Helium from Commonwealth Industrial Gases was passed through a liquid air cooled zeolite trap. This removed impurities, particularly water vapour as well as Oxygen and Nitrogen, from the Helium and hence enhanced the intensity of the Hopfield continuum by a factor varying from 20 - 50 %.

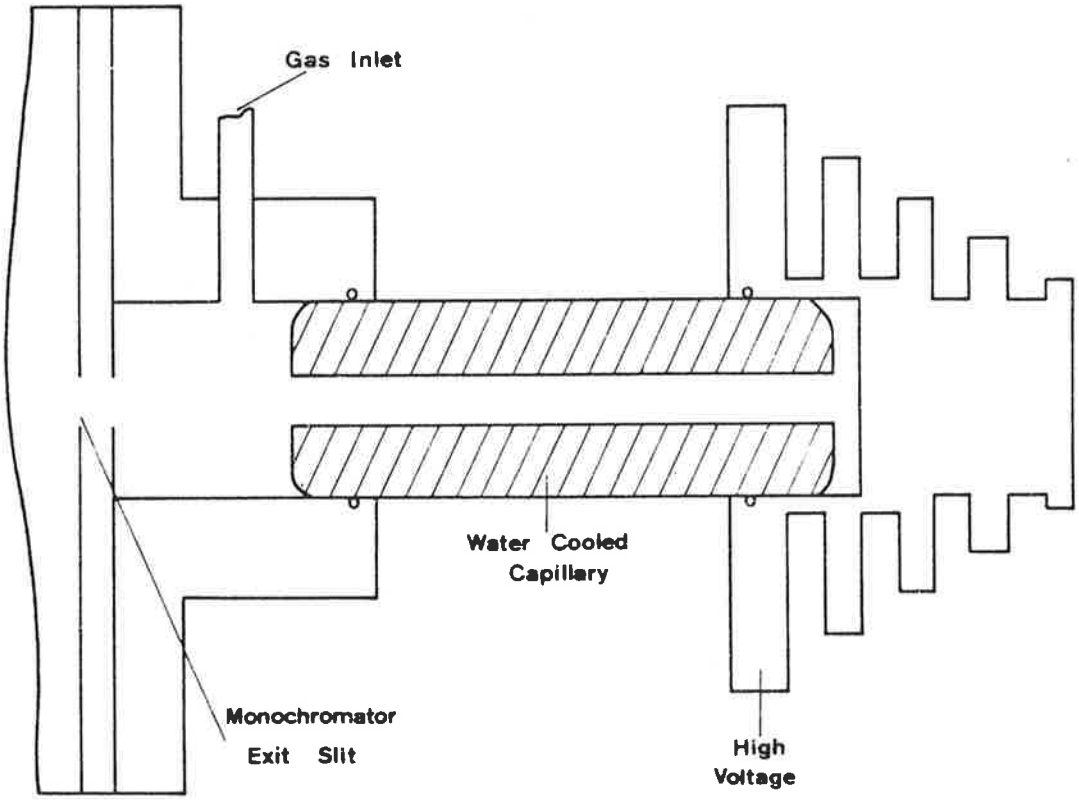

Fig. 2.2. The water-cooled capillary discharge light source.

2.2 THE MONOCHROMATOR

The monochromator used for these experiments was a 1 metre, near-normal incidence, scanning device (M^{c}Pherson; Model no. 225). The grating was a platinum coated, Bausch and Lomb replica grating with 1200 lines/mm and blazed for 80nm.

With the exit and entrance slits set to 100 μ, the resolution was 0.1nm which is more than adequate to distinguish autoionization resonances in photoionization cross-sections.

2.3 THE IONIZATION CHAMBER

The analyser was housed in a 15 cm copper chamber with its axis aligned at 54^{o} 33' to the photon beam, an arrangement which makes measurements almost insensitive to the angular distribution of the photoelectrons (see Section 1.4).*

Sensitivity to partial polarization of the light beam was removed by placing the axis of the analyser in a plane at 45^{o} to the Rowland plane of the monochromator.

This chamber, housing the ionization region and analyser, was pumped at each end by a 15 cm oil diffusion pump (Figs. 2.1 and 2.3). The ultimate pressure reached was about 5×10^{-6} Torr. Both pumps incorporated liquid air traps which were kept full when the pumps were in operation.

*Since the results for this thesis were taken, LINDEMANS et al (1979) (Appendix 3) have calculated that, for the geometry of the present apparatus, an angle of 55^{o} 33' would make the electron count rate truly proportional to the total cross-section. The maximum error this could produce is about 3 % for two processes which have different β values.

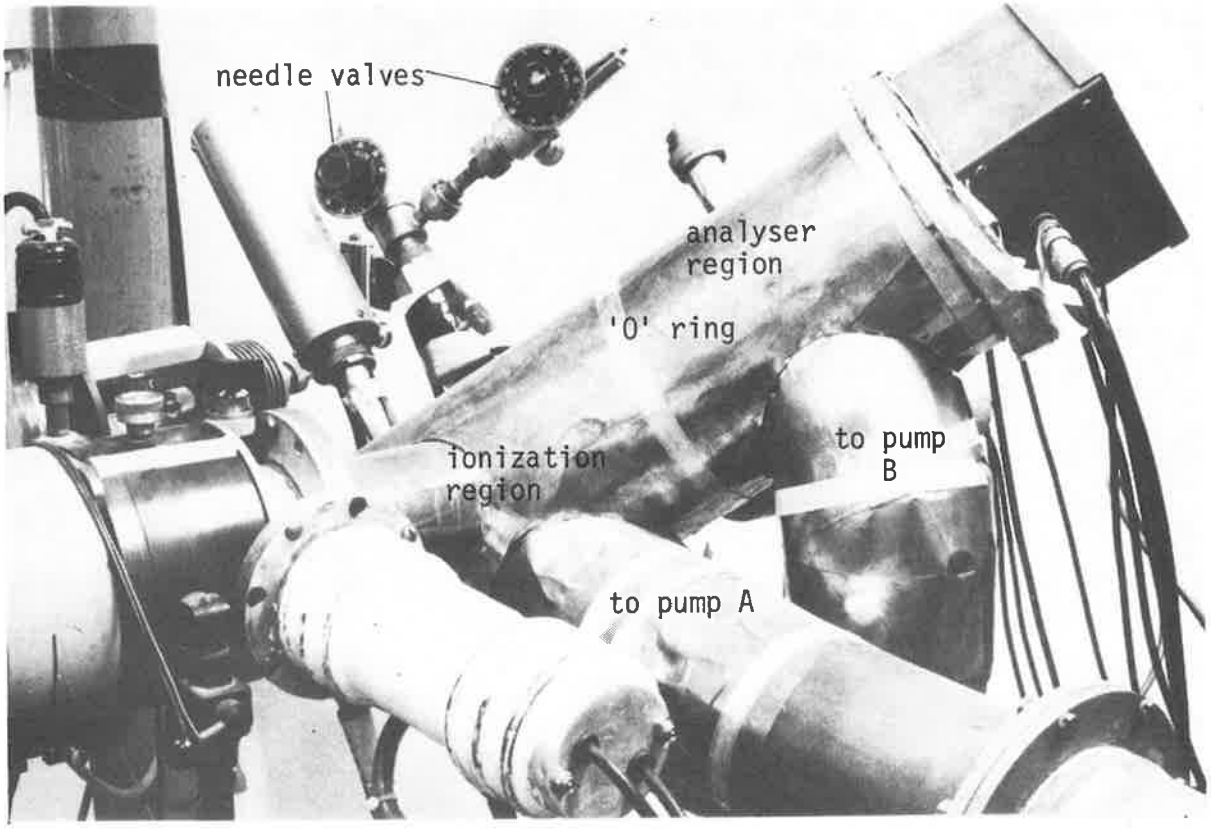

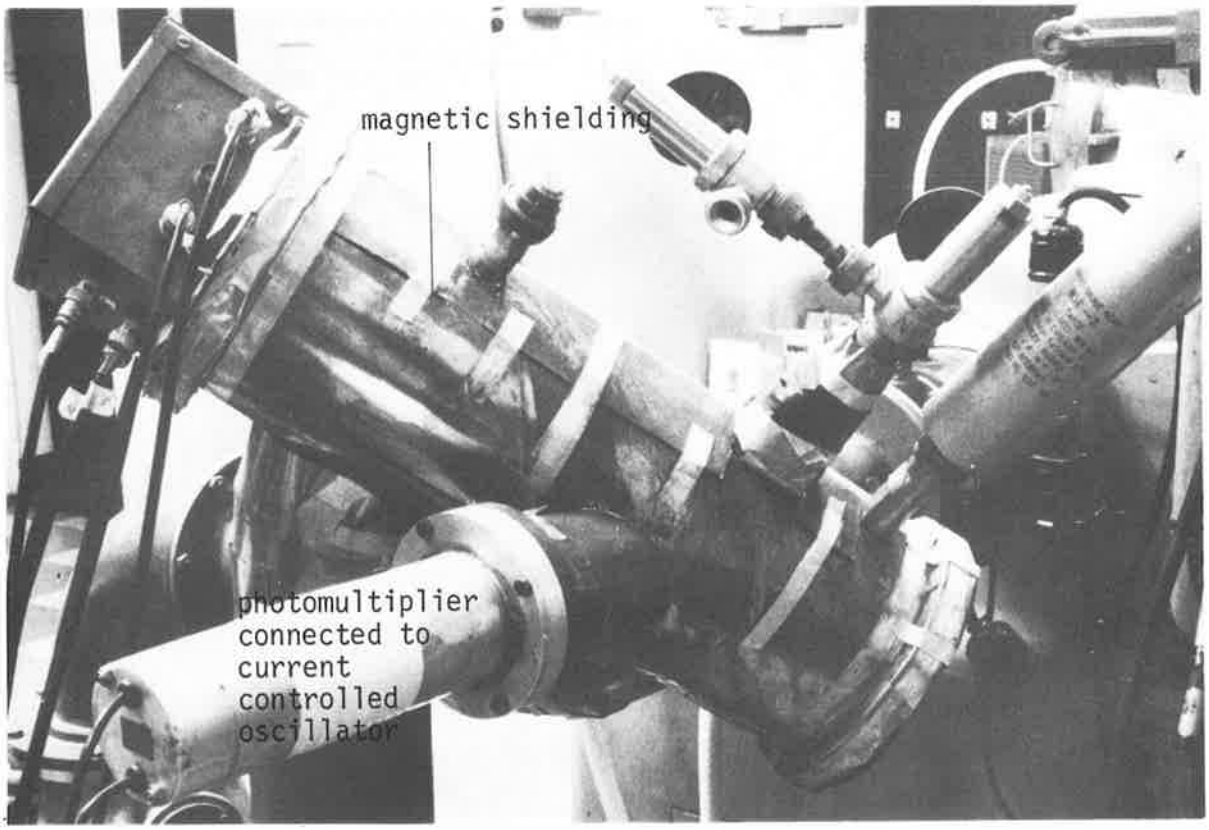

Fig. 2.3. Two views of the analyser chamber illustrating the angles of alignment.

2.4.1 Introduction to Photoelectron Spectrometers

A photoelectron spectrum is measured by varying the energy of photoelectrons allowed to reach the detector and recording the rate at which electrons of each energy arrive. Three main types of electron energy analysers or spectrometers are available:

a) magnetic focussing analysers

b) electrostatic focussing analysers

c) retarding potential analysers

These are discussed below.

a) Magnetic focussing analysers

Three examples of this kind are the cylindrical 180° magnetic field analyser (TURNER and MAY, 1966), the spherical 180° magnetic field analyser (FROST, M^{c}DOWELL and VROOM, 1965) and the double focussing magnetic analyser (FADLEY et al, 1969). Strictly speaking magnetic analysers are momentum not energy analysers as they separate electrons according to their velocities not their kinetic energies.

b) Electrostatic focussing analysers

This type of analyser, which uses an electrostatic field to deflect the electrons according to their kinetic energies, can be divided into four groups viz i) parallel plate, ii) cylindrical iii) spherical and iv) clyindrical mirror analysers. SEVIER (1972) describes these analysers, their characteristics and their uses. A more recent modification (GARDNER and SAMSON 1973, 1975, 1976) is the use of a pre-retarding/accelerating system coupled with a cylindrical mirror analyser. This reduces electron scattering effects and gives constant resolution so that peak areas measure photoelectron intensities directly.

Both magnetic and electrostatic focussing analysers are discussed by GELLENDER and BAKER (1974) who developed an equation which gave the maximum attainable resolution and transmission of these analysers.

c) Retarding potential analysers

In retarding potential analysers, a negative potential is applied to a grid or screen in front of or on the detector. By incrementally increasing this potential, electrons of energy less than that needed to overcome this potential are prevented from reaching the detector. A plot of detector signal against retarding potential produces an integral energy distribution curve.

A comparison of different kinds of retarding potential analysers is given in SEVIER (1972). Some of the common analysers used in PES are the cylindrical (eg. BLAKE and CARVER, 1967), spherical (eg. SAMSON and CAIRNS, 1968), hemispherical (eg. BAHR et al, 1969) and plane geometry (BERKOWITZ, 1967) analysers.

Another interesting paper on retarding potential analysers is by HUTCHITAL and RIGDEN (1972) who discussed the resolution and sensitivity of spherical grid retarding potential analysers.

The aim of all analyser designers is to obtain optimum resolution and high sensitivity simultaneously. Unfortunately these two factors conflict and so a compromise has to be reached.

Dispersion or differential analysers (magnetic and electrostatic focussing analysers) have the advantage of theoretically high resolution (as good as 10 meV for constant resolution instruments or about $\frac{\Delta E}{E}$ = 0.1 - 0.2 % if the resolution varies) but they need accurate machining and hence are more difficult to construct. Magnetic focussing analysers cannot measure low energy electrons because of the need for weak, uniform magnetic fields which would be disturbed by stray fields, and so are not much used these days.

Retarding potential analysers are inherently simpler and have a higher count rate which implies shorter measuring times and hence greater accuracy. The main disadvantage is that low energy electrons in a complex spectrum are difficult to examine due to statistical noise.

2.4.2 Choice of analyser for this thesis

In order to investigate the vibrational intensities from different auto-ionizing levels of diatomic molecules, an analyser with a resolution of better than 100 meV is needed to separate these vibrational levels. As the separation of the rotational levels (spacing $\sim$ 1 meV) was not of interest to this thesis, a resolution much better than this would have been wasted and would have been gained only at the expense of sensitivity. Since the intensity of the light entering the ionizing region was low because of the dispersion of the lamp's radiation by the monochromator, it was necessary to choose an analyser with a large electron collecting aperture. This was provided by a hemispherical grid retarding potential analyser which has a large collecting aperture for a given resolution (HEDDLE, 1971). This type of analyser also has the advantages of simplicity, stability and a well-behaved efficiency versus energy function.

For electrons from one energy level, the theoretical integral spectrum, which this analyser gives, is a step function with all electrons of energy greater than the retarding voltage being transmitted and no electrons of lower energy passing through the grids. Thus when the number of photoelectrons counted is plotted against the retarding voltage, a horizontal straight line up to a retarding voltage equal in magnitude to the ionization potential should be obtained. No photoelectrons should be recorded after this

voltage. Such a theoretical, "flat" spectrum is shown in Fig. 2.4(a). When electrons from more than one energy level are being counted, the spectrum consists of a series of step functions as shown in Fig. 2.4(b).

This integral form of the electron spectrum facilitates simultaneous scanning of the wavelength and electron energy to allow detection of electrons due to the same transitions. Because one can modulate from the top to the bottom of the step, a retarding potential analyser does not need the precision of tuning required by a differential analyser provided that the steps in the spectrum are well separated.

2.4.3 Details of the Spectrometer

The spectrometer consists of three elements; 1) the photoelectron source 2) the analysing grid system and 3) the photo-electron detector. These are shown in Fig. 2.5 and 2.6 and described below.

2.4.3.1 Photoelectron source

Photoelectrons generated in the ionization region enter the spectrometer through an inlet aperture of 1/8" diameter. These electrons then pass through a series of baffles which define the cone of acceptance of the photoelectrons. The main purpose of these baffles is to prevent the detection of non-radial electrons, which would otherwise have been deflected off the walls of the analyser and would have degraded the energy resolution of the analyser and increased the background count.

2.4.3.2 Grid System

Four grids were used in the analysers; an earth, a retarding, an accelerating and a focussing grid. These four

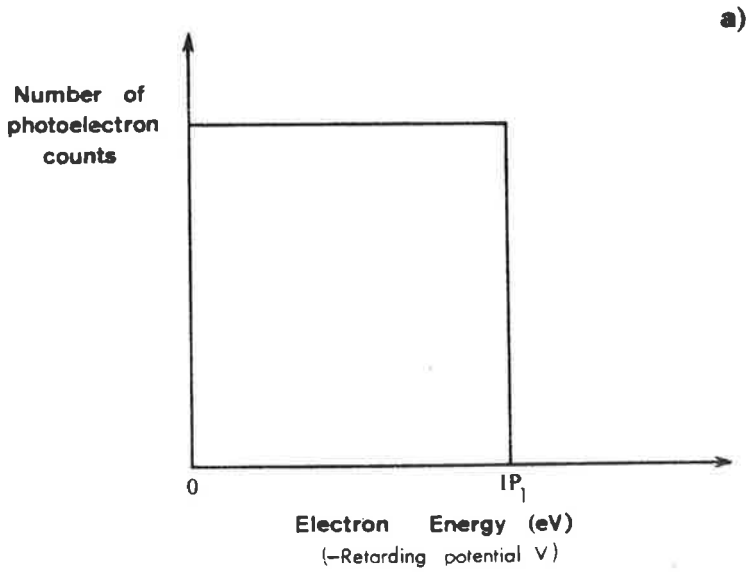

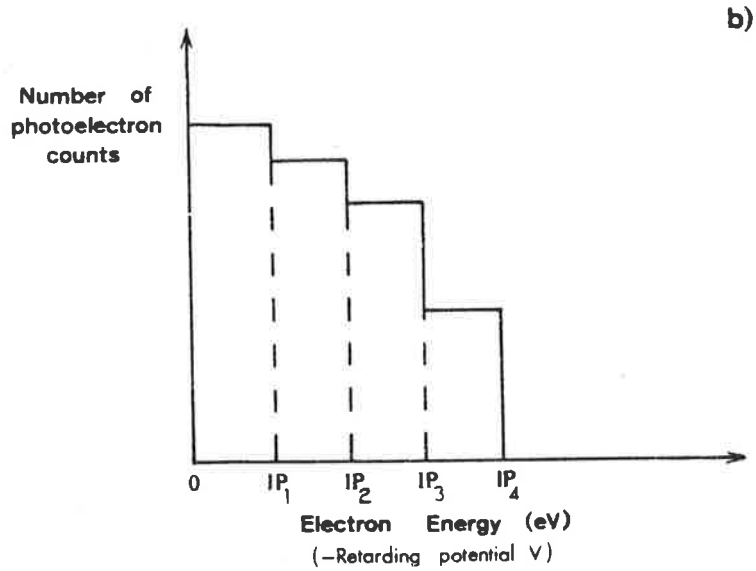

Fig. 2.4. Theoretical integral spectra.

a) Spectrum of mono-energetic electrons i.e. electrons from one state.

b) Spectrum of electrons from more than one state.

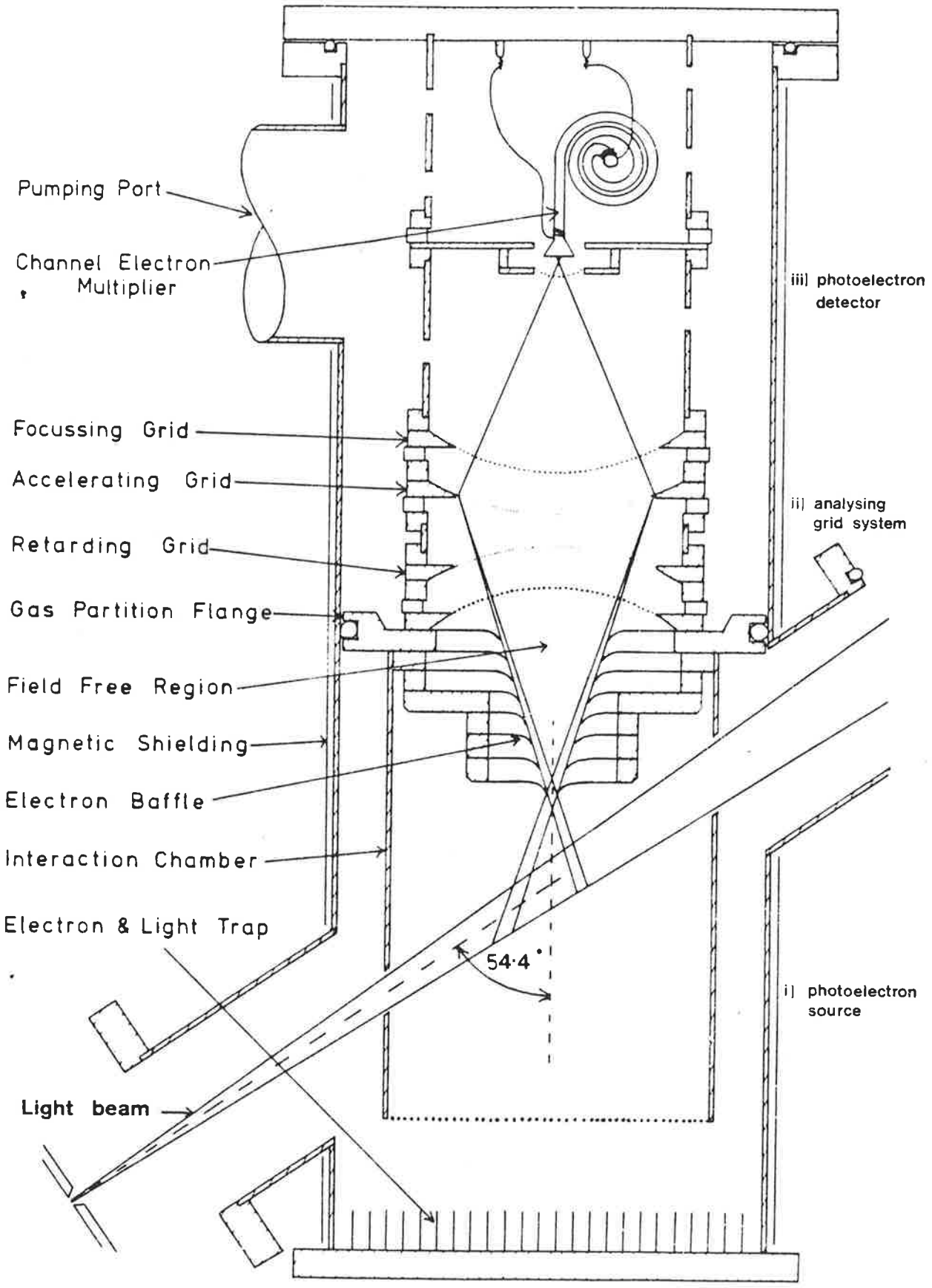

Fig. 2.5 Cross–section of the spectrometer (retarding grid electron energy analyser)

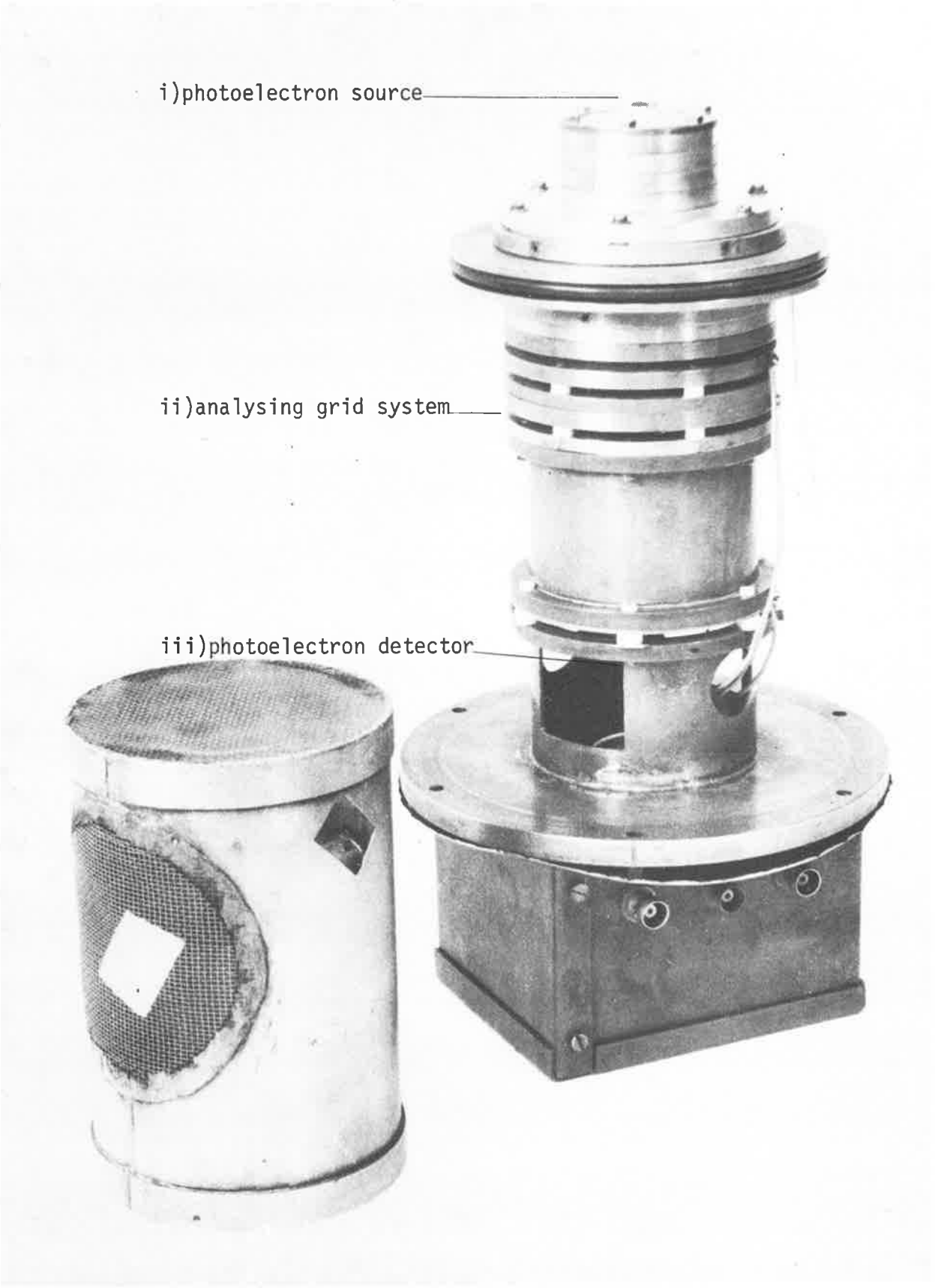

Fig 2.6 Electron energy analyser and interaction cage.

hemispherical grids were made of fine phosphor bronze mesh soldered onto brass rings (Fig. 2.7). The mesh was etched so that the earth and focussing grids were approximately 86 % transparent and the retarding and accelerating grids were about 78 % transparent giving a total transparency of about 45 %.

The grids were separated by spacers which were machined from Delrin or Teflon - both good, clean,non-compressible insulators which do not out gas badly under vacuum. The spacers were turned to a height which ensured that the earth grid and the retarding grid were concentric with the centre of the inlet aperture and the accelerating grid and focussing grid were concentric with the electron detector.

The earth grid, which had a radius of 50 mm, maintained a field free region in which the field of view of the analyser was defined by the baffles.

The next grid met by the electrons was the retarding grid whose electric field opposed their motion. Both the radius of this grid as well as the radius of the next grid - the accelerating grid - were 64 cms. The accelerating grid was used to give the electrons a constant energy to prevent them drifting onto the walls.

The final grid, of 50 cm radius, was the focussing grid which drew electrons in and focussed them onto the electron detector.

A wire mesh cage enveloped the front of the analyser (Fig. 2.6). This interaction cage was designed to provide a field free region which did not scatter electrons into the field of view of the analyser.

All the grids as well as the baffles and interaction cage were gold plated to minimize contact potentials and to eliminate stray electric fields.

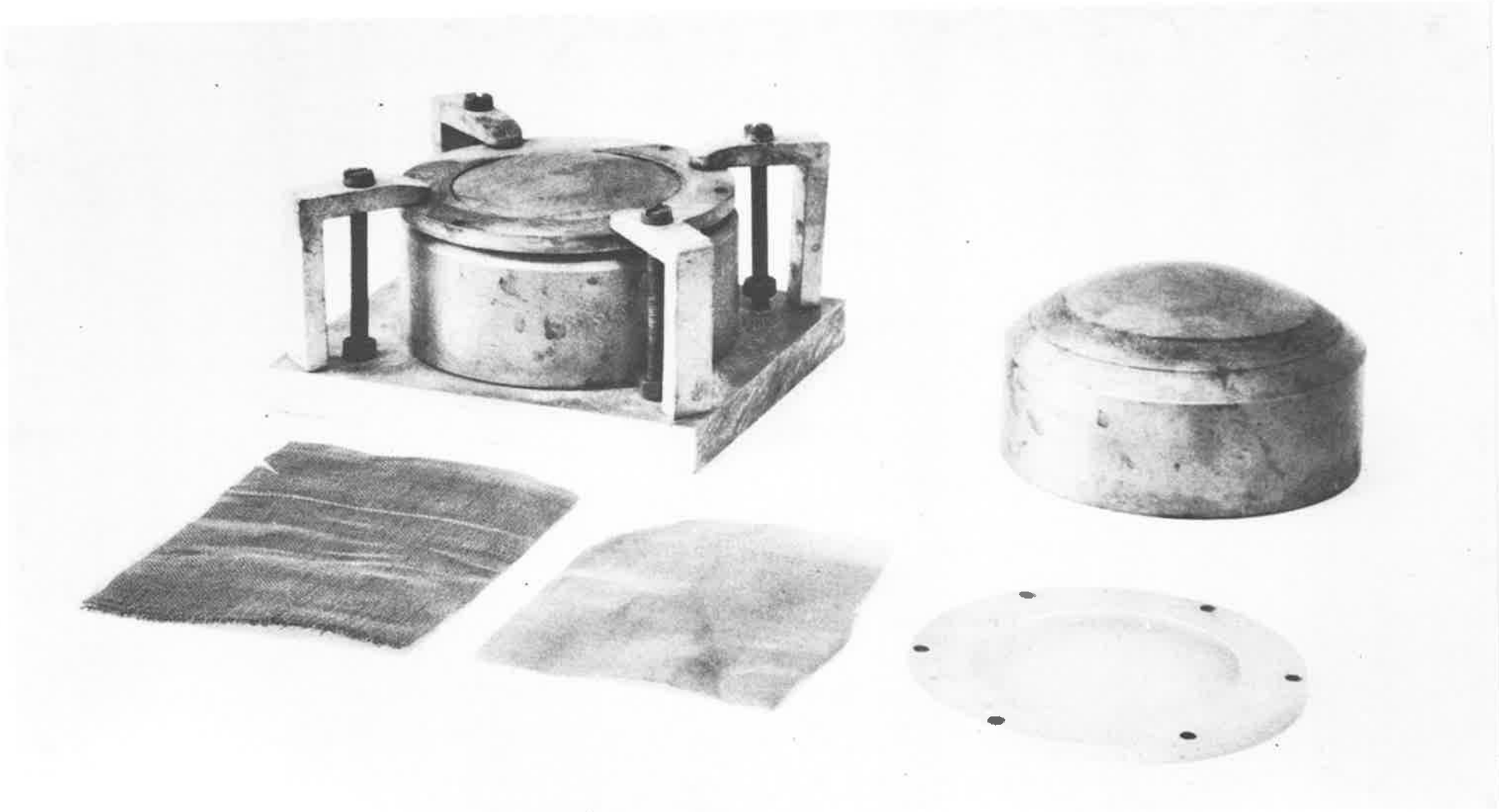

Fig .2.7. Construction of the spherical grids. Shown are samples of the two original mesh materials, the two aluminium mandrels, the method of mounting a grid, and a final plated grid.

2.4.3.3 Photoelectron detector

The individual electrons were detected using a low-resistance channel electron multiplier (Mullard type B419BL). These continuous dynode devices have a gain of the order of 10^8 with a nominal background pulse count rate of less than 2 Hz and an operational rate of very much less than this (less than 0.05 Hz). The channeltron produced negative pulses of less than 20 ns duration. The maximum allowable voltage across the channeltron was 3500 V.

The output of this type of curved multiplier is independent of the ambient pressure provided it does not exceed 5×10^{-4} Torr which was the maximum pressure in the channeltron regions used in any of the experiments for this thesis.

The channeltron was mounted on a Teflon block.

2.4.4 Operation of the Spectrometer

2.4.4.1 Applied Voltages

The earth grid was connected to ground via a wire joined to the rear of the analyser and hence onto the box containing the analyser.

The retarding potential applied was in the form of a negative staircase with an adjustable step size and duration (LINDEMANS, 1981). The smallest available step size was 2.5 mV and multiples of this up to 10 V were usually used. (Energies of up to 50 V could be obtained by making the step size larger). The output voltage of this supply was measured on a digital voltmeter. The potential was constant to $\pm$ 3 mV which was well within the required accuracy.

Much work was done initially to find voltages for the accelerating and focussing grids which gave maximum count rate and

a flat spectrum which was easy to analyse (see Section 2.4.2). Good results were obtained when the accelerating grid was tied to the retarding grid initially through a battery and variable resistor and finally through a fixed resistor chain so that $V_a = 0.968\ V_r$. This gave a spectrum which was flat to within 3 % for all electron energies up to 10 eV.

At most times the focussing grid was operated at 650 V. The voltage on the front of the channeltron was also found to affect the spectrum and this was set to the same voltage as the focussing grid to give the best results.

The voltage across the channeltron was kept at the maximum of 3500 V, which maximised count rate (Fig. 2.8).

These last three voltages were supplied by commercial, regulated power packs.

2.4.4.2 Gas, Pressure and Purity

The chamber which contained the analyser was divided into two sections by a flange with an 'O' ring seal between the vacuum chamber and the analyser (see Fig. 2.5 and 2.6). This seal was sprayed with a Teflon based lubricant to prevent tension between the 'O' ring and the walls causing distortion of the grids which would otherwise have lowered the electron count rate and affected the resolution.

This seal was designed to maintain a pressure differential between the ionization region into which the sample gas flowed and the analyser region which was pumped by one of the 15 cm oil diffusion pumps(pump B, Fig. 2.3). This arrangement allowed a higher sample gas pressure in the ionization region (up to 5×10^{-3} Torr) while the pressure in the analyser region was low enough to avoid degradation of the resolution by electron scattering (see Section 2.4.3.1) and to allow operation of the channeltron (below

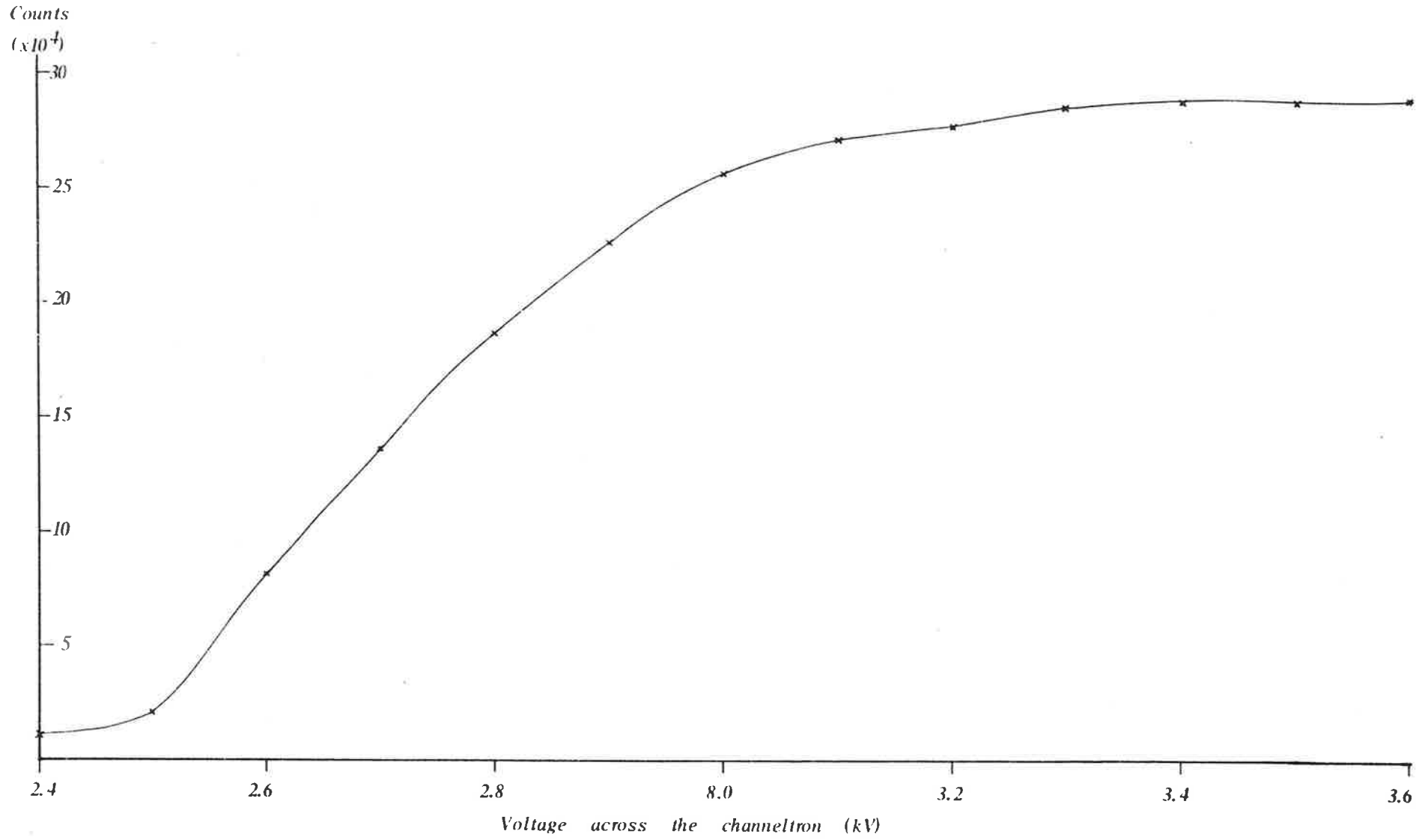

Fig. 2.8. Variation of counts as the voltage across the channeltron is increased.

5×10^{-4} Torr).

Gases entered the ionization region via two needle valves and a narrow pipe (Fig. 2.3). The needle valves produced good gas control and allowed a stable pressure to be maintained in the ionization region. In order to check for any pressure fluctuations, the pressure of the gas in the ionization region was monitored by a Pirani gauge, the output of which went to a chart recorder. Any spectra recorded for which the pressure variation was greater than 1 % in one scan were discarded.

An ionization gauge was used to measure the pressure in the analyser region. The gauge was switched off while recording data to prevent electrons from the gauge being counted as well as phtotelectrons.

The sample gases, supplied by Commonwealth Industrial Gases, were Argon (welding grade), Oxygen (medical grade), Xenon and Krypton (research grade). These were all 99 % pure or better. To purify them even more, they were passed through a cold trap. This trap consisted of a glass cold finger, filled with glass beads, which was kept at a temperature of about $-40^{\circ}C$ by a mixture of carbontetrachloride and chloroform, cooled to its freezing point. This trapped any substance with a boiling point above $-40^{\circ}C$ but allowed the sample gases to pass through (eg. boiling point of Oxygen is $-183^{\circ}C$, of Xenon is $-107^{\circ}C$).

2.4.4.3 Recording Spectra

Electrons, which were detected by the channeltron, produced negative 30 mV, 20 ns pulses at the output of the channeltron. These pulses passed into a fast amplifier which incorporated a discriminator. The discriminator level was adjusted to eliminate noise pules from the lamp and other sources.

The output from the amplifier went into an expander.

This device used up-down counters to produce a train of pulses with the same average frequency as the signal, but with a minimum pulse separation of 4 μs. This was the separation needed before the storage system would register individual pulses.

The storage system was a RIDL multi-channel store (model number 34-12b). The number of channels which could be selected for each spectrum was either 100, 200 or 400. The number of channels was usually chosen so that one channel corresponded to an energy increment small compared to the energy resolution of the analyser.

Each spectrum was recorded with multiple scans to prevent errors caused by long-term pressure drifts. The time for each scan was usually between one and two minutes.

The system also had the facility to allow for scanning of the wavelength by a monochromator drive which advanced the monochromator as the channel number and retarding potential were increased. This permitted the investigation of the variation of partial cross-sections with wavelength.

2.4.4.4 Light Intensity fluctuations

Figure 2.3 shows the position of the photomultiplier with sodium salicylate on the window, which was used to monitor the light intensity. In order to eliminate light fluctuation effects, the output from the photomultiplier went to a current controlled oscillator whose frequency was used to determine the time spent accumulating photoelectron counts in each channel. The higher the light intensity, the shorter the time spent at that partiuclar voltage.

2.4.5 Performance of the Spectrometer

In this section the performance of the analyser will be reviewed with reference to typical xenon spectra at 58.4 nm (Fig. 2.9(a) - (d)). The various characteristics of the spectra, the factors affecting the resolution, shape and background count as well as steps taken to produce optimal spectra will be discussed. The important features to note are the good resolution, the "flatness" of the spectra (see Section 2.4.2) and the low background count.

2.4.5.1 Resolution

From the spectrum (Fig. 2.9(d)), the experimental full width half maxima (FWHM) resolution is found to be 40 meV. This resolution is determined by -

a) the residual magnetic field inside the analyser
b) the size of the aperture
c) the photon resolution
d) the finite spacing of the grids
e) any large scale distortion in the grids
f) non-concentricity of the grids
g) contact potentials and
h) surface contamination.

a) Residual magnetic fields

The initial poor resolution of the analyser, caused by magnetic fields inside the analyser, was overcome by using magnetic shielding alloys. Two layers of Conetic and then an outer layer of Netic were placed on the outside of the chamber and pumping ports (Fig. 2.3). Another precaution taken was the use of only non-ferromagnetic materials inside the chamber. A five times improvement in resolution was obtained by these methods.

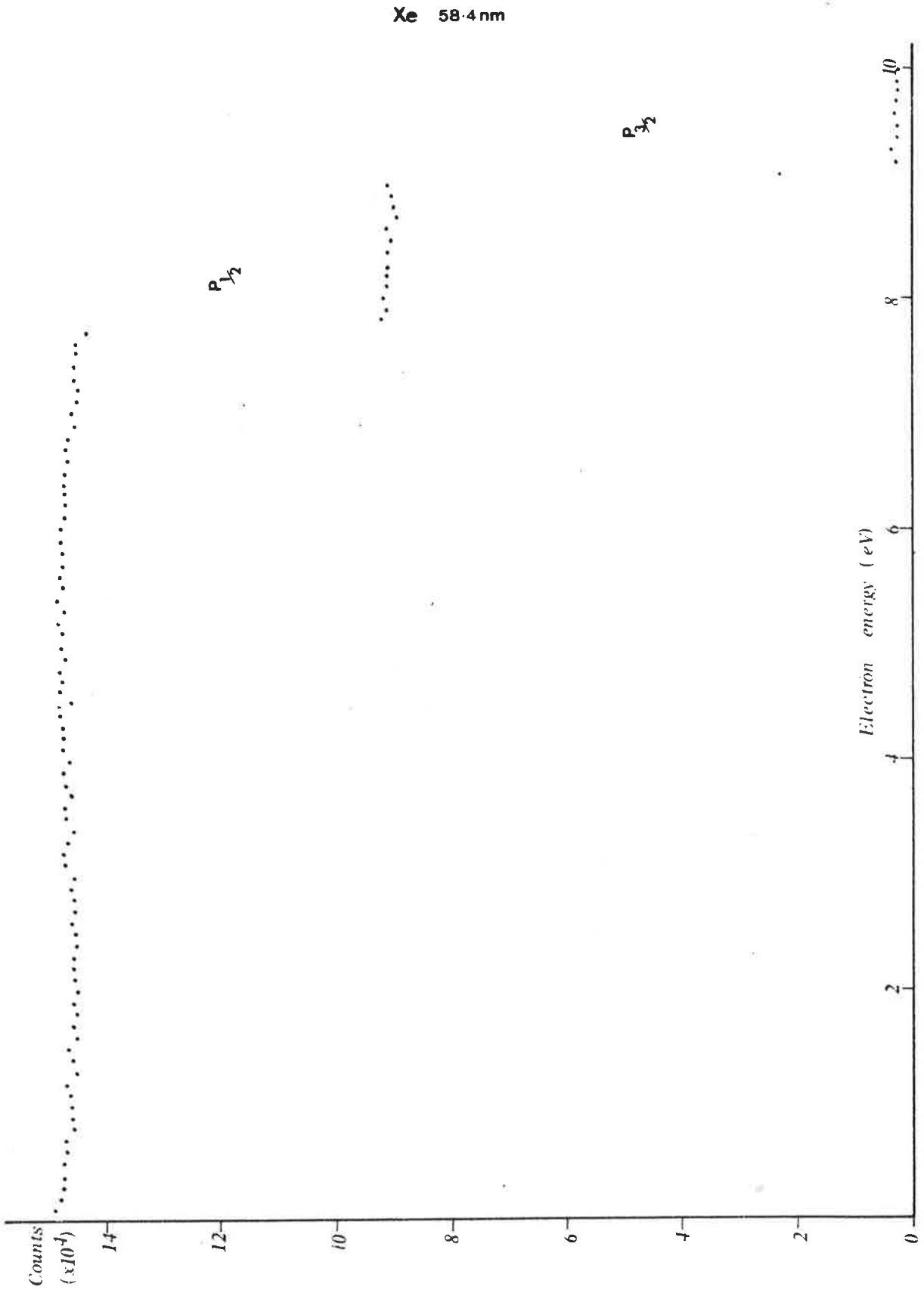

Fig. 2.9a). Total photoelectron spectrum of Xenon at 58.4 nm.

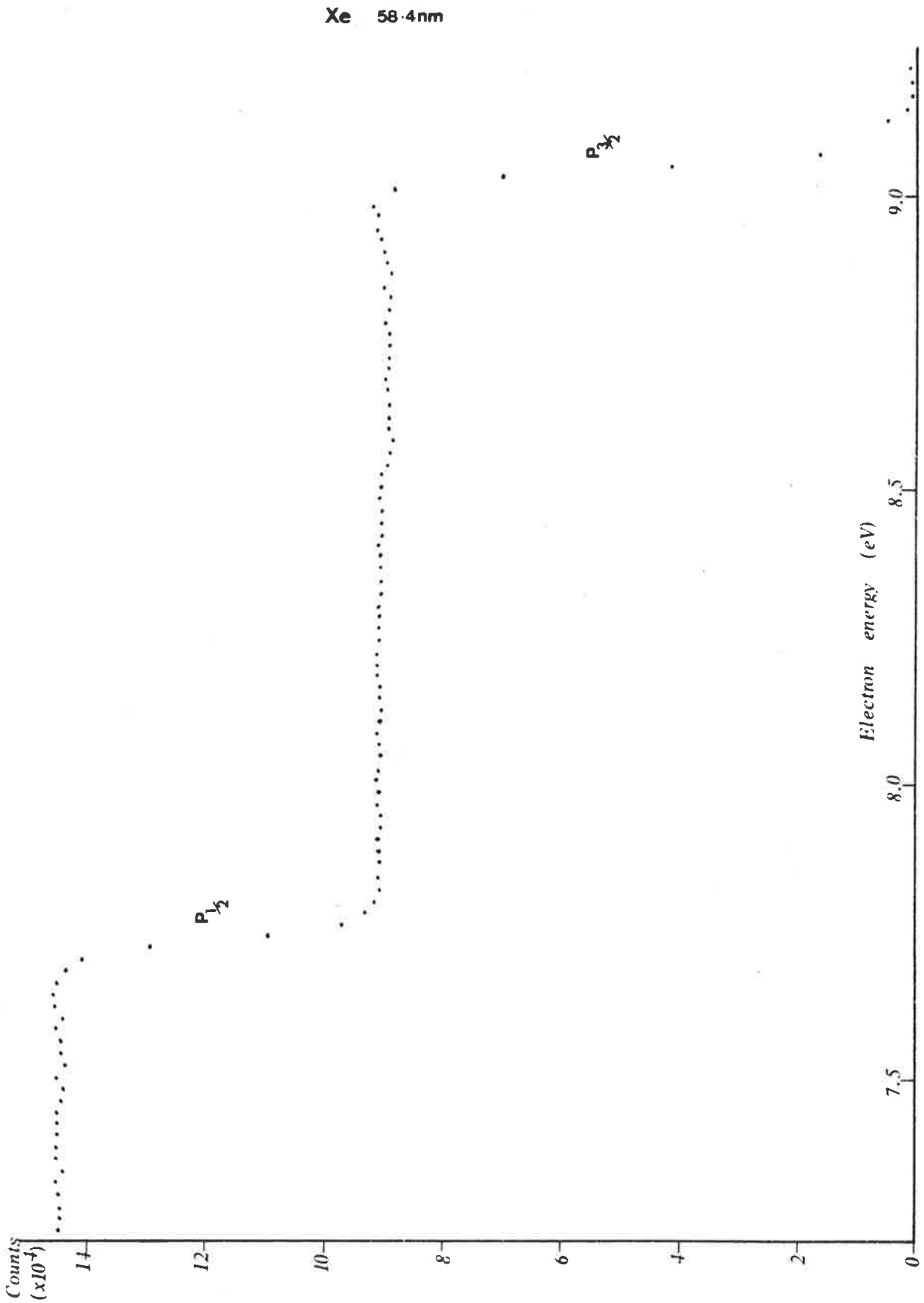

Fig. 2.9b). Photoelectron spectrum of the $^2P_{1/2}$ and $^2P_{3/2}$ states of Xenon at 58.4 nm.

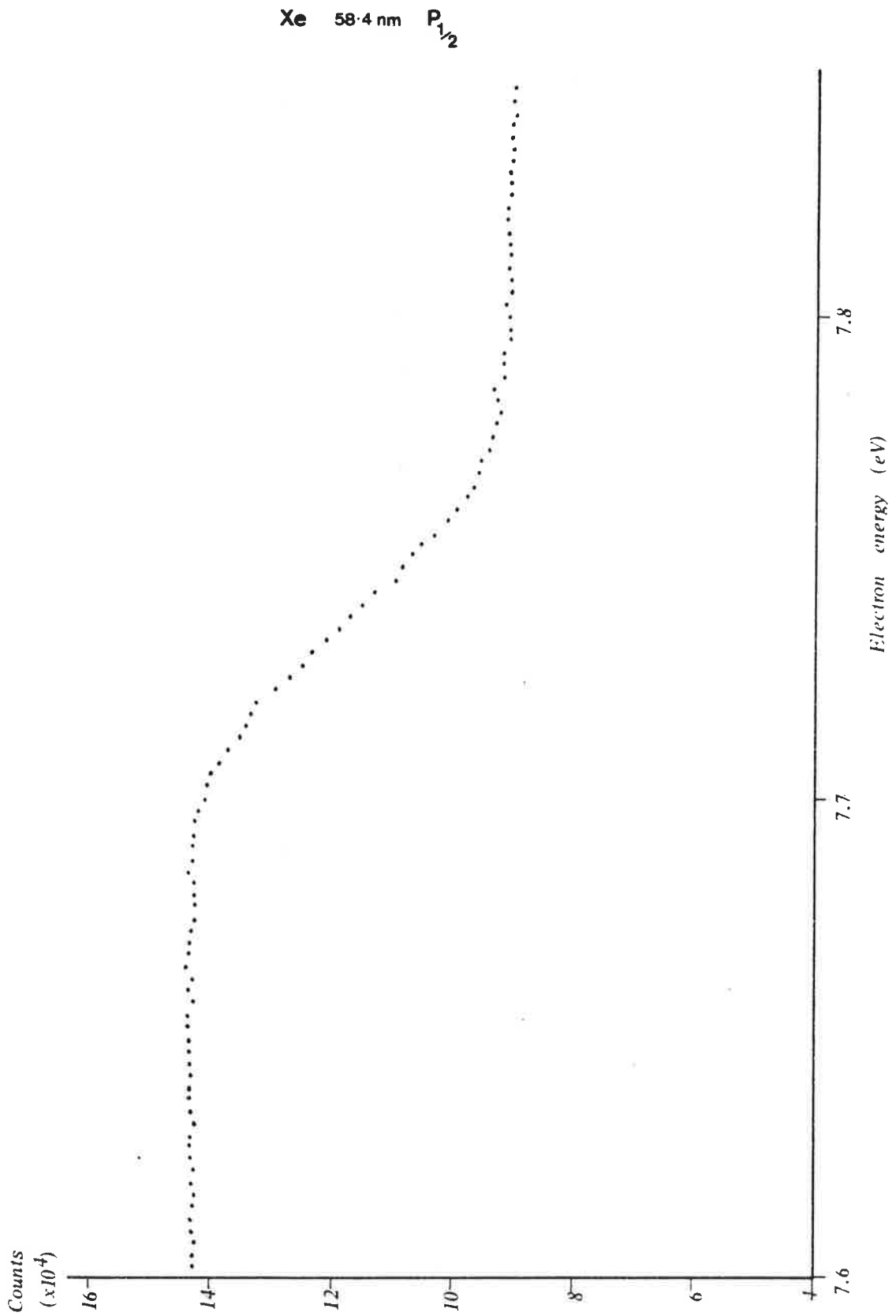

Fig. 2.9c). Photoelectron spectrum of the $^2P_{1/2}$ state of Xenon at 58.4 nm.

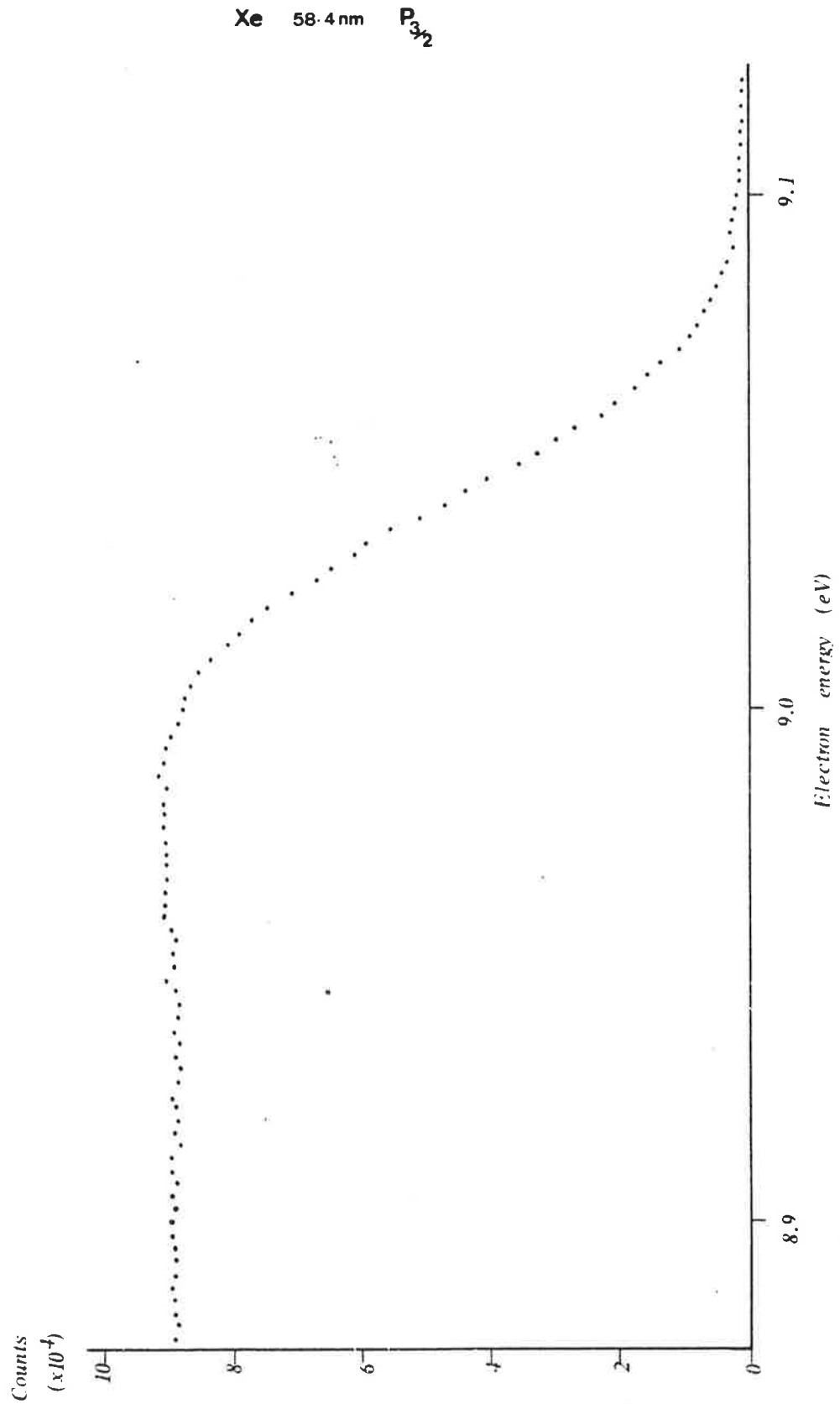

Fig. 2.9d). Photoelectron spectrum of the $^2P_{3/2}$ state of Xenon at 58,4 nm.

The residual magnetic field inside the chamber was measured to be 9×10^{-6} Tesla. According to HUTCHITAL and RIGDEN (1972), this would give a maximum resolution of about 30 meV. This resolution is independent of the electron energy. The magnetic field would also retard photoelectrons by a further 20 meV.

b) Size of the aperture

The resolution due to the finite size of the inlet aperture (1/8") was calculated on the geometry of the figure to be 0.06 % of the energy of the electron. Thus, at 58.4 nm, the resolution of 9 eV Xenon electrons would be about 5 meV.

c) Photon resolution

When the ultra-violet radiation is produced by exciting a resonance line of the lamp gas, the photon resolution is determined by the line width. For Helium at 58.4 nm this width is 5 meV. For other wavelengths, the resolution due to the spread of the light from the monochromator depended on the size of the entrance and exit slits e.g. when both were set at 100 μm, the wavelength resolution was about 0.1 nm. For the oxygen autoionizing lines of interest to this thesis at about 80.0 nm, this is equivalent to an energy resolution of 19 meV.

d) Finite spacing of the grids

Fine wire mesh with a wire spacing of 0.2 mm was used for the retarding and the accelerating grids to minimize the effects of field penetration. These effects contribute about 0.2 % to the energy resolution of the present analyser (HUTCHITAL and RIGDEN, 1972), or about 18 meV for Xenon at 58.4 nm.

e) Large scale distortion of the grids

As the grids were carefully made over a mould, it was felt that this factor did not make a significant contribution to the resolution of the analyser.

f) Non-concentricity of the grids

Careful machining and measuring of the height of the spacers holding the grids apart and the choice of a non-compressible nylon minimised this effect on the resolution (see Section 2.4.3.2).

g) Contact potentials and h) surface contamination

As discussed previously (Section 2.4.3.2), contact potentials were minimised by gold plating the analyser. Thorough cleaning removed surface contamination and hence diminished contact potentials as well.

An estimate of the theoretical minimum full width half maximum (FWHM) resolution R of Xenon at 58.4 nm is therefore -

$$R \sim (30^2 + 5^2 + 5^2 + 18^2)^{-\frac{1}{2}}$$

$$\sim 36 \text{ meV}$$

This can be compared with the FWHM experimental resolution in Figure 2.9 a) which is about 40 meV.

2.4.5.2 Cleanliness

Thorough cleanliness was essential. In early runs it was found that if a pumping accident occurred and oil contaminated the analyser, the apparent energy of the transitions of the spectra was shifted by up to 60 meV and the resolution degraded to 100 meV. A similar but gradual shift in energy of the spectra with time during normal operation of the apparatus also caused some initial concern.

These problems seemed to be overcome by thoroughly cleaning the analyser and chamber to remove any surface contamination which would cause space charging or inhomogenities in potentials. This was achieved by removing all the parts of the chamber and pumping ports and vapour degreasing them in a bath of AR grade trichloroethylene initially, followed by isopropyl alcohol. The analyser itself was taken apart and cleaned in an ultra sonic bath

as well as in the vapour degreasing bath.

Whenever a test run showed that the energy of a spectrum had shifted substantially, the analyser was again vapour degreased and the inside of the chamber was wiped clean. This ensured that the system was stable during runs and that maximum resolution was obtained (see Section 2.4.5.1).

2.4.5.3 Background Count

Electrons and photons scattered off the walls of the chamber as well as electrons from impurity gases contribute to the background count. Scattered electrons and photons were minimized by the use of aluminium honeycomb placed in front of the analyser (see Fig. 2.5) and impurities reduced by the cold trap (see Section 2.4.4.2).

By running a spectrum with no gas in the system, it was found that photoelectrons from the metals of the system contributed to the background. These could not be eliminated.

As would be expected, the background count increased with increase in gas pressure. It was only really significant for gases with low electron production cross-sections.

2.4.5.4 Linearity of count rate

a) Count rate vs Light intensity

The linearity of the system with increasing light intensity was tested by recording the number of electrons counted per second for the $^2P_{½} + {}^2P_{3/2}$ state of Argon at 58.4 nm and plotting this count rate against the current controlled oscillator frequency which is directly proportional to the light intensity (Section 2.4.4.4), (Fig. 2.10). The greatest deviation from the mid point was 2 % over a range of nearly 7,000 counts/second.

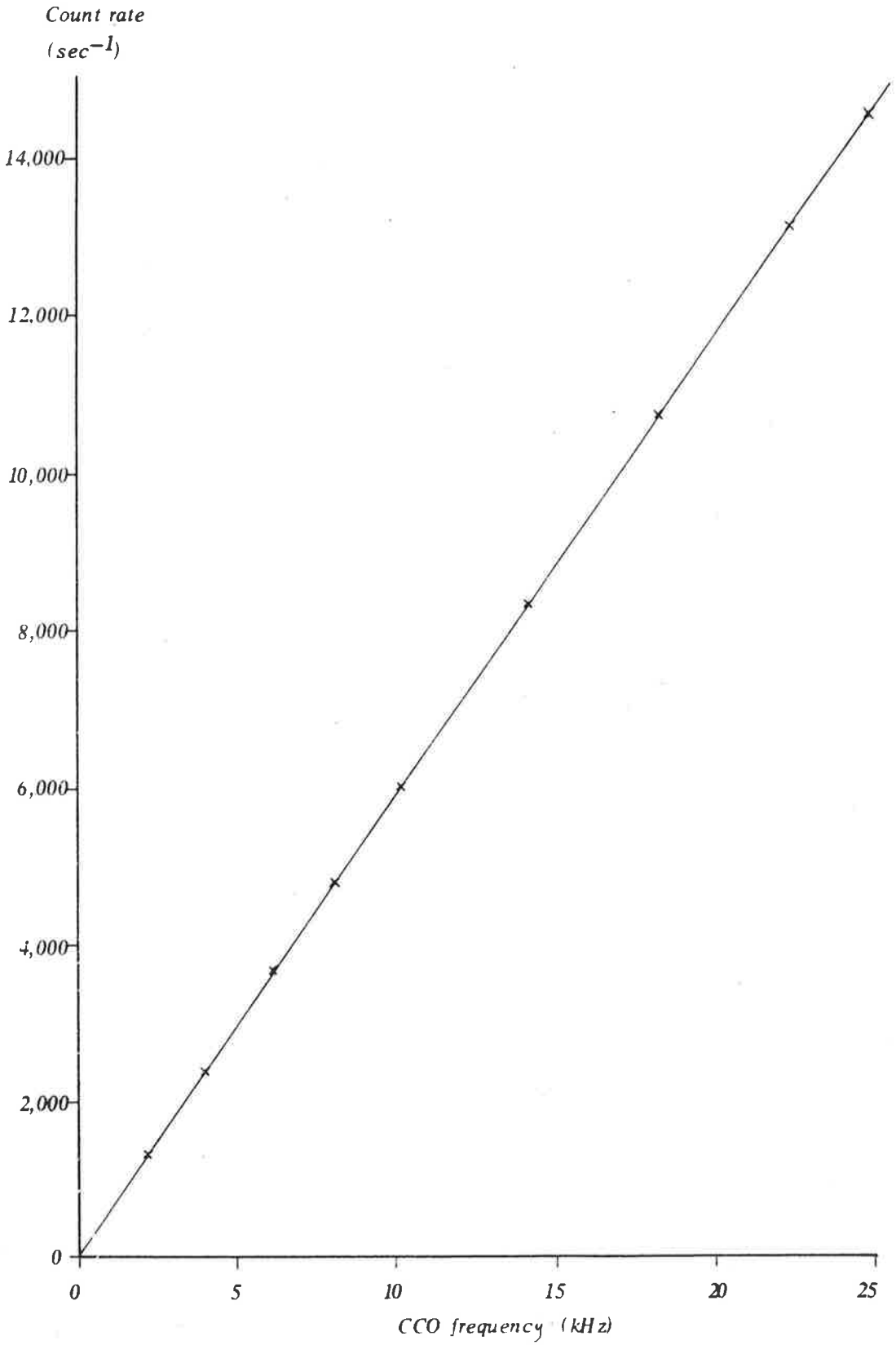

Fig. 2.10. Linearity of count rate versus light intensity.

b) Count rate vs Pressure

To investigate this, the ratio of the number of electrons produced by the $^2P_{½}$ state of Argon to the number of electrons produced by the $^2P_{3/2}$ state at 58.4 nm was calculated as the pressure was varied from 10^{-4} Torr to 10^{-3} Torr. The ratio varied by about 2 % indicating that the system was linear with pressure.

During normal operation, as pressure was monitored throughout scans, there would be no great variation in pressure and hence the count rate would not be affected.

2.4.5.5 Efficiency of the Spectrometer

The spectrometer described above does not collect electrons of different energy with the same efficiency. To be able to accurately calculate the true number of electrons produced at a particular energy, it is necessary to know how the efficiency of the spectrometer varies with electron energy.

In order to calculate the efficiency, Xenon spectra were run at the wavelengths and electron energies shown in Table 2.1. Argon spectra were also recorded up to electron energies of 3 eV.

Table 2.1 Xenon spectra for efficiency data

(nm)	101.4	99.6	99.0	97.8	97.2	96.4	95.0	93.8
E_{el}(eV)	0.097	0.318	0.394	0.547	0.626	0.732	0.921	1.09

As the gas pressures were not all the same for these spectra, scaling factors were needed. These were found by counting one equivalent point on each spectra at each wavelength while the gas pressure was kept constant. Background counts were also taken at wavelengths of 99.0 and 97.2 nm.

Because the absorption cross-sections of Xenon and Argon vary with wavelength, the number of counts from the photomultiplier at each wavelength was measured with and without gas in the system and hence the percentage absorption was calculated.

The number of electrons collected at each wavelength is proportional to the photoionization cross-section at that wavelength multiplied by the efficiency of the spectrometer. For rare gases, the photoionization cross-section is proportional to the absorption cross-section. Hence the efficiency of the analyser could be found by dividing the number of electrons counted at each wavelength by the absorption cross-section at that wavelength.

The results obtained by this method were unreliable due to fluctuations in lamp intensity which varied with lamp pressure and time. These caused large errors in the absorption data as the lamp intensity could not be assumed to be the same for the spectra obtained with and without the sample gas. When computed from these results, the efficiency of the analyser appeared to be constant, within the errors of the data, for electron energies greater than 100 meV and tended to zero at 0 eV. Subsequent measurements confirmed this (LINDEMANS et al, 1979; Appendix 3). This excellent characteristic allows for direct comparison of spectra by eye and also means that large errors due to rapid variation do not occur, and hence a more accurate efficiency correction can be made.

CHAPTER 3. DISCUSSION AND ANALYSIS OF RESULTS

INTRODUCTION

Chapter 2 contained a discussion of the characteristics and performance of the apparatus and in this chapter, results taken when the system was finally optimized are presented.

The method of analysis of these results is described in Section 3.1 and the results of this analysis are discussed in Section 3.2.

3.1 CURVE-FITTING

The simplest method of analysing the results makes use of the fact that the spectra recorded are fairly "flat" (see Sections 2.4.2 and 2.4.5 and Fig. 2.9 (a)). To a first approximation, therefore, branching ratios can be measured by firstly correcting for analyser efficiency and then by averaging over the flat parts of the spectra and subtracting the two averages to obtain a "step height". This is the procudure used for most of the analysis in this thesis.

The main difficulty involved in this method is estimating which points really do lie on the flat part. The way in which this was done is as follows.

Firstly an approximation to the step height of the most intense transition was made by ruling a line through an average value of the flat parts on either side of the step. As this average had to be guessed at by eye, the first inaccuracy arises. The position of the most intense transition was then taken at half this approximate step height. This method typically involved an error of about $\pm$ 1 channels, which corresponded to an energy of between 2.5 mV (e.g. Fig. 2.9 (c)) or 100 mV (Fig. 2.9 (a)). The positions of the "peaks" of the other transitions were then calculated from energy spacings in the literature.

Having established these positions, the next step was to decide which points lay on the "flat" part. The method adopted was to move to a new point which was up the step and away from the peak position by a number of channels which corresponded to approximately twice the F.W.H.M. resolution. The channel found in this way (channel A) was used as one of the points on the flat part. To find the others, the procedure was repeated but this time down the previous step. The number of photoelectron counts in the channel reached this time plus the counts from the points between this channel and channel A were then used to find the average count. This was repeated for all the flat parts and the step heights were found by subtracting these averages from either side of the peak.

Apart from the inaccuracy involved in finding the peak positions and the uncertainty in knowing if all the points used really are on the flat part, this method does not use all the data available. A more sophisticated technique with greater accuracy and which also makes full use of all the recorded data is needed, especially to analyse the oxygen autoionization data (Figs. 3.12 - 3.18) in which the higher vibrational levels cannot be fitted well by eye. These levels are the ones which are populated only on resonance and hence are of greatest interest. The count rate at these resonances is low and long data collecting periods are needed to provide enough counts to enable the vibrational transition intensities to be measured with sufficient accuracy to allow comparison with theory. To reduce the errors in the analysis and to make sure that some of the data collected is not wasted (as it is in the analysis by hand), a computer program to perform curve fitting was undertaken. Although the program was not developed to the stage where it could be used to analyse the results in this thesis, the curve fitting method will be described.

The first step, after correcting for analyser efficiency,

is to remove the background. This is done by recording a spectrum with no sample gas in the system and then subtracting this from the spectrum obtained when the gas is present.

The next step is to determine standard line shapes for monochromatic electrons of different energies. Table 3.1 shows the type of spectra recorded, together with the electron energies. The actual spectra are contained in Appendix 1.

Table 3.1 Standard Line Shapes

Gas	State	(nm)	E_{el}(eV)
Xe	$P_{3/2}$	58.4	9.09
Xe	$P_{1/2}$	58.4	7.78
Kr	$P_{3/2}$	58.4	7.21
Kr	$P_{1/2}$	58.4	6.55
Ar	$P_{3/2}$	58.4	5.46
Ar	$P_{1/2}$	58.4	5.28
Xe	$P_{3/2}$	73.6	4.72
Xe	$P_{1/2}$	73.6	3.41
Kr	$P_{3/2}$	73.6	2.85
Kr	$P_{1/2}$	73.6	2.18
Ar	$P_{3/2}$	73.6	1.09
Ar	$P_{1/2}$	73.6	0.908

Thus lineshapes can be found for electron energies between 0.9 and 9.1 eV. For energies in between these points, the lineshapes must be obtained by interpolation.

Finally, a suitable fitting program is needed to synthesise the measured spectra from these standard profiles. The program must combine these line shapes to produce a statistical best fit to the data. The spectra must be fitted "height-wise" which gives the branching ratios and "energy wise" to provide the position of the peak. To simplify the procedure, the energy spacings

between the different states can be taken from the literature (e.g. NATALIS, 1979 for oxygen) and the program need then only vary one energy.

Such a program is provided by sub-routine CURFIT (BEVINGTON, 1969) which makes a least squares fit to a function using an algorithm of MARQUARDT (1963). This algorithm combines a gradient search with the method of linearizing the fitting function to minimize χ^2, (χ^2 is a measure of the "goodness" of fit and is given by $\chi^2 = \sum_i \left(\frac{1}{\sigma_i^2} (Y_i - Y(x_i))^2 \right)$ where the σ_i are the uncertainty in the data points Y_i and $Y(x_i)$ is the fitting function).

The fitting function to be used in this program is a combination of scaled lineshapes. The parameters A_j, which are to be optimised, are the scaling factors and the energies of the peaks. The method of least squares finds the optimal value of the parameters A_j by minimizing χ^2 with respect to each of the parameters simultaneously by using $\frac{\partial \chi^2}{\partial A_j} = 0$.

When the fitting function is non-linear, as is the case here, χ^2 may be considered to be a continuous function of the n parameters A_j describing a hypersurface in n-dimensional space and the space can be searched for the appropriate minimum value of χ^2. One way of performing this investigation is to use the gradient search method in which the direction of travel in the parameter space is along the gradient of χ^2. To look for the minimum, a search is conducted along the direction of the original gradient in small steps and the value of χ^2 is calculated after each step until χ^2 rises again. The gradient is then recalculated and the search begins again in a new direction. The procedure is then repeated until χ^2 is minimized.

An alternative way of minimizing χ^2 is to expand the fitting function as a function of the parameters A_j by a Taylor's

expansion i.e. $y(x) = y_0(x) + \sum_{j=1} \left(\frac{\partial y}{\partial A_j}(x) \, \delta A_j \right)$

The method of linear least squares can then be used to determine the optimal values for the parameter increments δA_j. In this method, χ^2 is minimized with respect to each of the parameter increments δA_j by setting the derivatives equal to zero.

In Marquardt's routine, the gradient search is used inititially as it approaches the minimum well when for away but is inefficient nearby. The method of linearizing the fitting function converges rapidly to the minimum from points close by and so takes over from the gradient search when the search comes close to the minimum.

3.2 ANALYSIS OF RESULTS

3.2.1 Introduction

Most of the results presented here were analysed by hand as described above. The energy spacings used for oxygen were taken from NATALIS et al (1979) and those for nitrogen from COLLIN and NATALIS (1969). As the analysis is approximate, only general trends will be discussed.

One spectrum (Fig. 3.6) was analysed by a preliminary version of the program described in Section 3.1.

The experimental conditions for each spectrum are contained in Appendix 2. Note that in many of the spectra the position of the peak does not occur at the theoretical energy. This is due to the presence of stray magnetic fields (see Sec. 2.4.5.1) as well as dielectric surface contamination (Sec. 2.4.5.2).

3.2.2 Nitrogen at 58.4nm

Figures 3.1 to 3.4 show spectra of nitrogen taken at 58.4nm. Figure 3.1 is a spectrum over the range from 0v to 6.25 V encompassing the three electronic states of the ion which can be populated at this wavelength.

The difficulties of obtaining accurate measurements at low electron energies due to statistical noise (Sec. 2.4.1) are demonstrated in Figure 3.2 (N_2 $X^1\Sigma^+$ (v'' = 0) $\rightarrow$ N_2^+ $B^2\Sigma^+$ (v' = 0, 1, 2)). It is obvious that the v' = 0 transition is the strongest and that the intensity of the v' = 1 transition is about one tenth of the intensity of the v' = 0 transition but it is not possible to measure the v' = 2 transition intensity.

Figure 3.3 (N_2 $X^1\Sigma^+$ (v'' = 0) $\rightarrow$ N_2^+ $A^2\Pi_u$ (v' 0 to 8)) and Figure 3.4 (N_2 $X\,^1\Sigma^+$ (v'' = 0) $\rightarrow$ N_2 $X^2\Sigma_g$ (v' = 0, 1, 2)) involve electrons of higher energy and have less scatter. Hence these

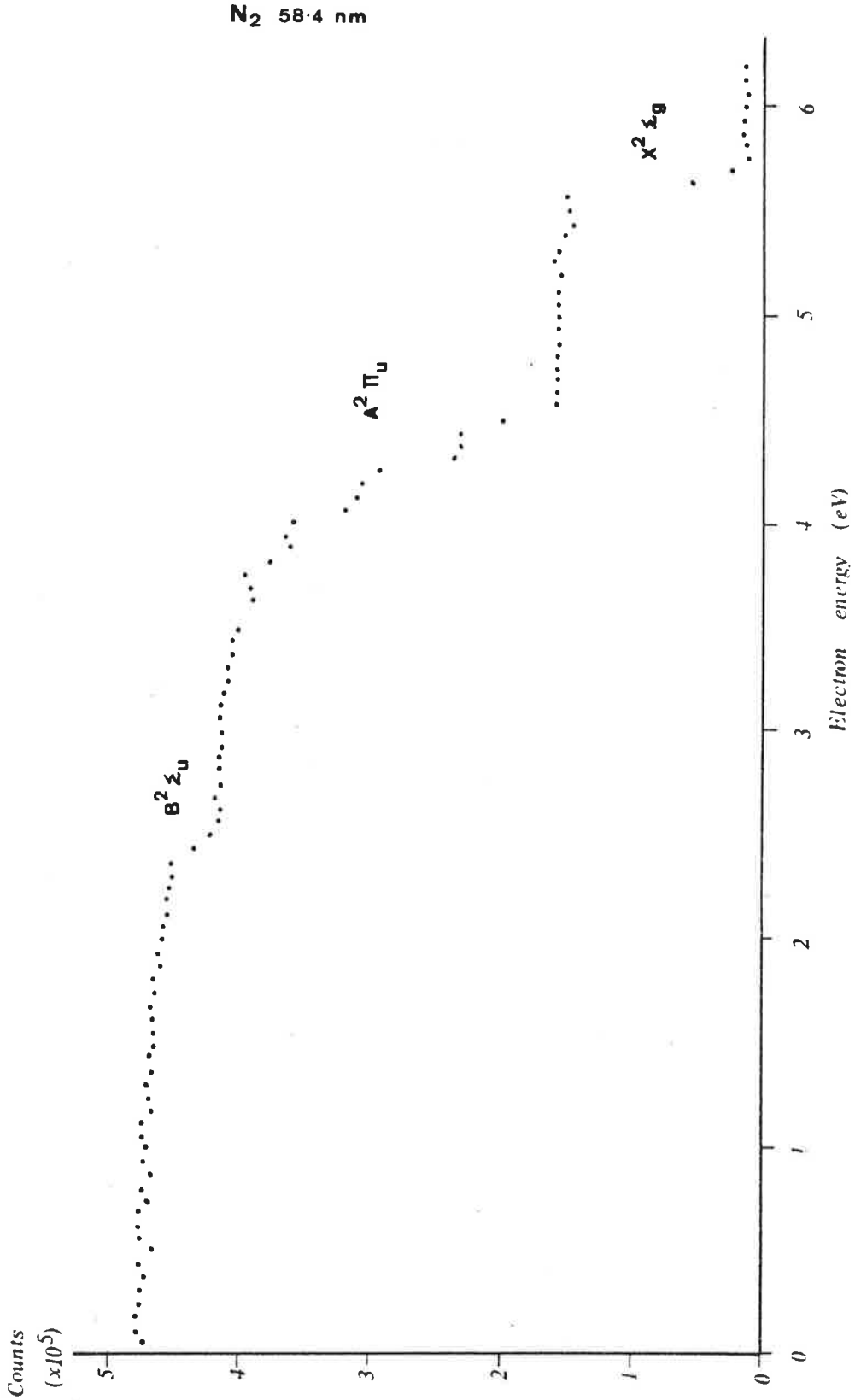

Fig. 3.1. Photoelectron spectrum of nitrogen at 58.4 nm showing all available states of the ion.

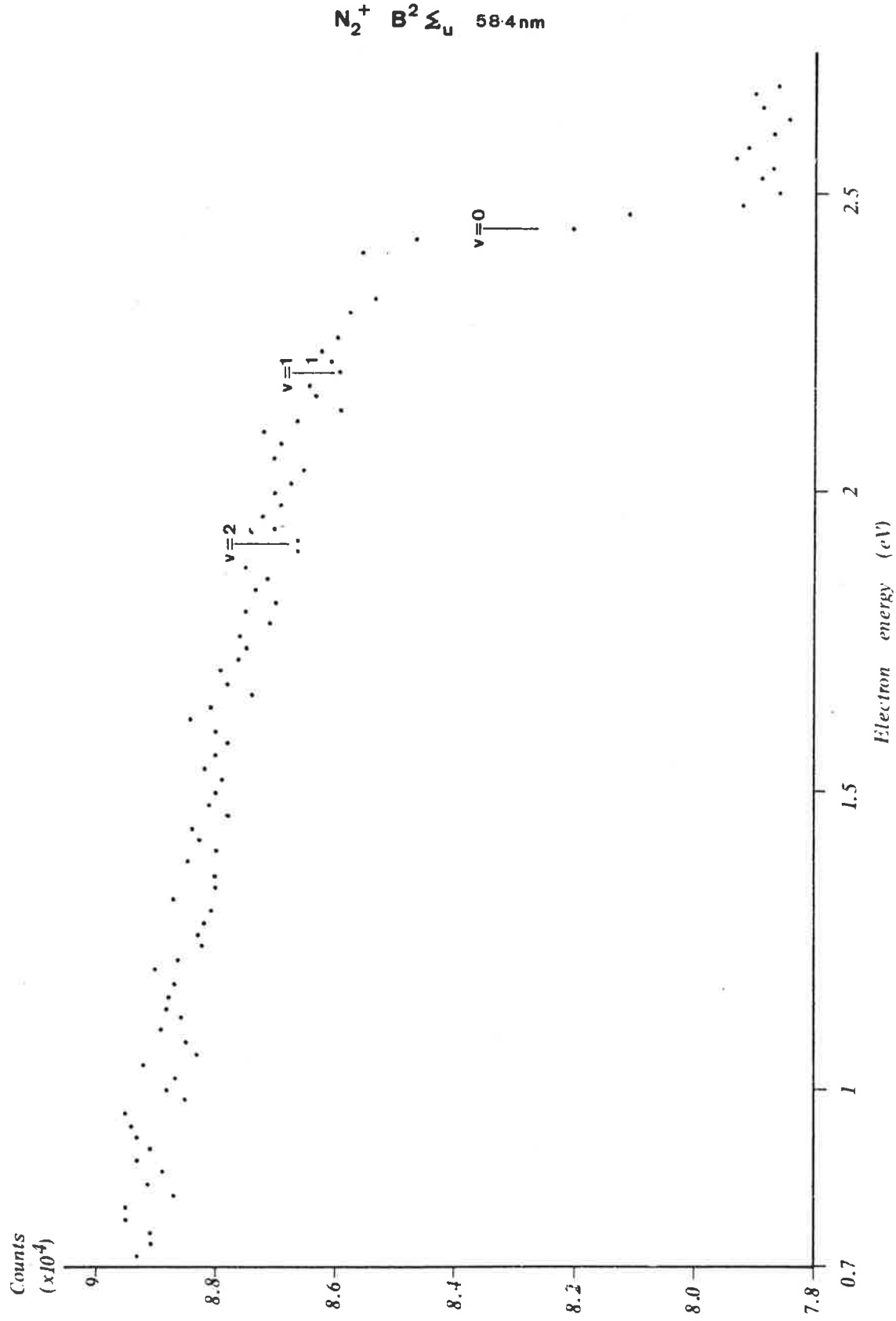

Fig. 3.2. Photoelectron spectrum of the $B^2\Sigma_u$ state of the nitrogen ion at 58.4 nm.

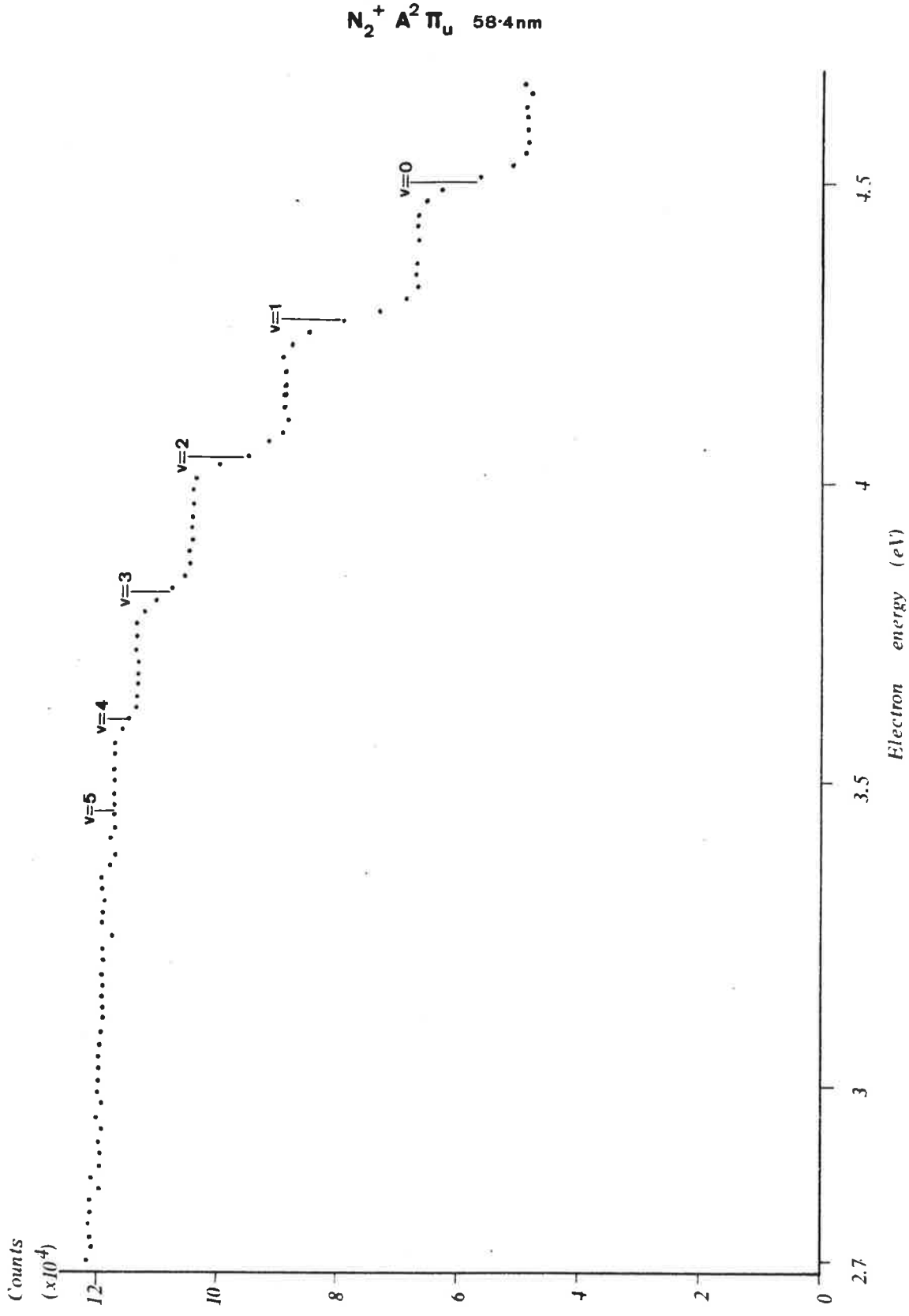

Fig. 3.3. Photoelectron spectrum of the $A^2\Pi_u$ state of the nitrogen ion at 58.4nm.

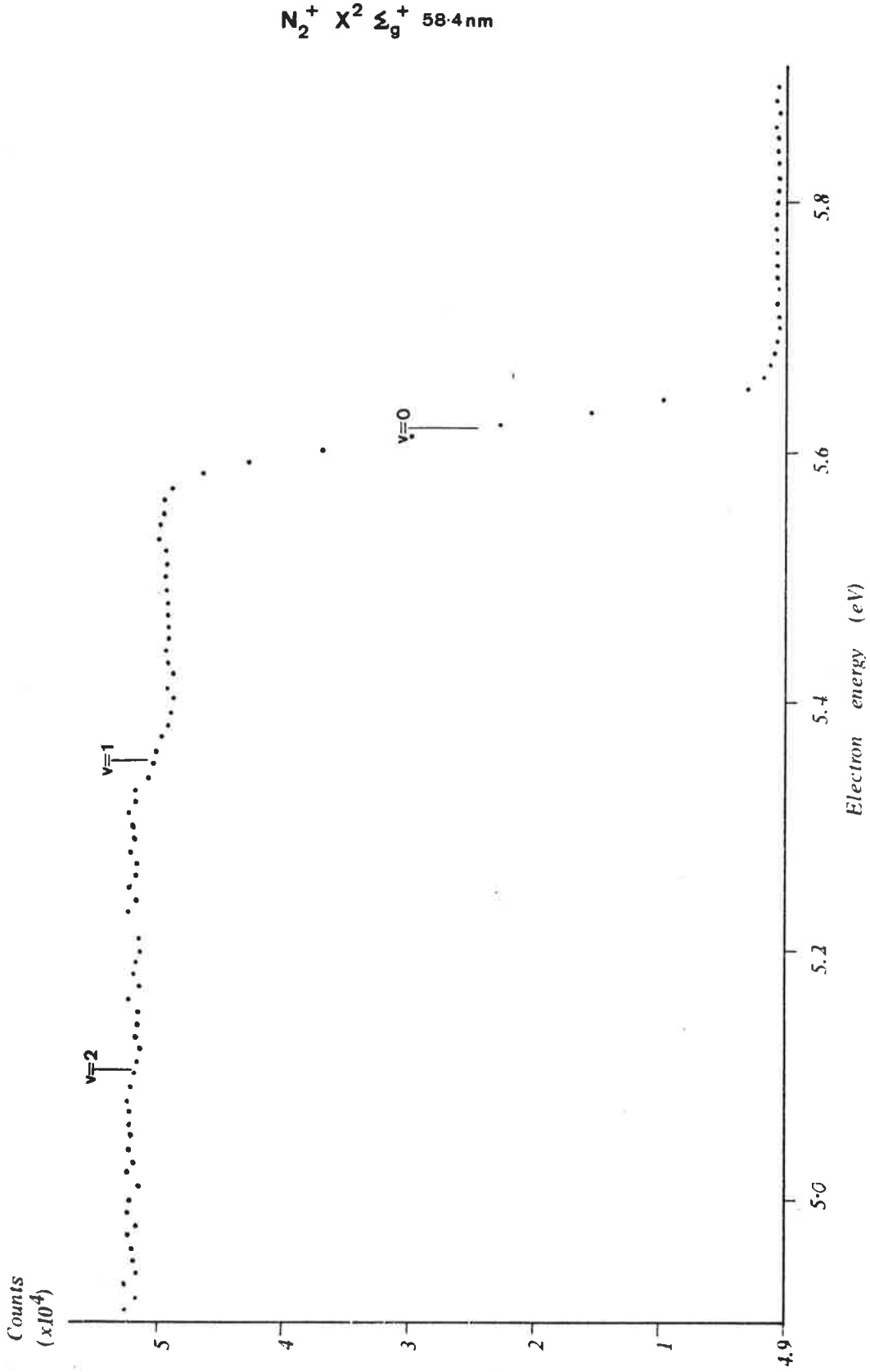

Fig. 3.4. Photoelectron spectrum of the ground state of the Nitrogen ion at 58.4nm.

were able to be analysed by hand. Table 3.2 shows a comparison of the results from this thesis with others from the literature as well as with calculated Franck-Condon factors. The agreement between the present work and other experimental results as well as with Franck-Condon factors is good considering, the accuracy of the analysis method.

Table 3.2 Experimental Vibrational Intensities and FCF for transitions N_2 $X\ ^1\Sigma^+(v" = 0)$ to the ionic levels v' shown

		Experimental Results		FCF (b)
State	v'	Present	(a)	
$A^2\Pi_u$	0	92	87.1 ± 3.1	84.9
	1	100	100.0 ± 2.8	100.0
	2	72	76.3 ± 1.5	68.0
	3	42	43.5 ± 2.9	35.3
	4	16	19.1 ± 2.4	15.7
	5	9	7.09 ± 0.77	6.37
	6	-	2.51 ± 0.40	2.43
	7	-	1.70 ± 0.34	0.89
	8	-	0.37 ± 0.17	0.32
$X^2\Sigma_g^+$	0	100	100.0	
	1	5	9.27	
	2	0.3	0.59	

a) GARDNER and SAMSON (1974a)

b) ALBRITTON et al (from (a))

3.2.3 Oxygen at 58.4nm

Spectra of oxygen recorded at 58.4nm are shown in Figures 3.5 to 3.10. Figure 3.5 is a photoelectron spectrum of the five electronic states of the ion.

Of particular interest to this thesis is Figure 3.6, which shows the transitions from $X^3\Sigma_g^-$ (v" = 0) to the vibrational levels of the $X^2\Pi_g$ state of the ion. Table 3.3 shows the measured

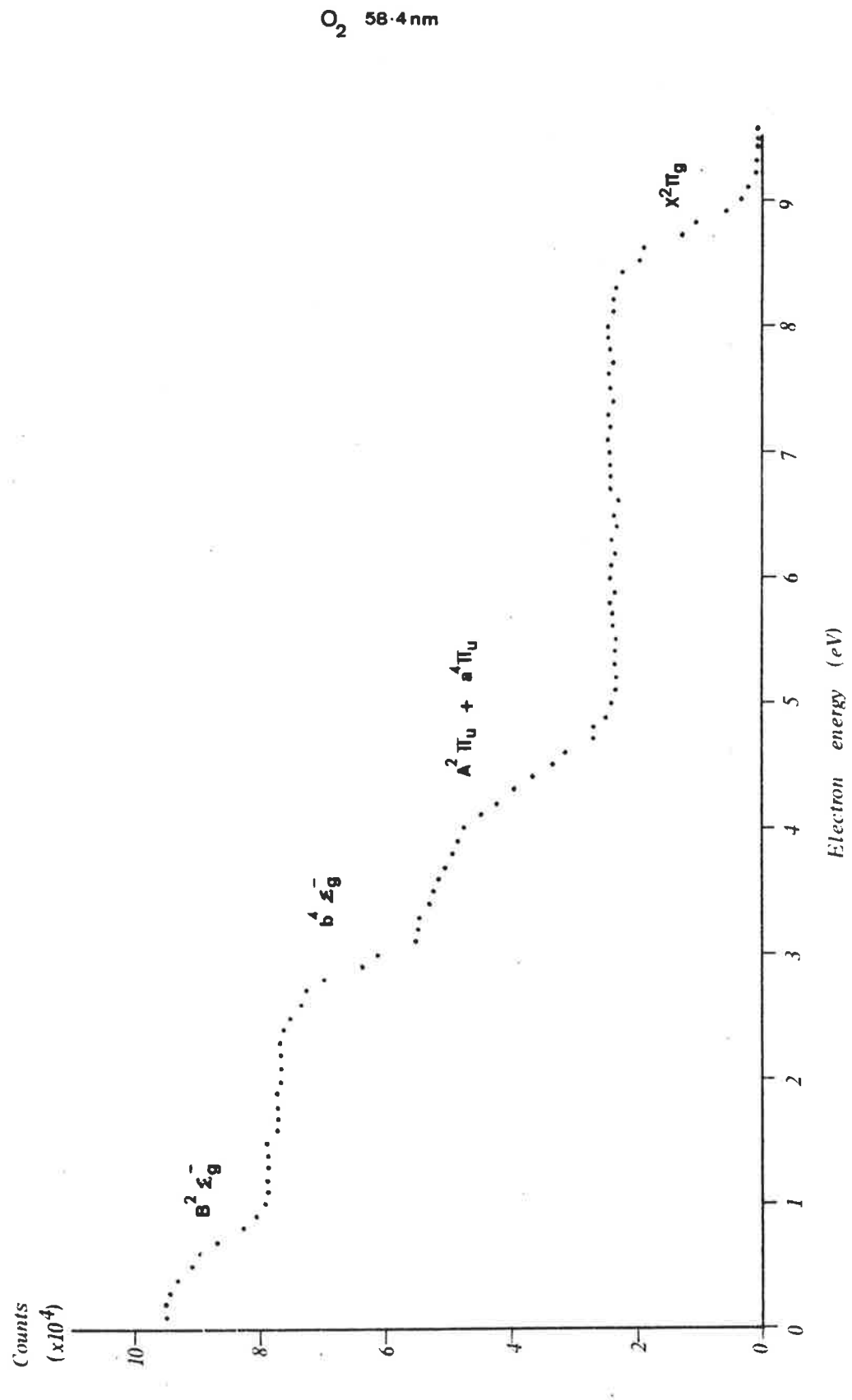

Fig. 3.5. Photoelectron spectrum of Oxygen at 58.4nm showing all available states of the ion.

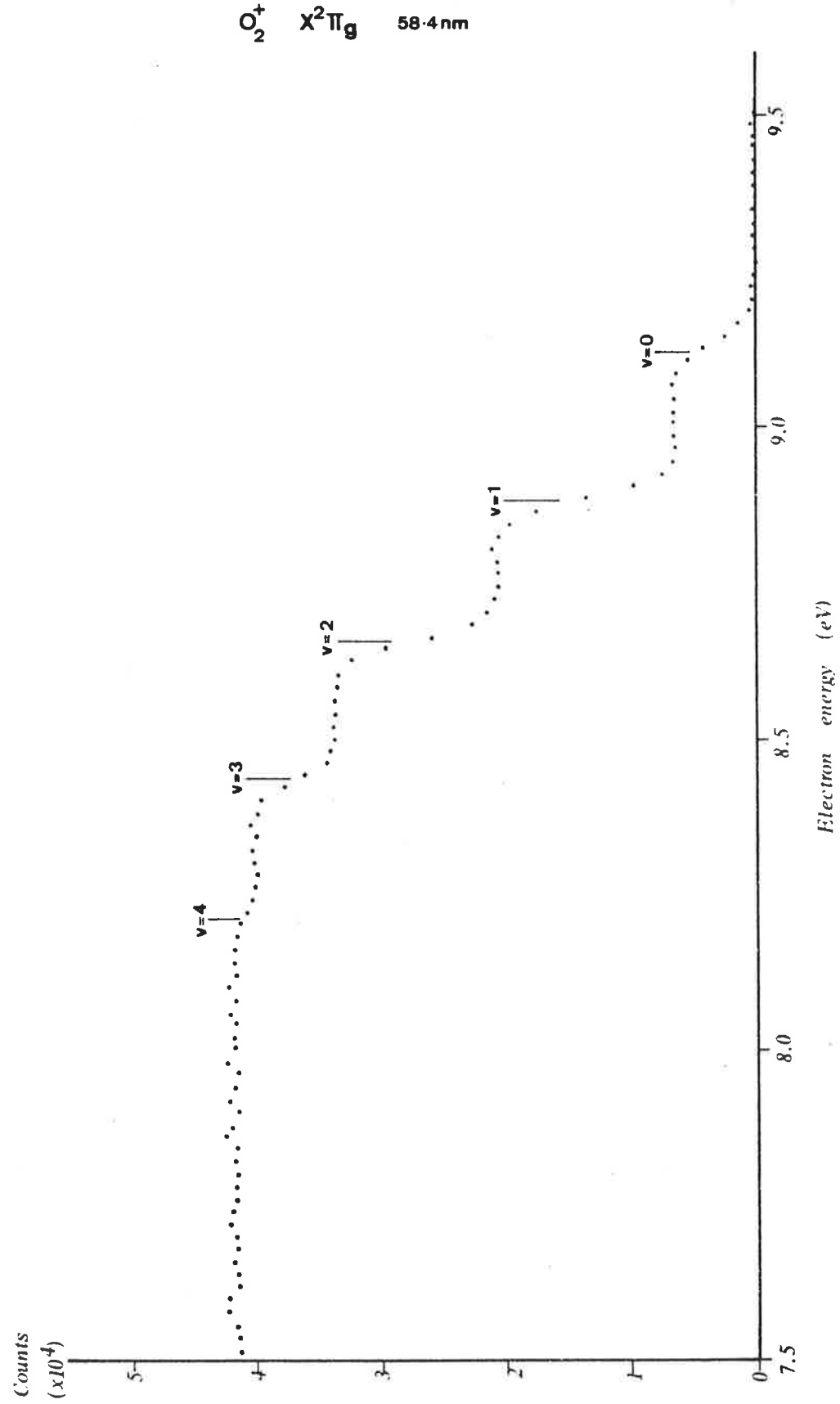

Fig. 3.6. Photoelectron spectrum of the ground state of the Oxygen ion at 58.4nm.

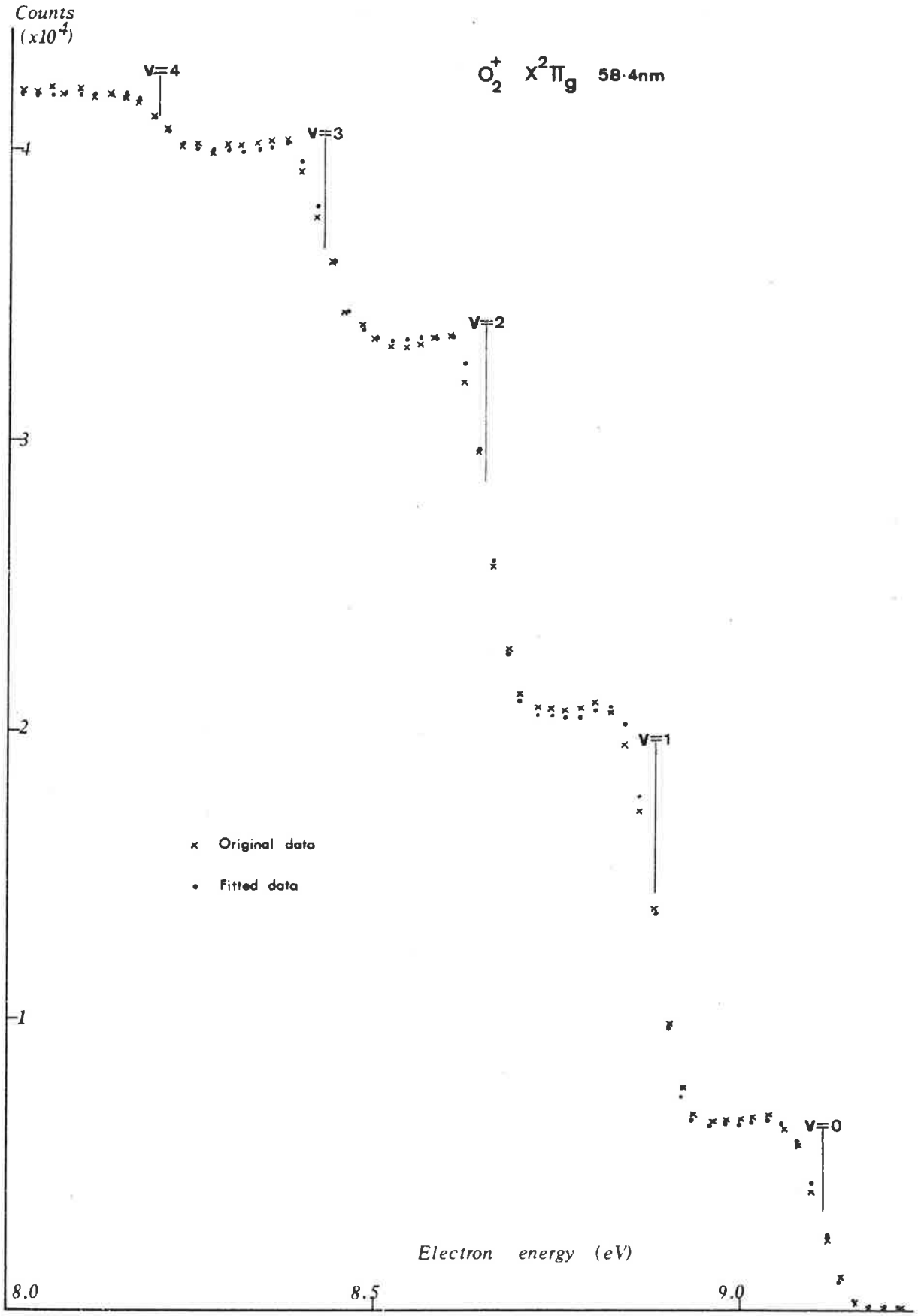

Fig. 3.7. Comparison of the fitted and raw data for the photoelectron spectrum of the ground state of the Oxygen ion at 58.4nm.

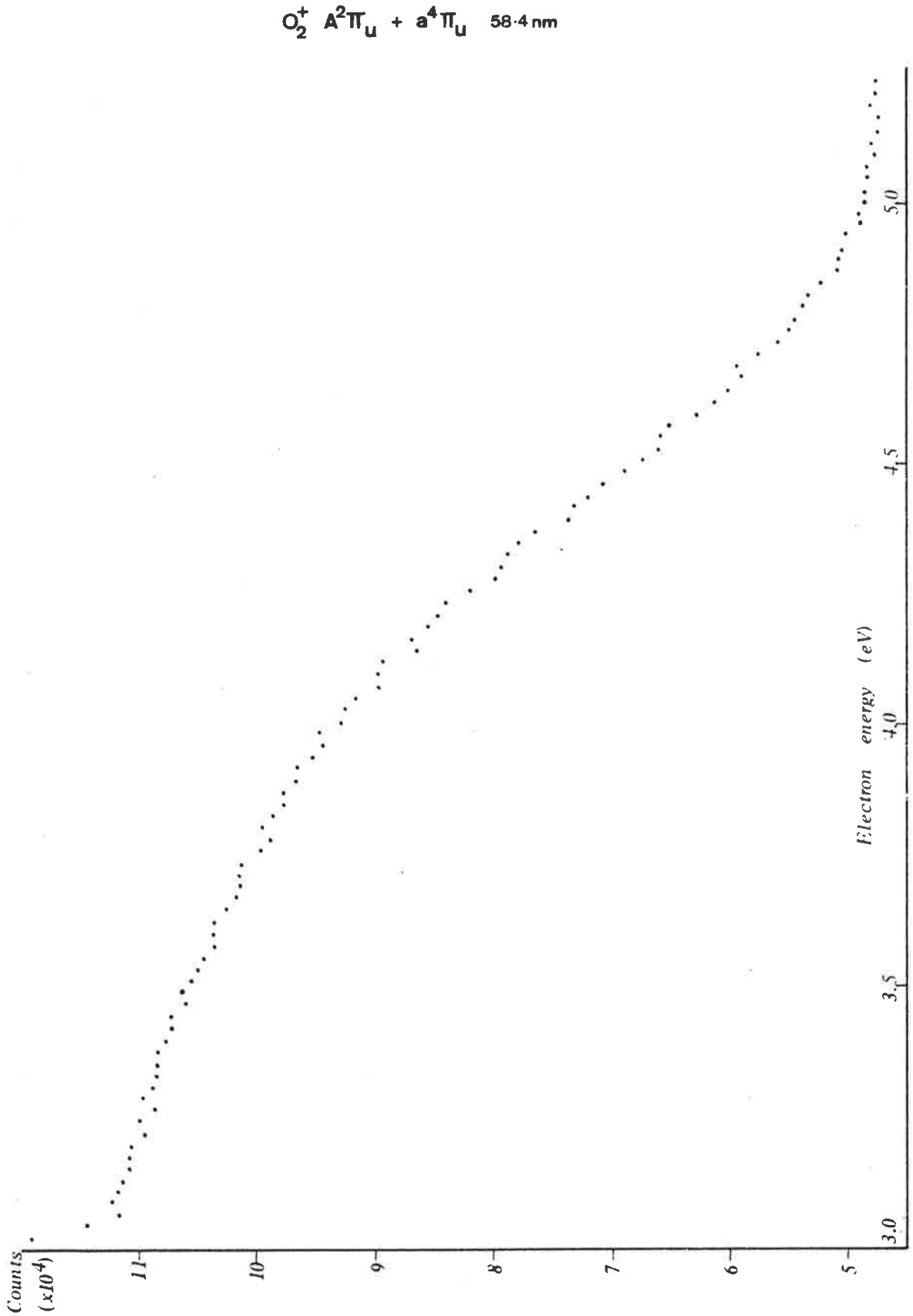

Fig. 3.8. Photoelectron spectrum of the $A^2\Pi_u$ and the $a^4\Pi_u$ states of the Oxygen ion at 58.4nm.

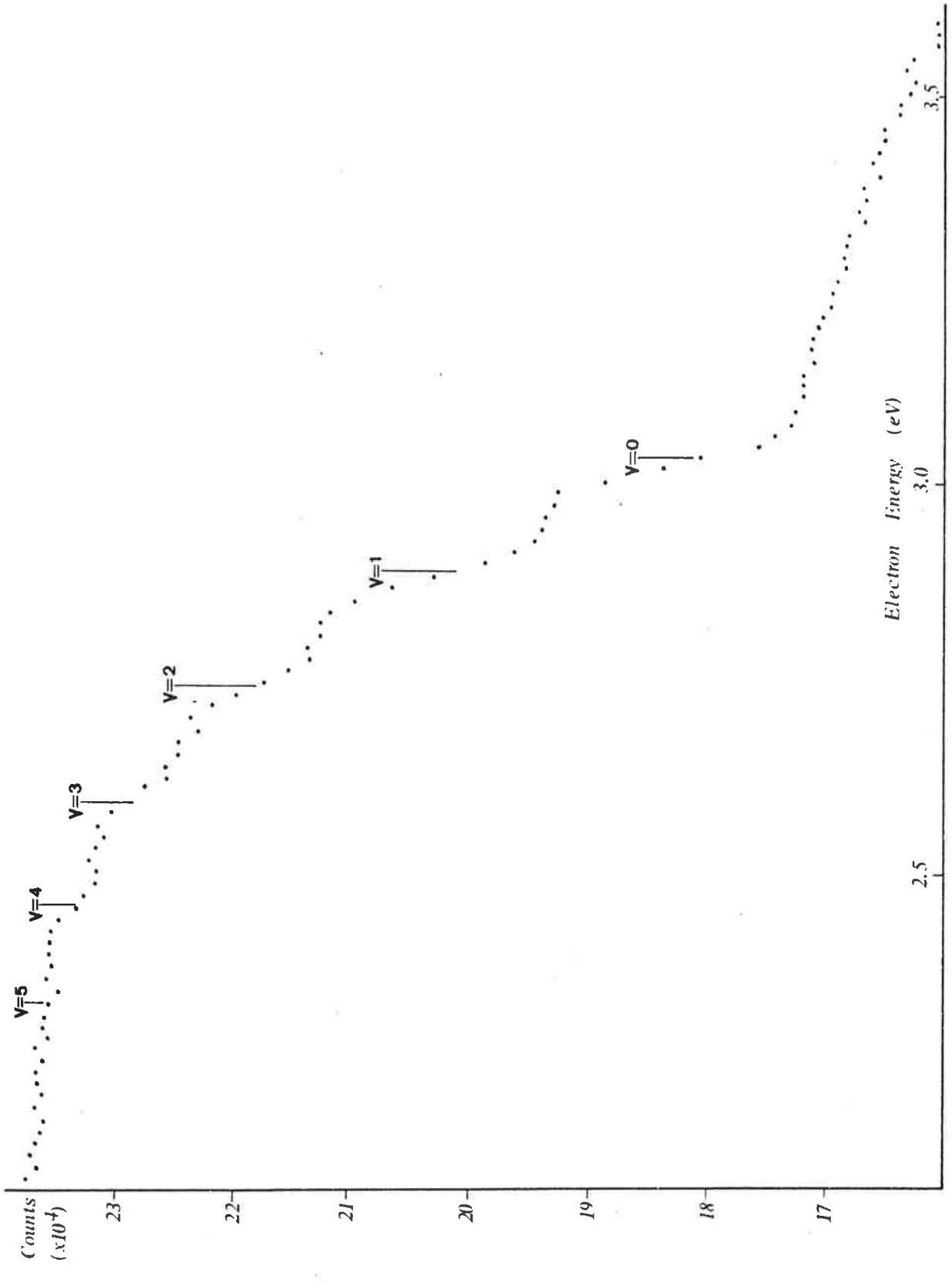

Fig. 3.9 Photoelectron spectrum of the $b\Sigma_g$ state of the Oxygen ion at 58.4nm.

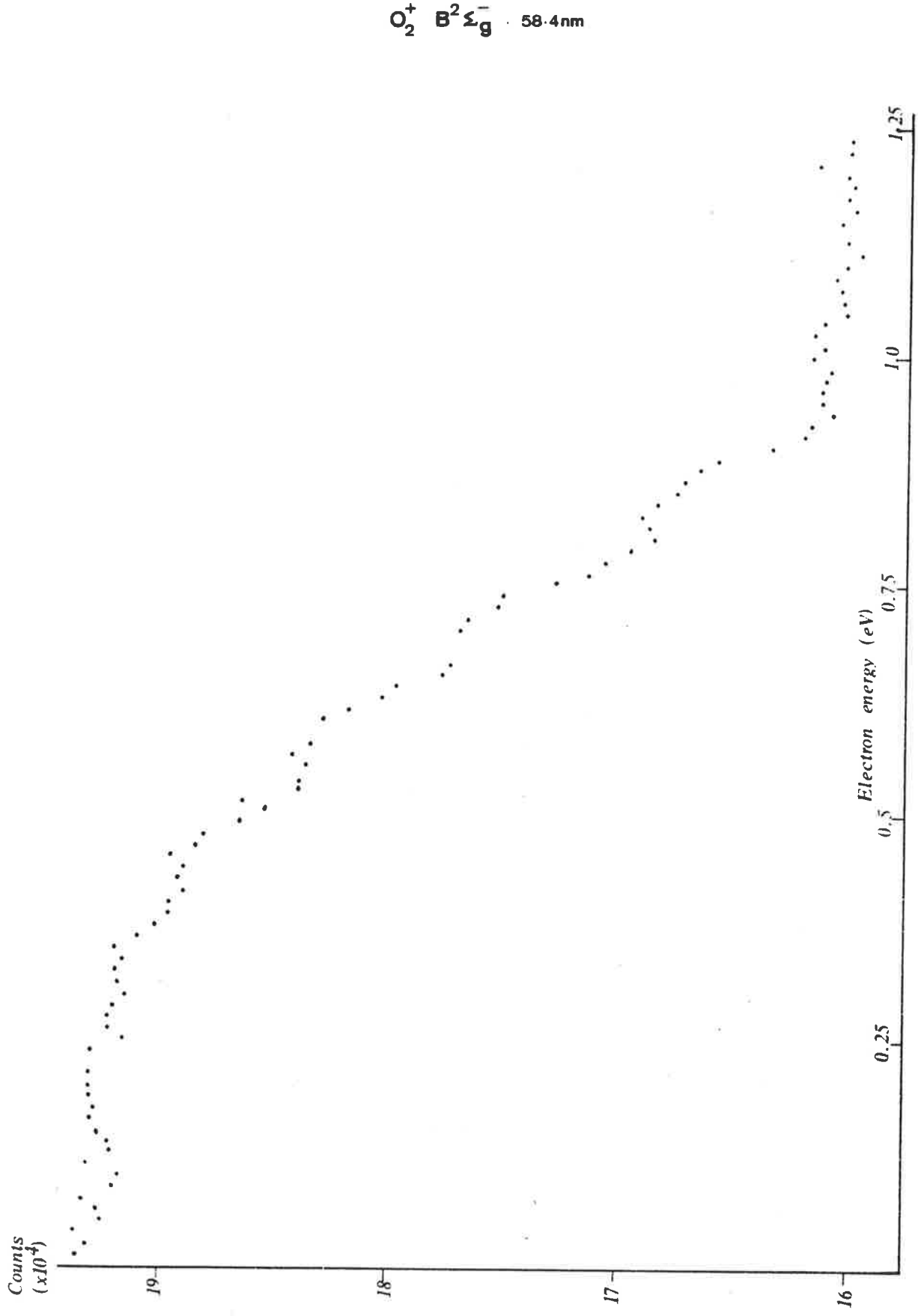

Fig. 3.10. Photoelectron spectrum of the $B^2\Sigma_g^-$ state of the Oxygen ion at 58.4nm.

intensities calculated from this spectra 1) by analysis by hand and 2) by the curve-fitting routine (Section 3.1) and compares them with experimental results (GARDNER, 1976) and with a range of results from many PES values compiled by NATALIS et al (1979). Calculated Franck-Condon factors are also included.

Table 3.3 Experimental vibrational Intensities and FCF for transitions from O_2 $X^3\Sigma_g^-$ (v" = 0) to the ionic levels v' shown.

State	v'	Experimental Intensities				FCF[c]
		Present Work (1)	Present Work (2)	Gardner(1976)[a]	Natalis[b]	
$X^2\Pi_g$	0	45	45.1 ± 0.4	46.7 ± 1.8	43 → 47	51.7
	1	100	100.0 ± 0.8	100.0 ± 5.0	100	100.0
	2	92	91.8 ± 0.9	91.6 ± 3.2	91 → 95	79.6
	3	46	46.4 ± 0.8	46.1 ± 2.1	44 → 49	33.7
	4	13	13.4 ± 0.6	15.4 ± 0.5	14 → 16	8.17

1) Results from Figure 3.6 analysed by hand

2) Results from Figure 3.6 analysed by curve-fitting routine (Sec. 3.1)

a) GARDNER and SAMSON, 1976

b) NATALIS et al, 1979

c) ALBRITTON et al from KRUPENIE, 1972

These results show that 1) the equipment produces good intensities 2) averaging over the flat parts and subtracting the averages is a reasonable method of analysing the data and 3) the computer program produces a satisfactory fit to the data, indicating that the program has the ability to analyse photoelectron spectra. (Figure 3.7 shows the fitted and raw data superimposed).

These very encouraging results demonstrate that the technique has great potential in the measurement of vibrational intensities.

The other point to note is the discrepancy between the

Franck-Condon factors and the measured intensities. GARDNER and SAMSON(1974b) suggest that they are not only those due to continuum ionization but also contain contributions from nearby autoionizing resonances. This is borne out by the fact that their results at 30.4nm are in much closer agreement with the calculated Franck-Condon factors.

The energy spacings between the vibrational levels can also be calculated from the spectra and these are shown in Table 3.4 along with results measured by other PES groups.

Table 3.4 Energy spacings of vibrational levels of $O_2^+ X^2\Pi_g$

v'	Present Work (1)	(2)	Natalis(1979)	Dromey(1979)	Edquist(1970)
0 → 1	229	230	232	232	232.4
1 → 2	227	228	229	228	227.9
2 → 3	221	220	227	224	223.6
3 → 4	226	228	221		219.9

The results calculated by hand (1) were found by taking the channel number corresponding to the midpoint of the step and using the fact that 1 channel = 20 meV. The curve-fitting results (2) were computed by allowing the energy spacings to be parameters involved in the program. These two methods gave results in agreement with each other but the last two values are not consistent with those of other workers presumably due to statistical scatter at lower electron energies. This points out the desiribility of using reputable energy spacings from elsewhere instead of allowing them to be varied either by eye or by the program.

Table 3.5 presents the results for the $b^4\Sigma_g^-$ and the $B^2\Sigma_g^-$ states.

Table 3.5 Experimental vibrational Intensities and FCF for transitions O_2 $X^3\Sigma_g^-$ (v" = 0) to the ionic levels v' shown

State	v'	Present	Gardner 1976[a]	FCF[b]
$b^4\Sigma_g^-$	0	100	100.0 ± 3.2	100.0
	1	91	86.8 ± 2.2	82.4
	2	53	54.3 ± 0.6	40.1
	3	36	33.7 ± 1.0	15.3
	4	18	18.4 ± 2.6	
	5	4.4	5.2 ± 0.5	
$B^2\Sigma_g^-$	0	87	86.2 ± 8.5	
	1	100	100.0 ± 5.7	
	2	86	80.2 ± 5.7	
	3	66	51.9 ± 7.8	
	4	34	35.3 ± 1.8	
	5	12	12.2 ± 0.7	
	6	8	1.4 ± 0.8	

a) GARDNER and SAMSON, 1974 (b)

b) ALBRITTON et al from (a)

Again adequate agreement is obtained although the $B^2\Sigma_g^-$ (v' = 3) seems to be high.

The results for the $b^4\Sigma_g^-$ are very different from the calculated Franck-Condon factors. GARDNER and SAMSON (1974b) pointed out that a dip in the photoionization cross-section near 59.0nm, which indicates the presence of an autoionized window resonance, appears in the cross-section for the production of this state and hence it will show the most perturbed vibrational distribution at 58.4nm.

The absence of Franck-Condon factors for the $B^2\Sigma_g^-$ state is due to the fact that this state predissociates and hence not enough spectroscopic data is available to calculate potential

energy curves.

Figure 3.8 shows the $a^4\Pi u$ state as well as the $A^2\Pi u$ state. It is not possible to separate those states by eye and so no vibrational intensities have been calculated for them.

3.2.4 Autoionization in oxygen in the region 87 - 90nm.

Figure 3.11, which illustrates the variation in photoelectron counts as the wavelength is scanned from about 90nm to 87nm, shows the positions of the wavelengths used in Figure 3.12 to Figure 3.18. The naming of the resonances is from DEHMER and CHUPKA (1975). Spectra were recorded at four J level (J_0 - J_3) autoionizing resonances, one at an un-named resonance X between J_0 and J_1, and at two so-called off-resonance positions, one between J_0 and J_1, (OR_1), and another between J_1 and J_2 (OR_2).

These results are presented in Table 3.6. The values for the J_1 state are an average obtained from those in Table 3.7. The latter table shows results of spectra taken on J_1 at different gas pressures and wavelength resolution.

Comparison of the results in Table 3.6 is not really valid because 1) the method of analysing by hand is not very accurate particularly at low electron energies, 2) no attempt has been made to correct for analyser efficiency which will be important at very low electron energies (see Section 2.4.5.5) 3) there was a known wavelength variation during the recording of J_1 (d) and J_2 and possibly in others 4) the wavelength resolution is 0.13nm for J_0, X, J_1, J_2 and some of J_1 but 0.2nm for off-resonance spectra and 5) the spectra did not have the same total counts which means that the intensities cannot be measured to the same accuracy. The only points worth noting are that 1) on resonance more of the higher vibrational levels are populated than at the off-resonance positions 2) the X resonance has a markedly different distribution from that

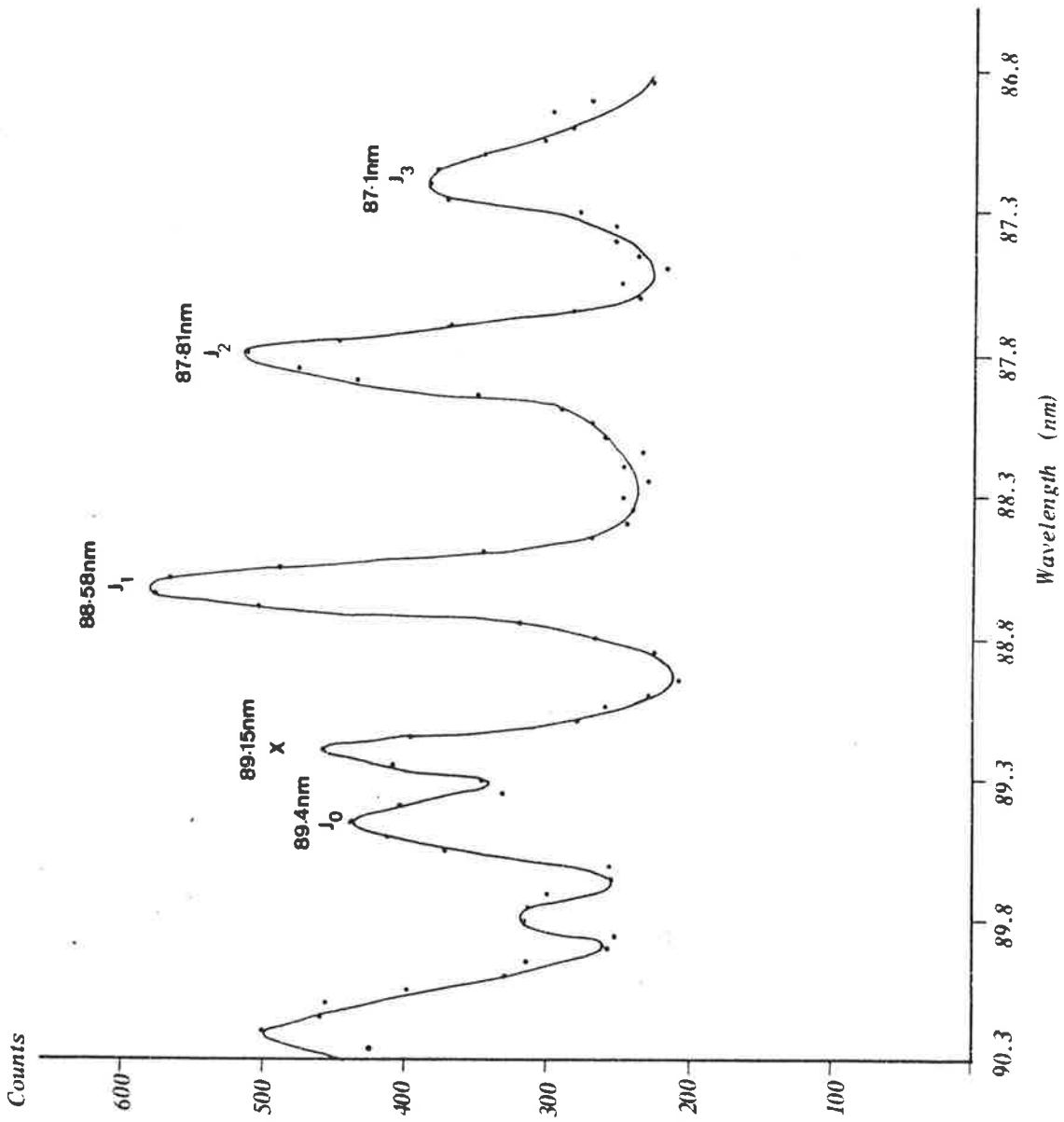

Fig. 3.11. Total electron count obtained as the wavelength was scanned across the J levels of Oxygen.

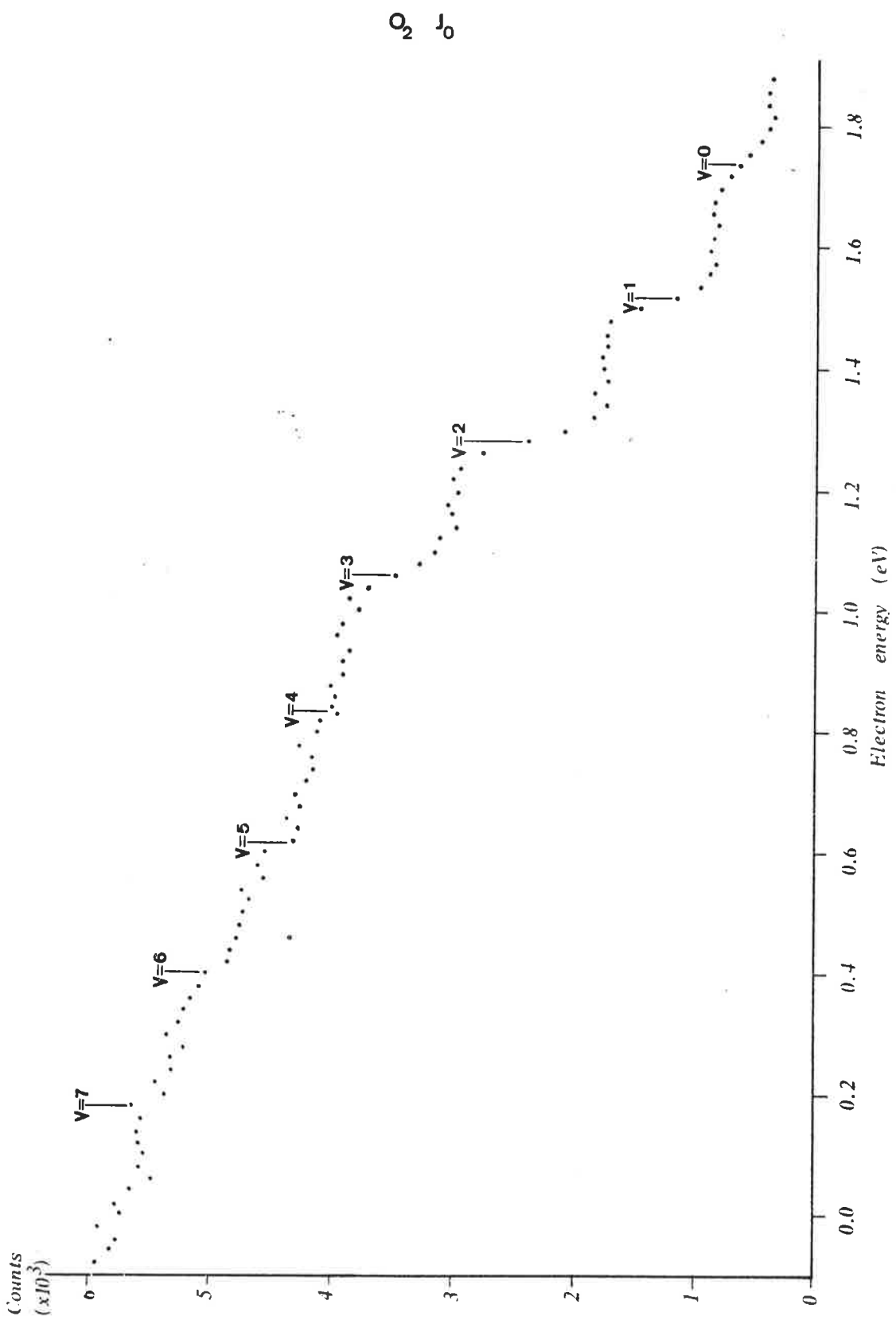

Fig. 3.12. Photoelectron spectrum recorded at the v = 0 level of the J autoionizing progression of Oxygen.

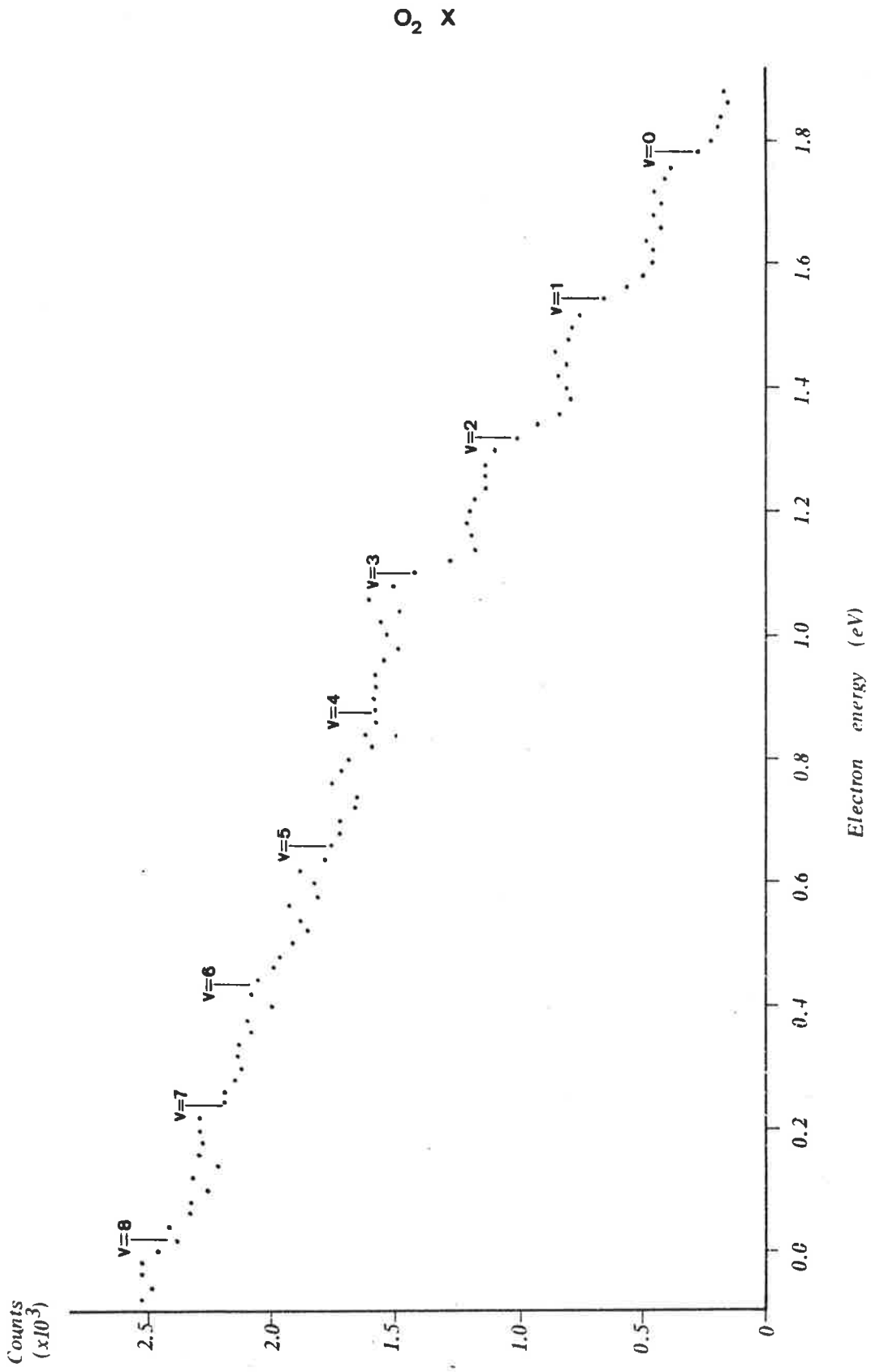

Fig. 3.13. Photoelectron spectrum recorded at an unknown resonance of Oxygen at 89.2nm.

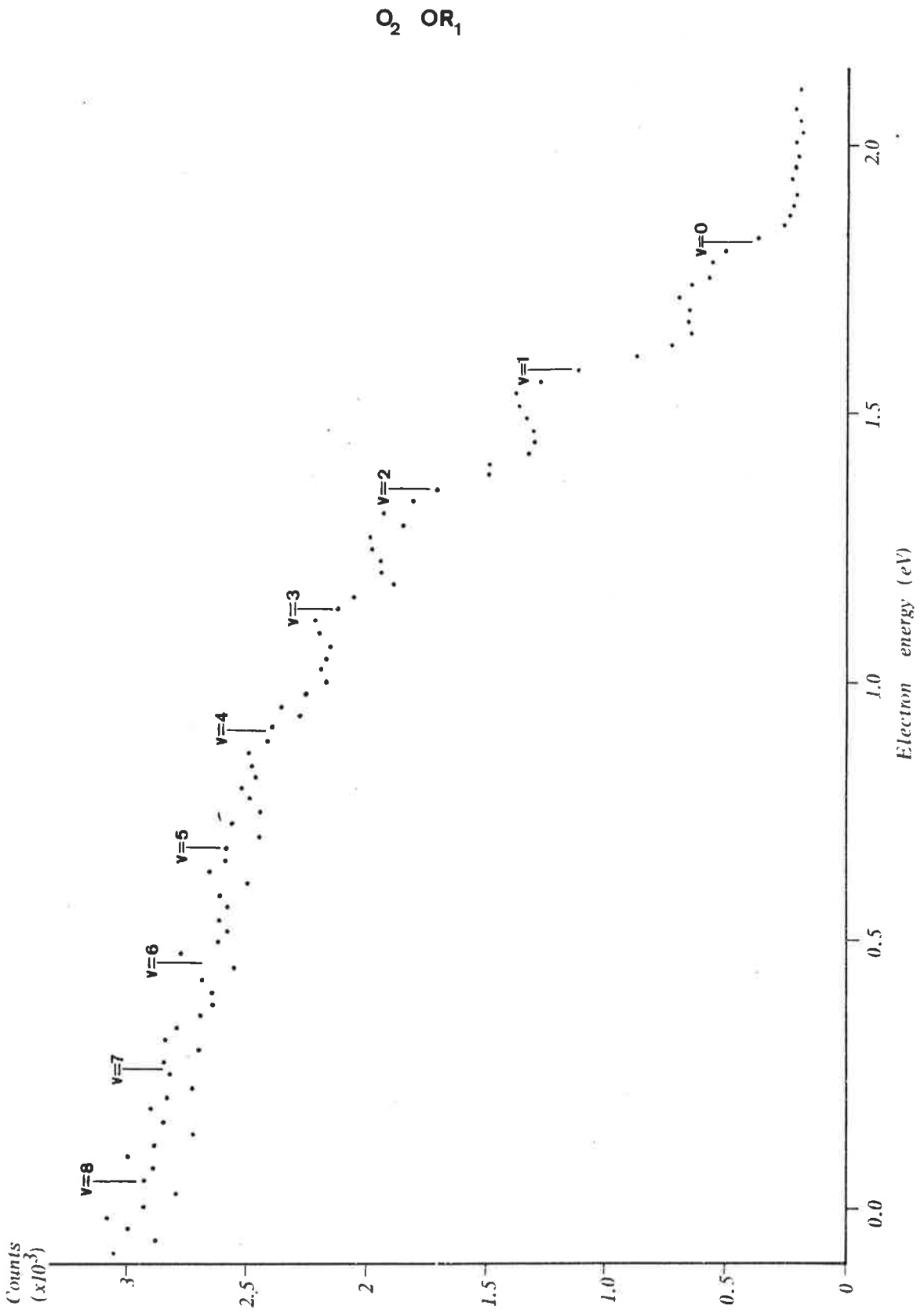

Fig. 3.14. Photoelectron spectrum recorded between the v = 0 and v = 1 levels of the J autoionizing progression of Oxygen.

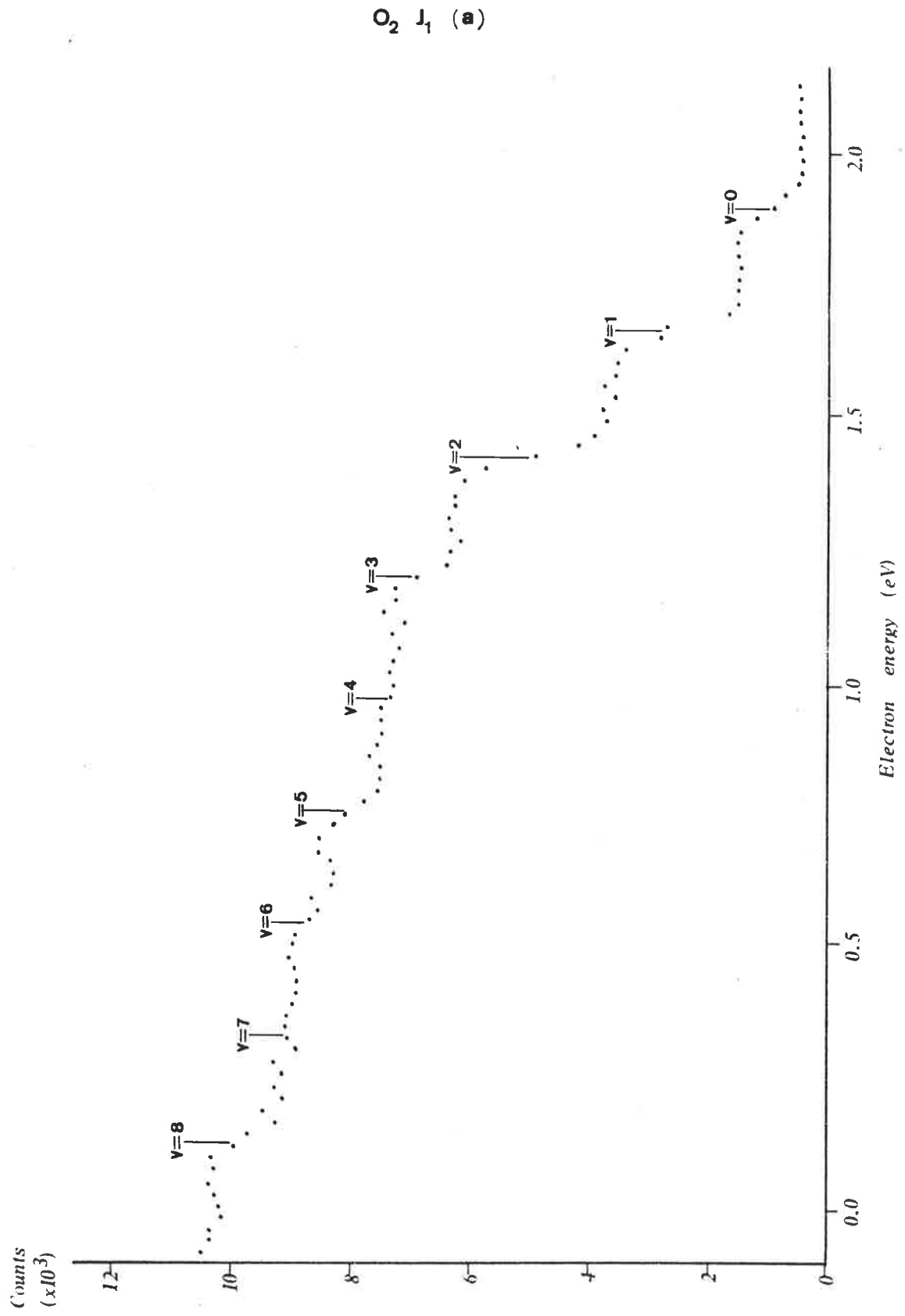

Fig. 3.15a). Photoelectron spectrum recorded at the v = 1 level of the autoionizing progression of Oxygen using a pressure of 0.6mu and a wavelength resolution of 0.2nm.

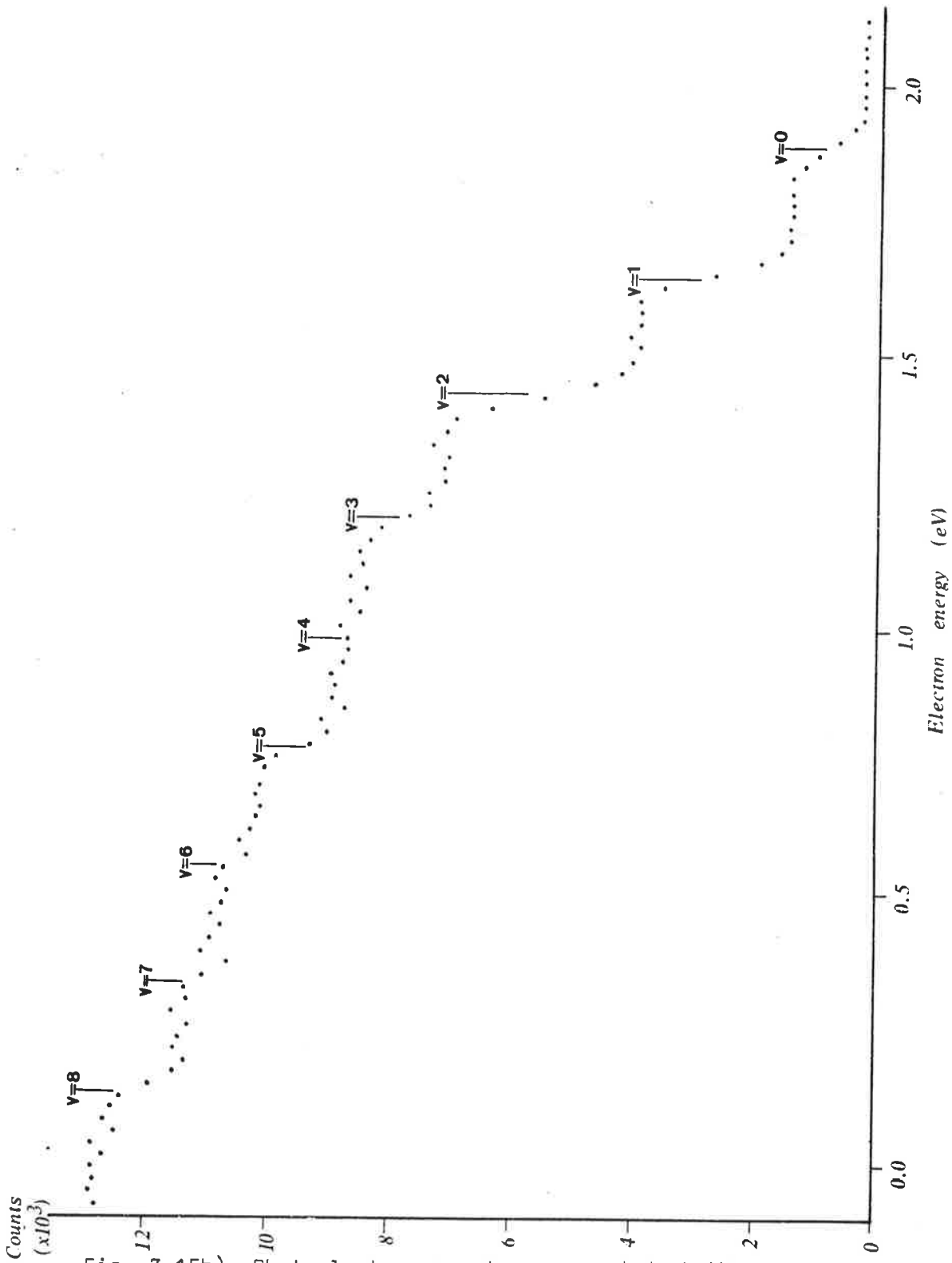

Fig. 3.15b). Photoelectron spectrum recorded at the v = 1 level of the J autoionizing progression of Oxygen using a pressure of 3 mu and a wavelength resolution of 0.2nm.

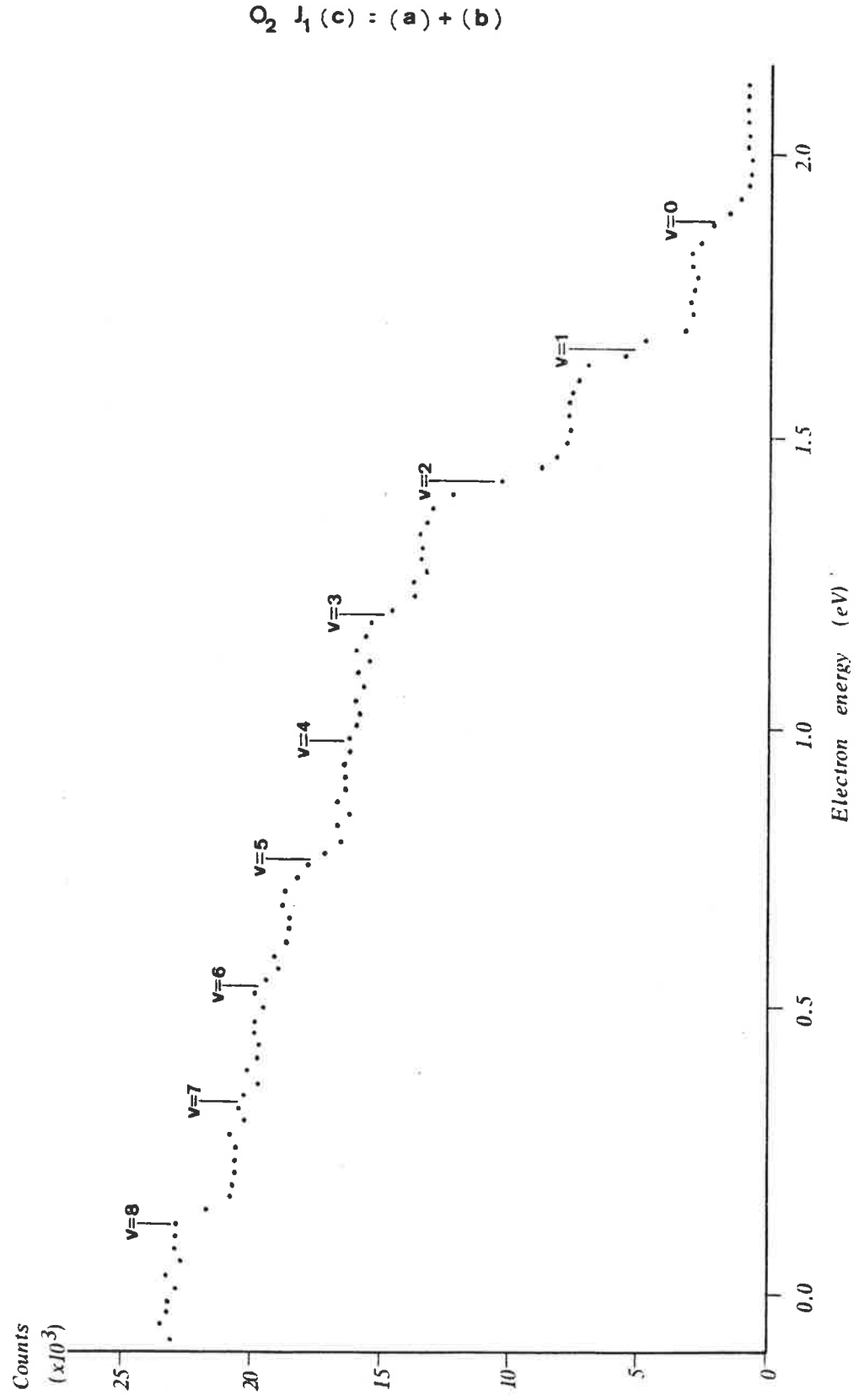

Fig. 3.15c). Combined photoelectron spectrum obtained by adding counts from 3.15a) and b).

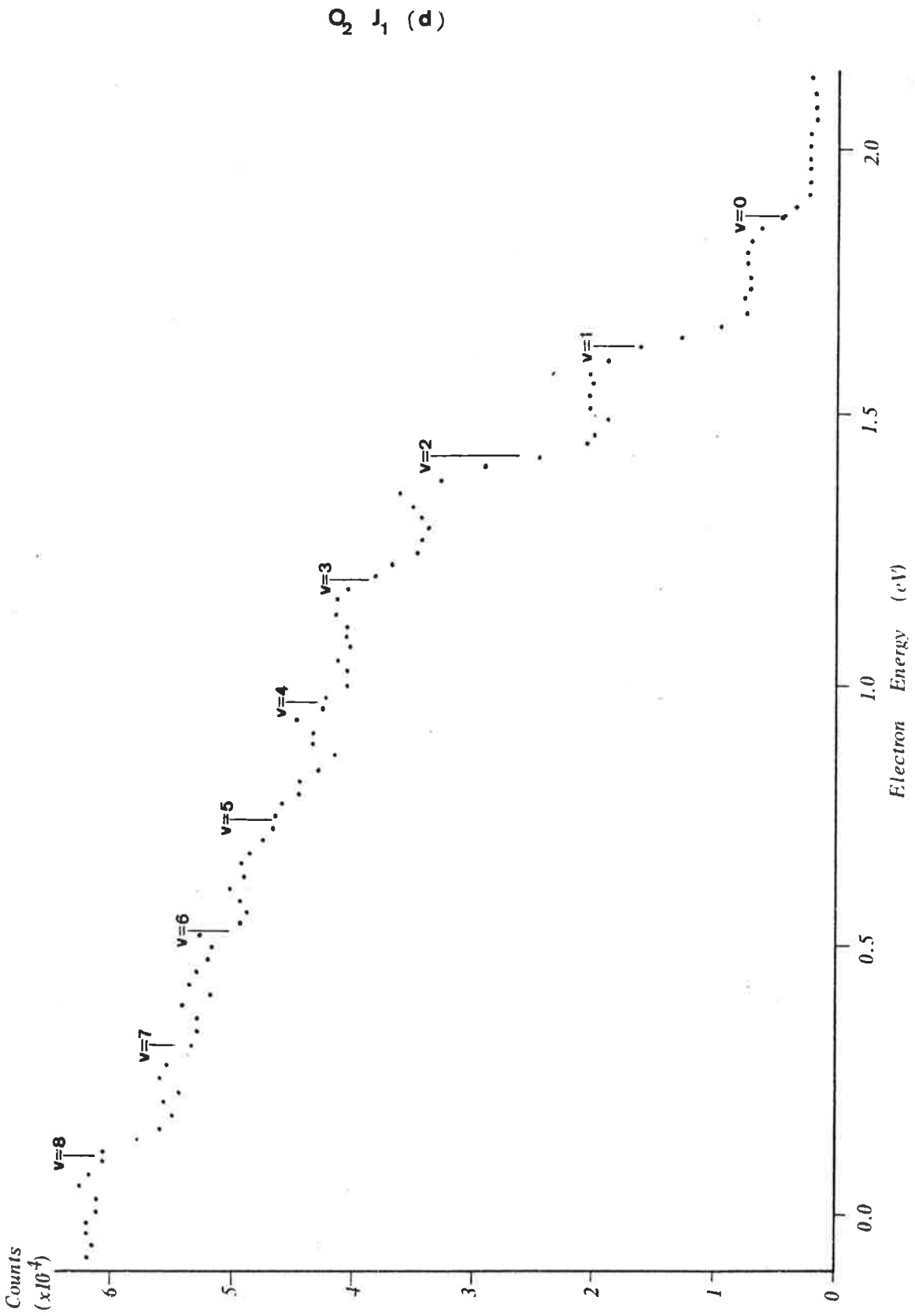

Fig. 3.15d). Photoelectron spectrum recorded at the v = 1 level of the J autoionizing progression of Oxygen using a pressure of 3 μ and a wavelength resolution of 0.1nm.

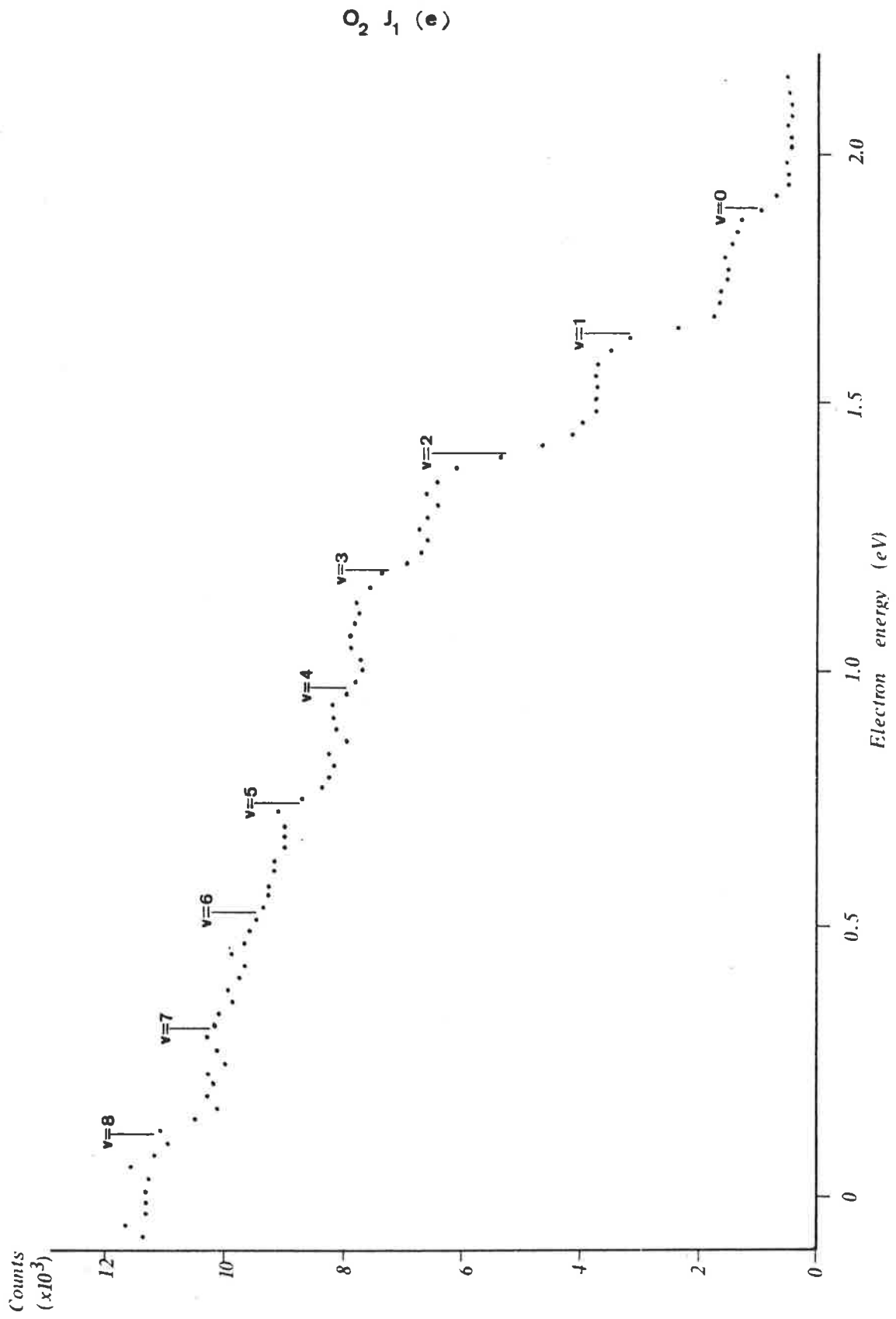

Fig. 3.15e). Photolectron spectrum recorded at the v = 1 level of the J autoionizing progression of Oxygen using a pressure of 3 μ and a wavelength resolution of 0.13nm.

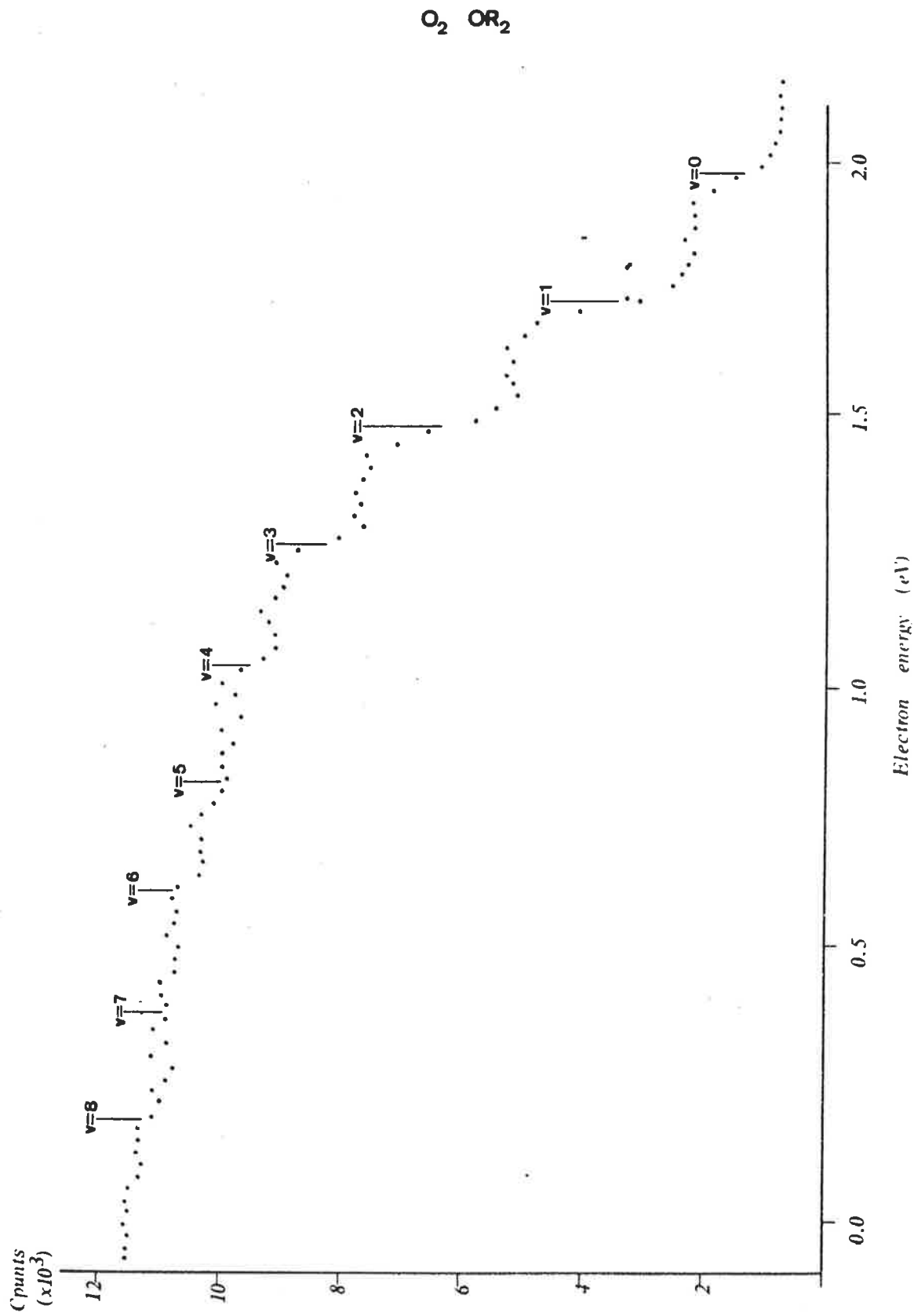

Fig. 3.16. Photoelectron spectrum recorded between the v = 1 and the v = 2 levels of the J autoionizing progression of Oxygen.

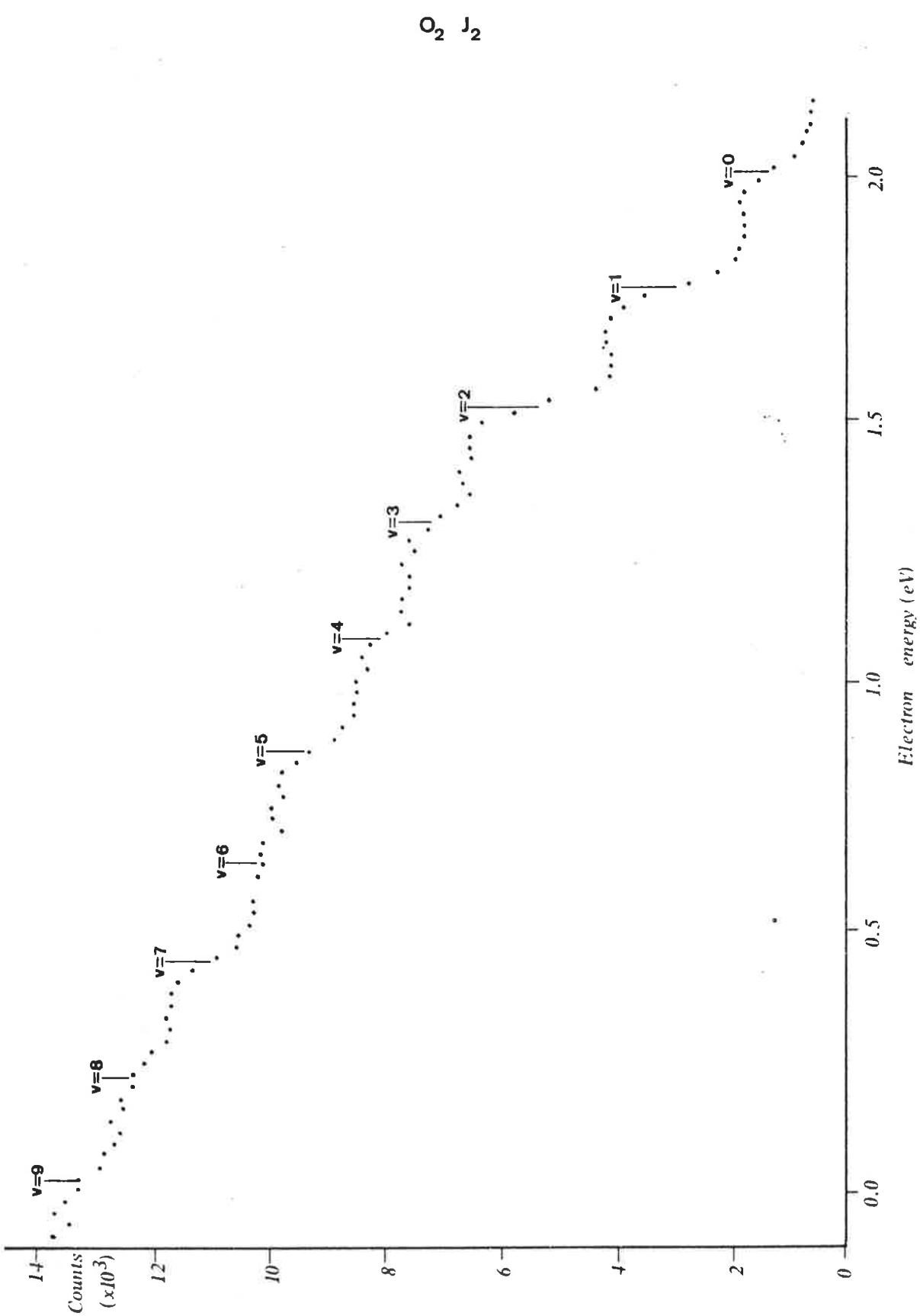

Fig. 3.17. Photoelectron spectrum recorded at the v = 2 level of the J autoionizing progression of Oxygen.

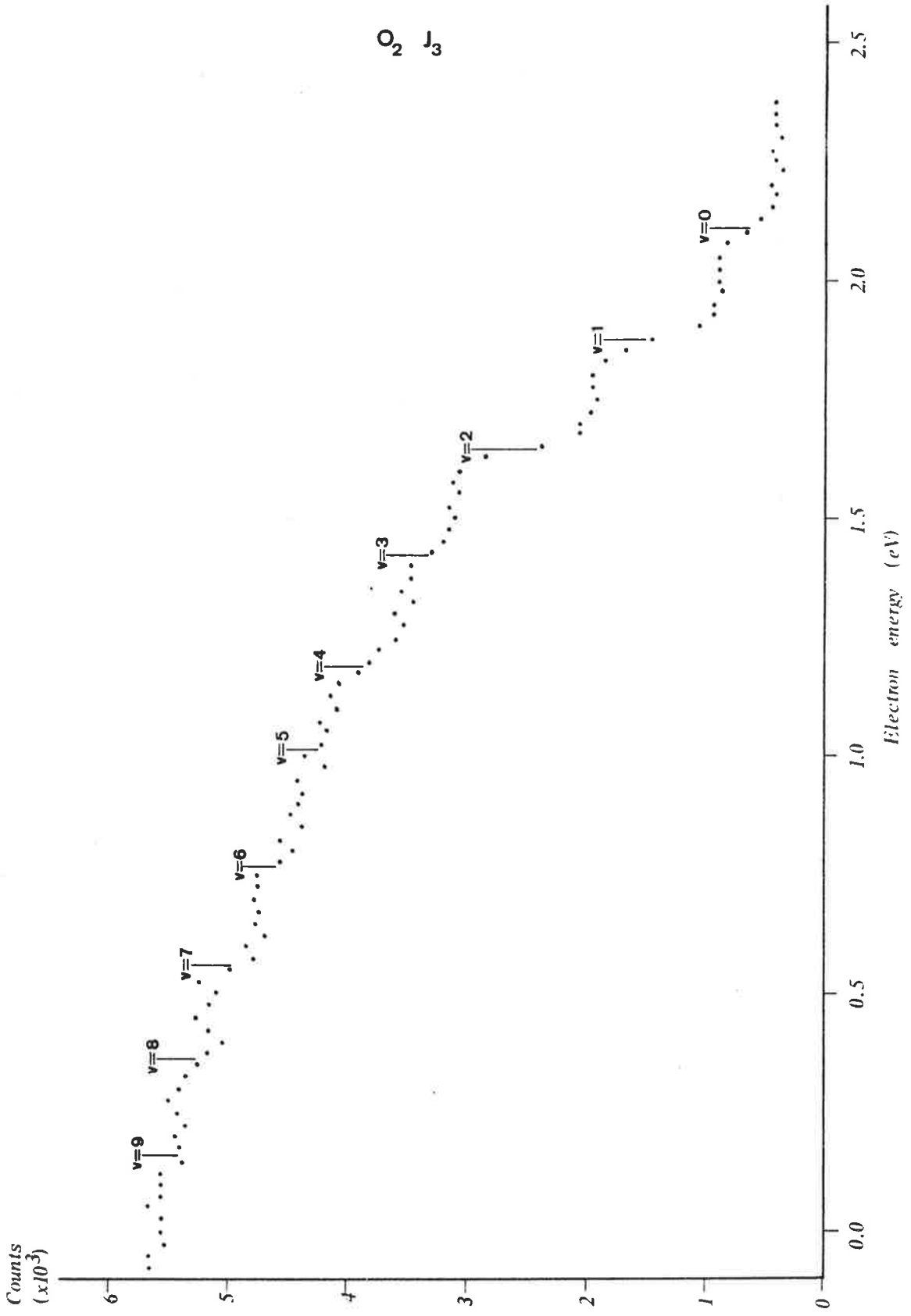

Fig. 3.18. Photoelectron spectrum recorded at the v = 3 level of the J autoionizing progression of Oxygen.

Table 3.6 Experimental vibrational intensities for $O_2^+ X^2\Pi_g$ populated through various autoionizing resonances.

v'	J_0	J_1	J_2	J_3	OR_1	OR_2	X
0	0.08	0.09	0.09	0.09	0.15	0.14	0.13
1	0.16	0.21	0.18	0.20	0.26	0.28	0.18
2	0.23	0.25	0.19	0.22	0.21	0.23	0.16
3	0.16	0.10	0.08	0.09	0.09	0.14	0.17
4	0.06	0.03	0.07	0.12	0.11	0.06	0.09
5	0.09	0.09	0.11	0.04	0.04	0.04	0.08
6	0.12	0.06	0.04	0.07	0.03	0.03	0.12
7	0.04	0.04	0.11	0.08	0.07	0.03	0.08
8	0.06	0.11	0.07	0.05	0.04	0.04	0.13
9			0.08	0.03		0.01	

Table 3.7 Experimental vibrational intensities for $O_2^+ X^2\Pi_g$ at J_1 resonance.

	0.2nm photon resolution			0.1nm	0.13nm
	0.6u	3u	½u + 3u	3u	3u
	a)	b)	c) = a+b	d)	e)
0	0.10	0.09	0.10	0.09	0.09
1	0.22	0.20	0.21	0.21	0.20
2	0.26	0.25	0.26	0.25	0.25
3	0.09	0.11	0.10	0.10	0.12
4	0.04	0.03	0.03	0.03	0.03
5	0.08	0.10	0.09	0.11	0.09
6	0.06	0.06	0.05	0.06	0.05
7	0.03	0.05	0.04	0.03	0.05
8	0.11	0.11	0.12	0.12	0.11

of the J levels and 3) the so called off-resonance spectra clearly contain some contribution from resonances (cf Franck-Condon factors in Table 3.3) and show a greater discrepancy from the Franck-Condon factors than does the spectrum at 58.4nm (Section 3.2.3 and Fig. 3.6). This suggests that the autoionizing resonances in this region overlap and so there is no true off-resonance position between the peaks.

Table 3.7 seems to indicate that, to the accuracy of the analysis, no significant difference is caused either by pressure or photon resolution. The latter could be explained by assuming again that the resonances overlap as indicated by the fact that the higher vibrational levels are populated at the "off resonance" positions.

The results presented in this chapter do indicate that the apparatus described in Chapter 2 is capable of producing vibrational intensities particularly at autoionizing resonances. The next chapter will deal with problems still to be sorted out and future work to be done.

CHAPTER 4 FUTURE DEVELOPMENT

4.1 INTRODUCTION

The results presented in chapter 3 show that the system is obviously capable of producing good quality data but that 1) some modifications still need to be made to the equipment and 2) the analysis routine requires further development. These points will be discussed in this chapter as well as suggestions for future research work.

4.2 MODIFICATIONS TO THE EQUIPMENT

As discussed in Section 2.4.5.2, it was imperative to keep the analyser and ionizing region as clean as possible in order to produce reliable results. Any pumping accident, caused either by human error or power failure, deposited oil on the analyser. To protect the analyser as well as the diffraction grating, whose reflectivity is lowered by oil films from pumping accidents, pneumatically operated valves with failsafe operation should be installed to isolate the ionizing chamber and monochromator from all the pumps. Such a precaution would 1) increase the time available for data collection as no time would then be wasted cleaning up after accidents and 2) ensure that conditions in the system remained more stable.

The variation of the wavelength during scans, which was mentioned in Section 3.2.4, was later found to be caused by expansion in the monochromator as the pumps heated up. If protection valves were added to the system as described above, the pumps could then be safely left on all the time. This should eliminate the wavelength drift.

The system also needed to be modified to improve the

measurement of the efficiency function (Section 2.4.5.5). This requires the recording of more accurate absorption data which could be obtained by monitoring the light entering as well as leaving the ionization region. An extra photomultiplier placed at the exit of the monochromator i.e. in front of the ionizing region would record any fluctuations in the lamp intensity as well as any variations due to the different reflectivity of the grating at different wavelengths. The absorption cross-section as a function of wavelength would then be found by dividing the difference in count rate from the two photo-multipliers (this difference being proportional to the light flux absorbed in the region viewed by the analyser) by the sum of the count rates (which is proportional to the average light flux in the region viewed by the analyser). The efficiency is then calculated by dividing the electron count by the absorption cross-section. This method has been used by LINDEMANS et al (1979) and the dependence of the collecting efficiency of the analyser has been accurately recorded (Section 2.4.5.5). They showed that the efficiency remains constant within a few percent for electron energies greater than 100 meV but for energies less that this, the efficiency has to be carefully measured and then taken into account when analysing the data.

Because the efficiency is basically constant, it need not be checked very often. Measurements should be taken occasionally to determine the efficiency at low electron energies as well as at a few higher energy values to see that no great change has occurred. This can be done simply by using a rare gas and the two photon beam detectors using the method described in Section 2.4.5.5 and above.

The addition of the second photomultiplier also allows the electron count rate to be made independent of sample gas pressure fluctuations as well as of lamp intensity variations. The independence is achieved by dividing the number of electrons counted at a particular energy by the difference in photomultiplier count rates and hence

eliminates the need to monitor the sample gas pressure and then discard those scans with pressure variations greater than 1% (Section 2.4.4.2).

As explained in Sections 1.4 and 2.3, a further modification to the system which is needed is to change the angle of the axis of the electron energy analyser to the light beam from 54^{o} 44' to 53^{o} 33'. This change, which was made after completion of the work for this thesis, ensures that future results will be independent of the angular distribution of the photoelectrons.

4.3 ANALYSIS PROGRAM PROBLEMS

The difficulties encountered with the curve-fitting program discussed in Section 3.1, also need to be considered.

Firstly a method of obtaining a suitable background spectrum which accounts for pressure and time variations is needed. A spectrum run with no gas in the ionization region shows that photoelectrons are emitted from the metal walls of the chamber. Impurities which are not removed by the cold trap (Section 2.4.4.2) also contribute to the background. It is not possible to find how the metal spectrum changes with increases in sample gas pressure and also, unless the percentage and nature of the impurities are known, no true background can be removed from the spectrum to be fitted. The metal spectrum is presumably incorporated in the standard line shape and, if impurities are considered negligible, the simple procedure of scaling the standard line shape, background and all, to fit the spectrum being analysed may be sufficient. Preliminary attempts at this procedure seemed to indicate that this was valid.

The system must also be pumped for a considerable time after cleaning (Section 2.4.5.2) so that the cleaning fluids do not produce background counts.

Secondly the variation of the resolution of the analyser

with electron energy may need to be taken into account. This may be allowed for by using the experimental line shapes which are recorded at different energies.

Thirdly, another factor that may also have to be considered is that the standard line shapes described in Section 3.1 and shown in Appendix 1 were taken at lamp resonance lines and most of the interesting spectra are recorded at wavelengths where the radiation comes instead from the Hopfield continuum which has a different light resolution and shape.

The resolution of HeI line at 58.4nm is about 5 meV but for wavelengths in the Hopfield continuum, the photon energy spread varies from about 20 meV at 90nm to 40 meV at 60nm. (These spreads correspond to a wavelength resolution of 0.1nm obtained with the exit and entrance slits set to 100 μ (Section 2.2)). The experimental resolution for spectra measured at lamp resonance lines (i.e. with insignificant photon spread) varies from about 20 meV for 1 volt electrons to about 40 meV at 9 volts. Thus for low energy electrons or for spectra run at short wavelengths the photon energy spread is comparable to the analyser resolution.

To test whether the wavelength resolution does make any significant difference to the standard line shapes, the spectra should be repeated at wavelengths close to 58.4nm or 73.6nm but this time using light from the Hopfield continuum.

An auxiliary test would be to run, for instance, a Xenon $P_{3/2}$ spectrum at 82.8nm (electron energy of 2.85 eV) and compare this with the Krypton $P_{3/2}$ spectrum at 73.6nm (electron energy also of 2.85 eV). This may also reveal any anomalies in the line shape caused either by "idiosyncrasies" of the gas used or by a difference in background since the 82.8nm spectrum would need to be run for a much greater time due to the lower light intensity.

If the tests described above indicate that it is

necessary to include the change in wavelength resolution, the following will have to be done. The wavelength resolution will have to be determined by recording the photomultiplier count as a function of wavelength across e.g. the Lyman α line of Hydrogen and calculating the spread at full width half maximum. This will then need to be compared to a similar scan across the 58.4 and 73.6nm lines.

Fourthly, the experimental line shapes need to be smoothed to produce a suitable curve for the curve-fitting program. This can be done, for example, by using another subroutine of Bevington's (BEVINGTON, 1969). Here, each data point is replaced by a new value which takes into account the neighbouring points ($Y_i' = \frac{Y_{i-1} + 2Y_i + Y_{i+1}}{4}$).

Fifthly, as the line shapes are taken at discrete energies, a method of interpolating between these energies to produce suitable line shapes at all energies is needed. If the variation in shape is gradual and smooth, a linear interpolation between equivalent smoothed points may be sufficient. The decision as to which are equivalent points needs to be investigated - perhaps the energy of the peak could be used as the reference point. This peak position could be found by differentiating the spectrum numerically, drawing the differentiated spectrum and finding the position of the maximum.

Many of these problems could be overcome by finding an analytical function with parameters which can be varied with electron energy. This function would then take into account the difficulties caused by the change in resolution and the difference in shapes using radiation from resonance lines or the Hopfield continuum, as well as eliminating the need for smoothing of the data and interpolation betwen energies. LINDEMANS (1981) has attempted to find such a function.

Two other problems which arose in the analysis of the data were encountered in the curve-fitting program itself. These were; -

1) knowing what value of X^2 indicated a good fit and 2) knowing whether the errors it gave were sensible. More work needs to be done on these two points.

4.4 FUTURE RESEARCH WORK

Now that the apparatus described in this thesis is known to produce good photoelectron spectra, particularly at autoionizing resonances (Figures 3.12 - 3.18, Section 3.2.4), more data should be taken. The preliminary results for the autoionizing levels in oxygen described in Section 3.2.4 should be repeated but with the following changes.

Firstly, a similar maximum count is needed for all spectra in order to make more accurate comparisons between the vibrational intensity distributions at different wavelengths.

Secondly, the pumps should be switched on continuously to avoid the problem of a wavelength drift during scans as described above.

Thirdly, the spectra should be repeated at higher wavelength resolution to see if contributions from nearby resonances can be excluded. (If the neighbouring resonances overlap, it will not be possible to eliminate the effects of other resonances, as discussed in Section 3.2.4).

These new experimental results will then need to be analysed with a curve-fitting program, such as that described in Section 3.1, and which incorporates in it solutions to the problems raised in Section 4.3 as well as an accurate efficiency correction for low energy electrons (Sections 2.4.5.5 and Section 4.2).

The heights of the steps of the fitted spectra will then be proportional to the intensities of the transitions to the various vibrational states of the $X^2\Pi_g$ state of the oxygen ion at the

particular wavelength used. These vibrational levels are of three types; type 1 - those populated directly from the ground state of the molecule only, type 2 - those populated both from the ground state and through the autoionizing level and type 3 - those populated through the autoionizing level only. There are thus three different types of vibrational intensities each associated with one of the 3 different types of vibrational levels. These vibrational intensities can then be compared with those predicted by theory (e.g. the Fano-Mies theory presented in Section 1.3.3).

This particular theory requires an off-resonance spectrum. As discussed in Sections 3.2.4 and 3.2.3, neither the spectra taken between the J autoionizing levels nor the spectrum at 58.4nm are truly off-resonance spectra; the former either because of overlapping resonances or because of the use of too low a wavelength resolution and the latter because of the presence of a nearby autoionizing resonance. GARDNER and SAMSON (1974 (b)) suggest that a spectrum recorded at 30.4nm would be more appropriate (Section 1.3.4).

If higher wavelength resolution spectra show that neighbouring resonances really do overlap in the region of interest the theory will have to be modified to include contributions from other resonances.

CONCLUSION

This thesis has shown that results similar to those obtained and analysed by the methods described in Chapters 2 and 3 and with the modifications discussed in Chapter 4 will lead to greater insight into the process of autoionization in diatomic molecules.

APPENDIX 1

Figs. A1 – A11 show spectra which would be used to obtain a set of standard line profiles for use in the curve-fitting program discussed in Sec. 3.1.

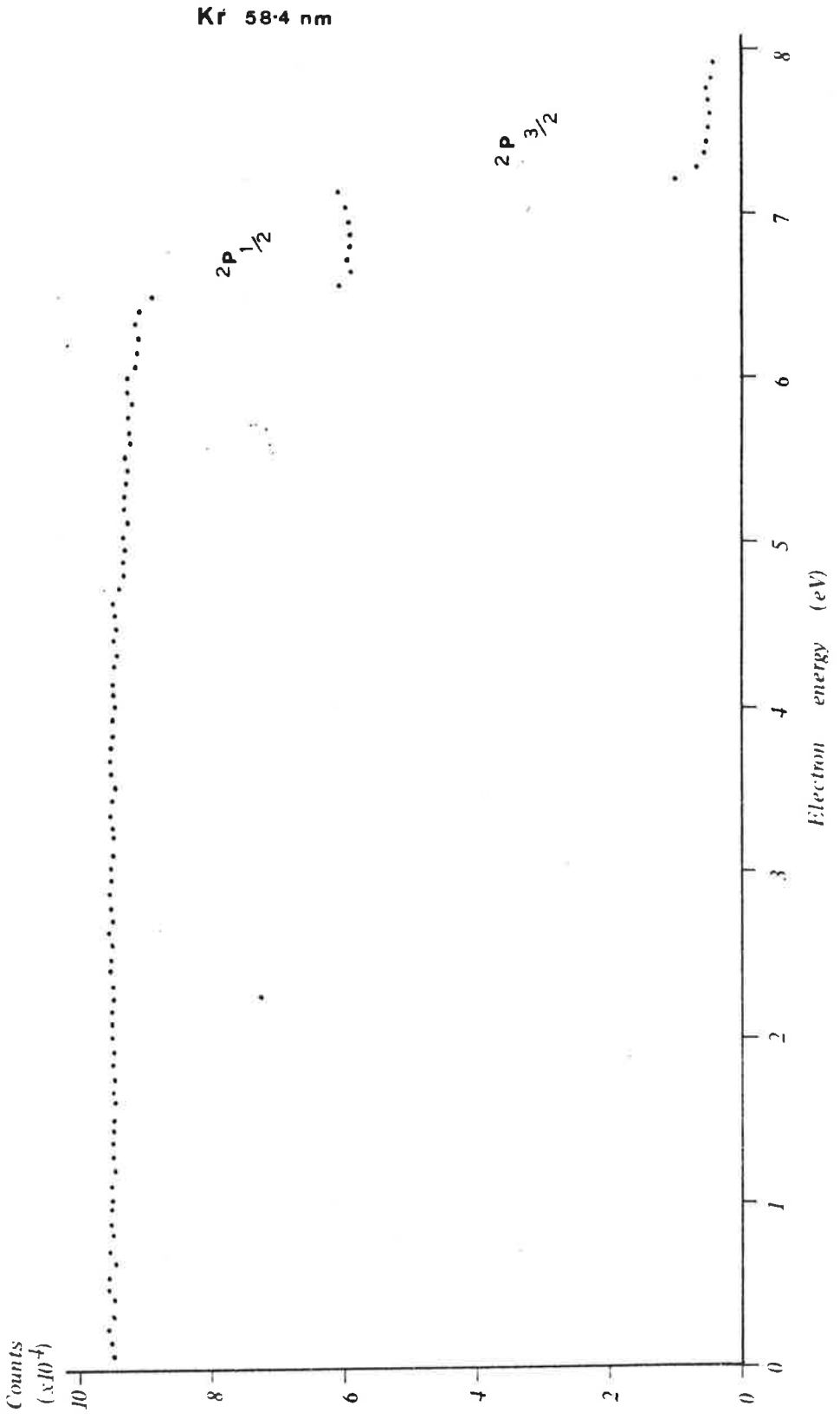

Fig. A1. Total photoelectron spectrum of Krypton at 58.4nm.

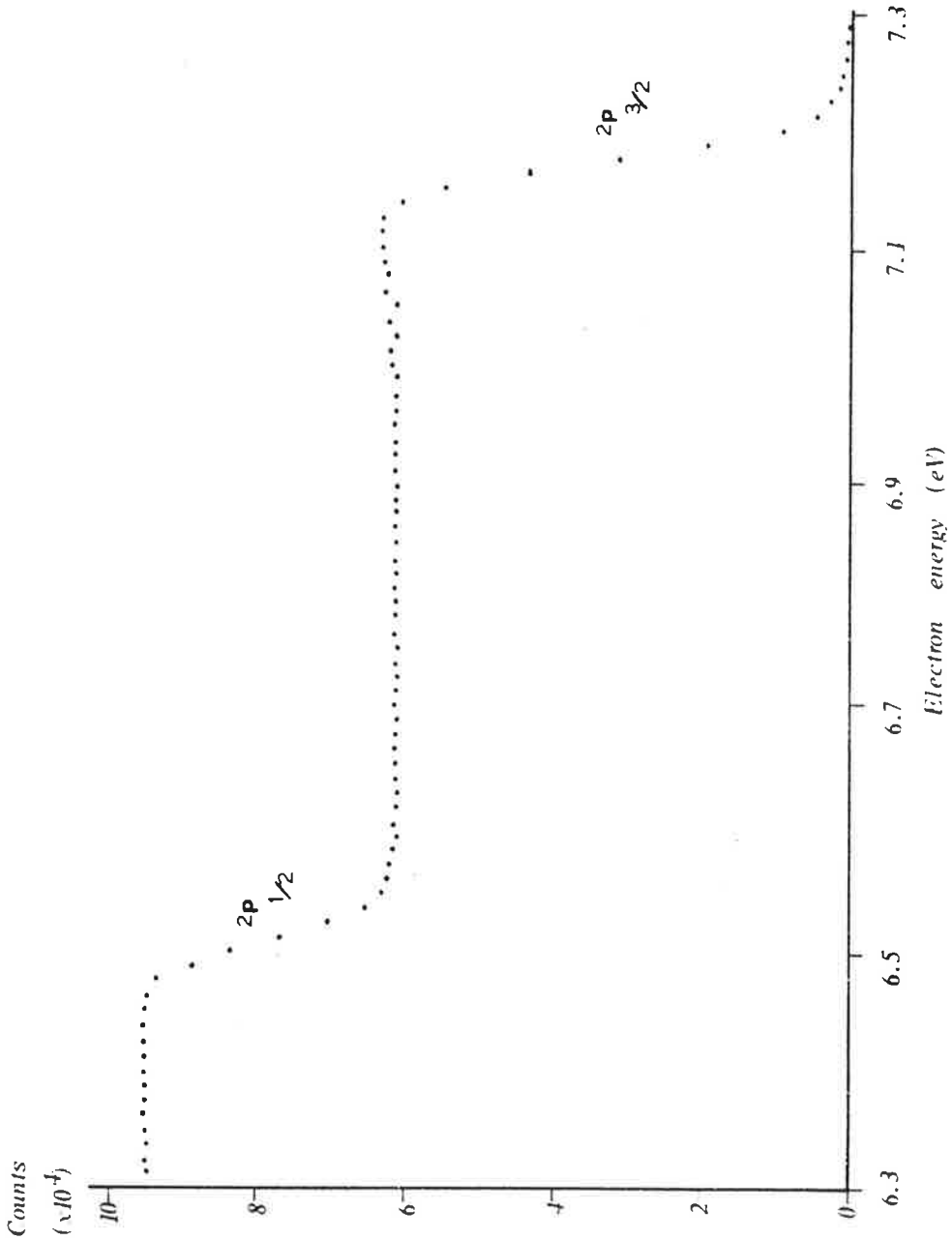

Fig. A2. Photoelectron spectrum of Krypton at 58.4nm scanned across the $^2P_{1/2}$ and $^2P_{3/2}$ states.

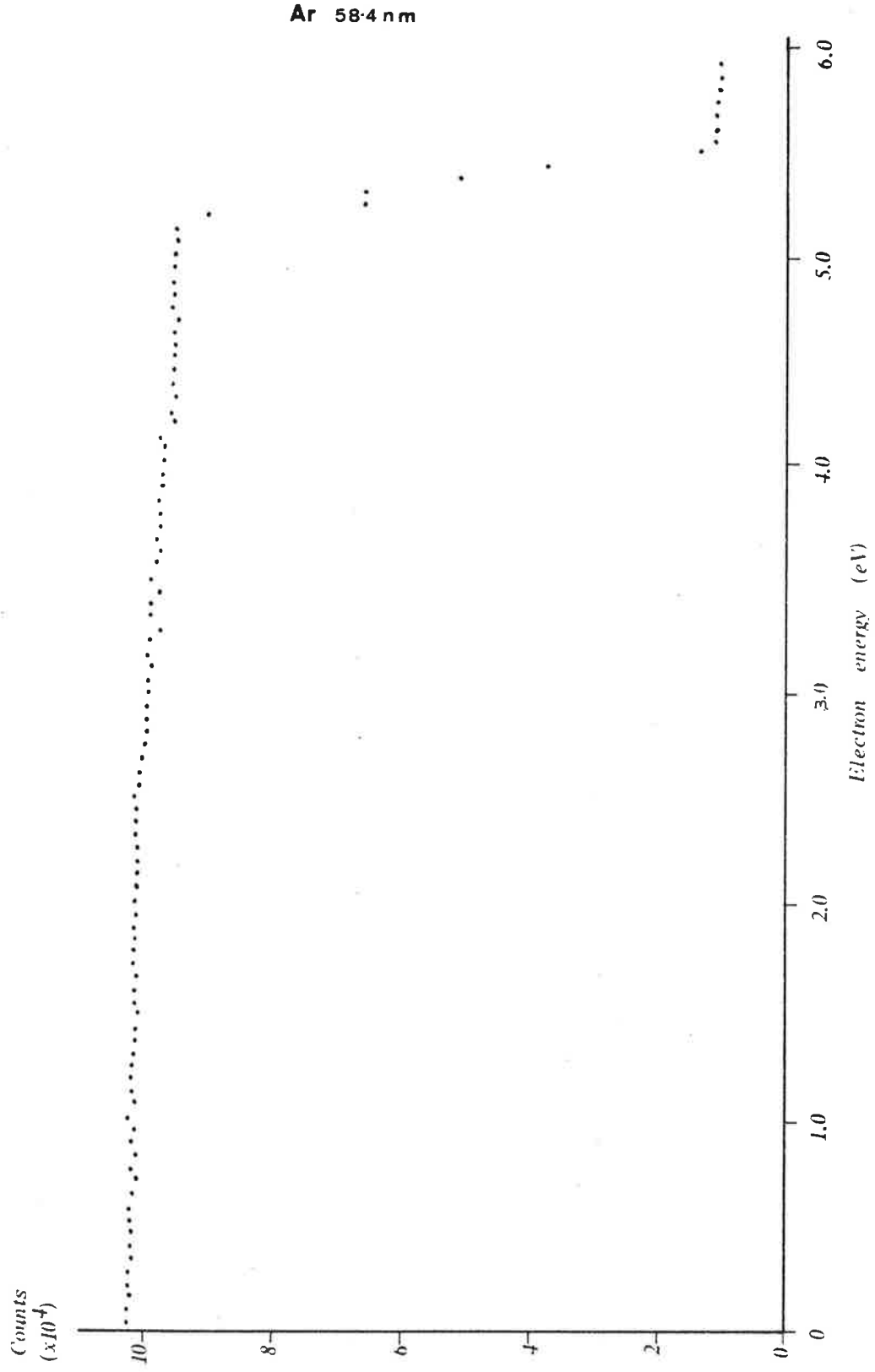

Fig. A3. Total photoelectron spectrum of Argon at 58.4nm.

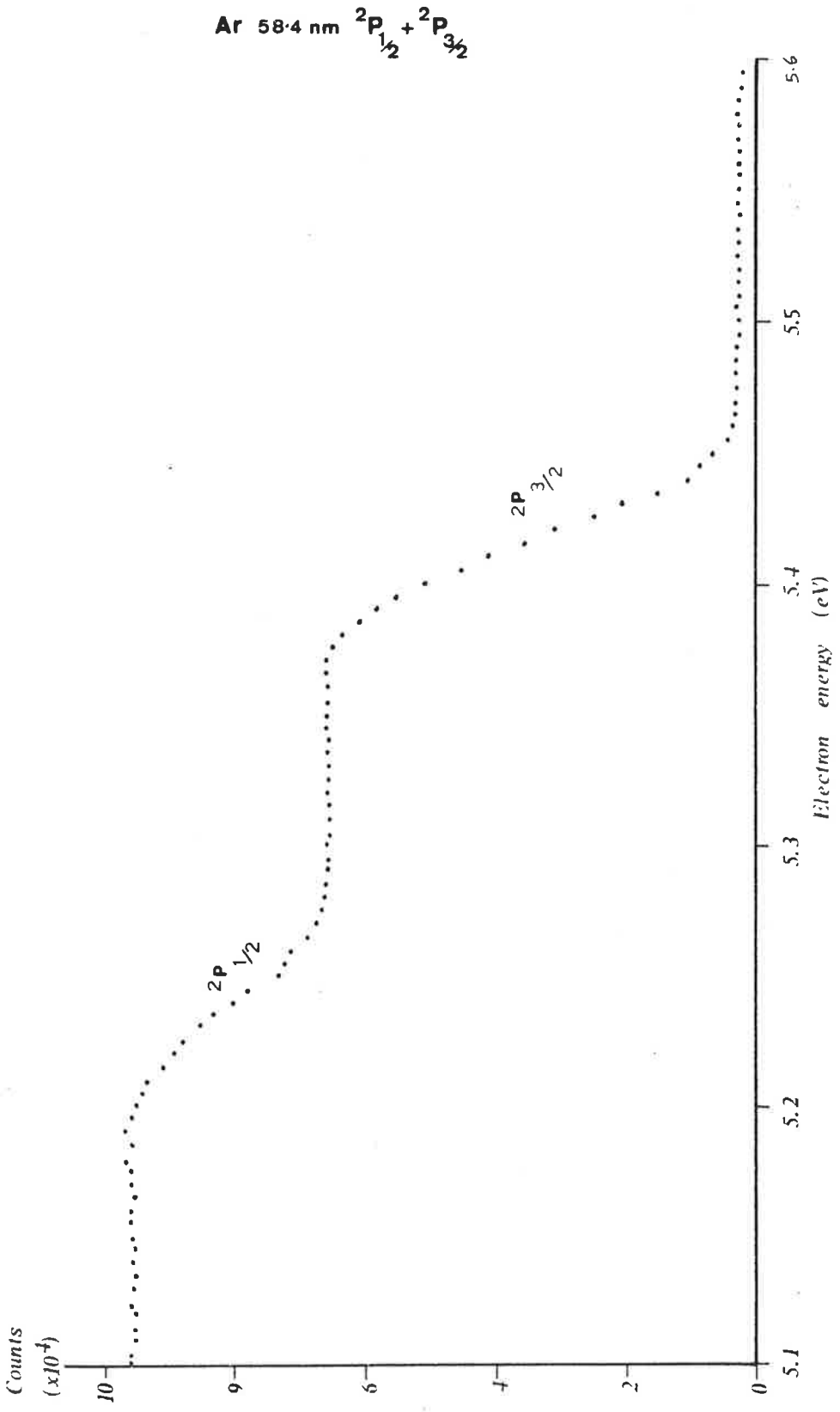

Fig. A4. Photoelectron spectrum of Argon at 58.4nm scanned across the $^2P_{1/2}$ and $^2P_{3/2}$ states.

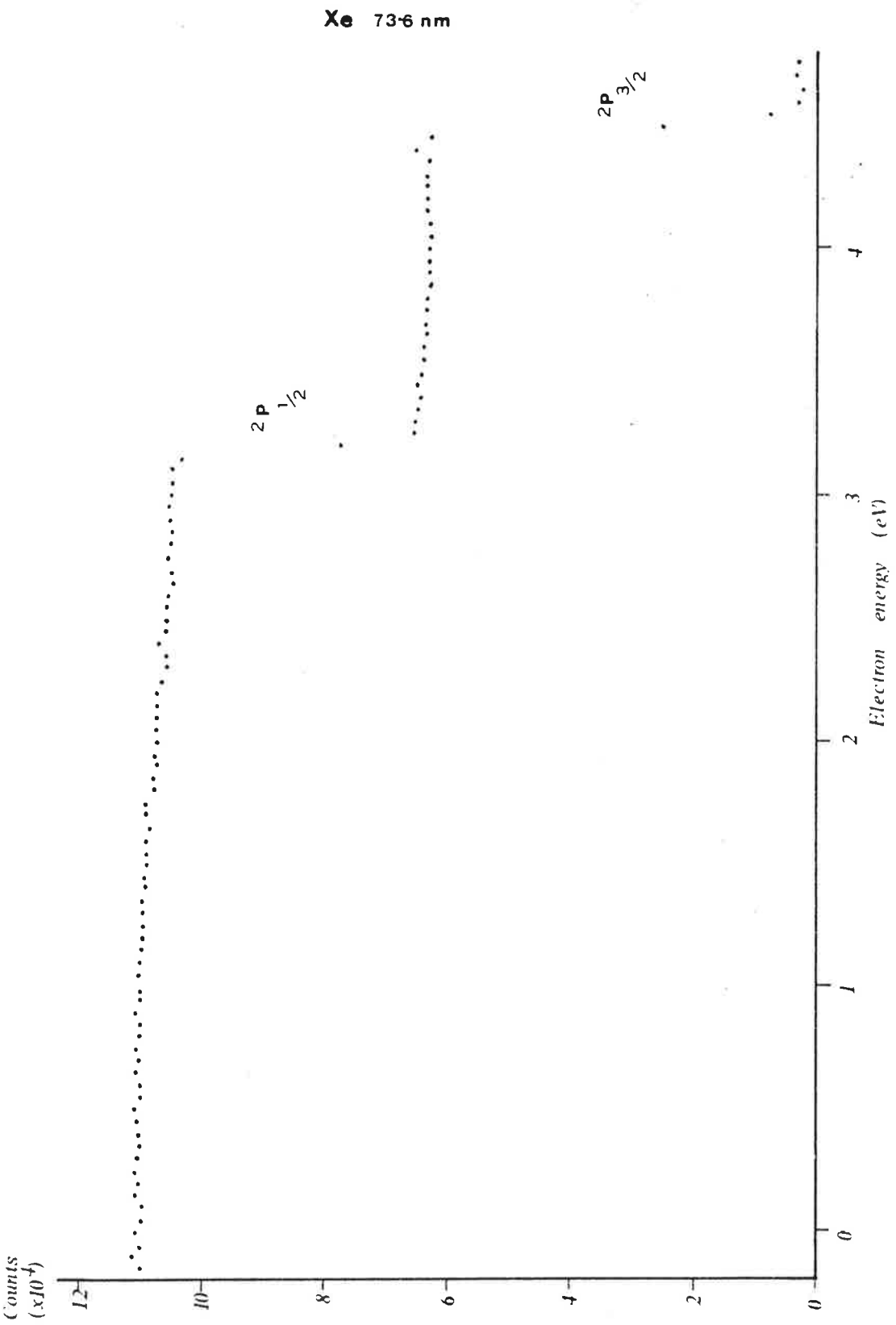

Fig. A5. Total photoelectron spectrum of Xenon at 73.6nm.

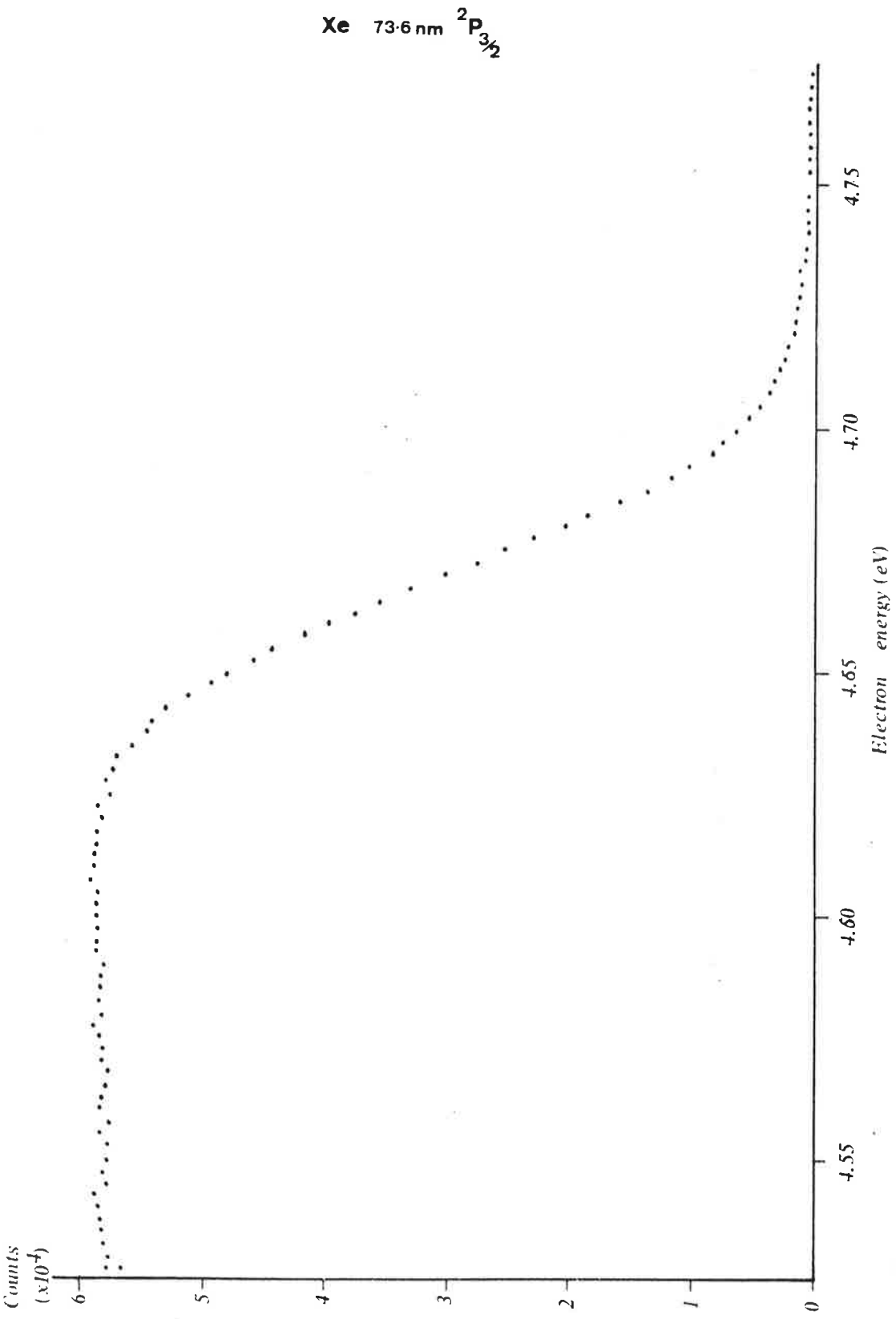

Fig. A6. Photoelectron spectrum of the $^2P_{3/2}$ state of Xenon at 73.6nm.

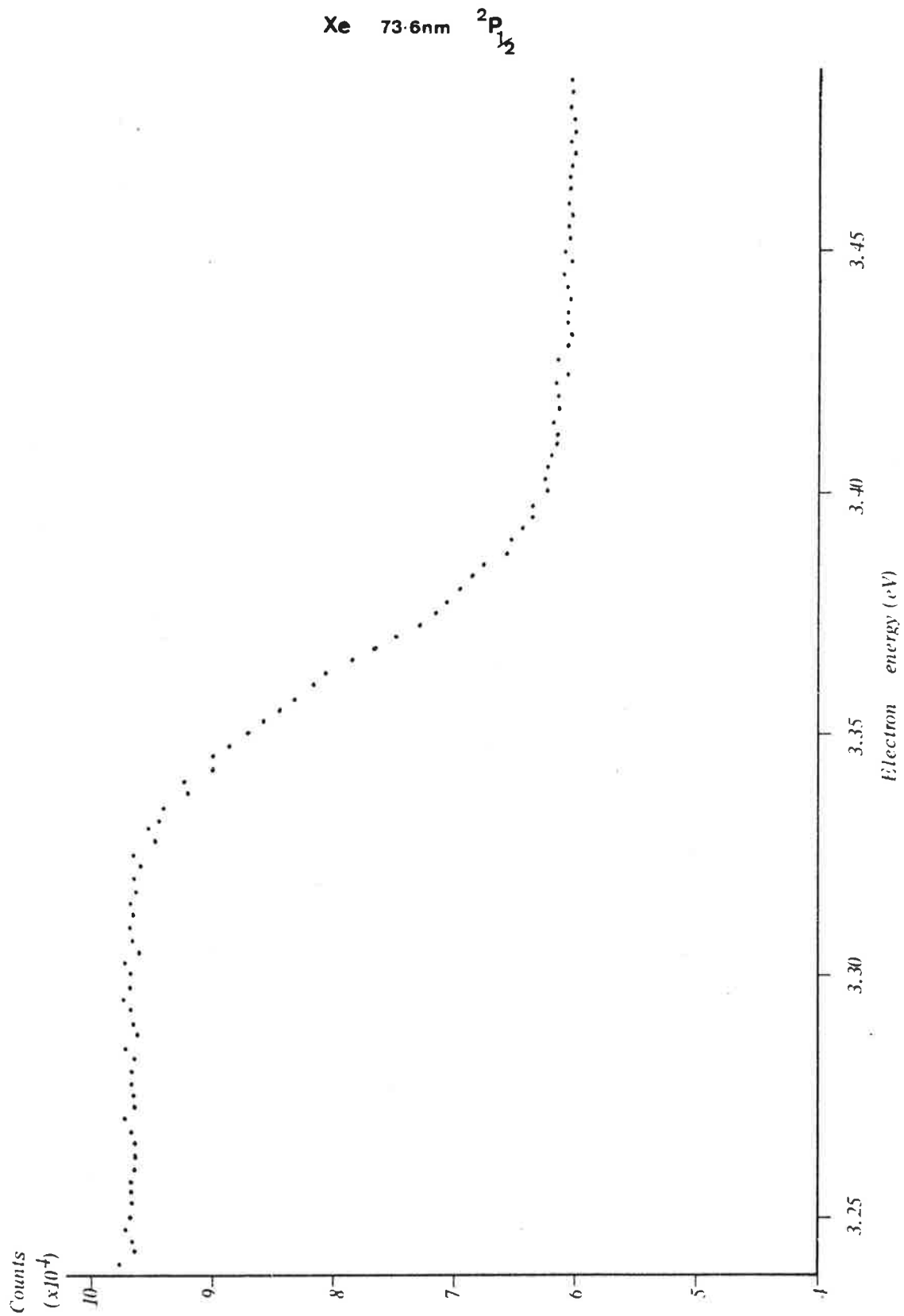

Fig. A7. Photoelectron spectrum of the $^2P_{1/2}$ state of Xenon at 73.6nm.

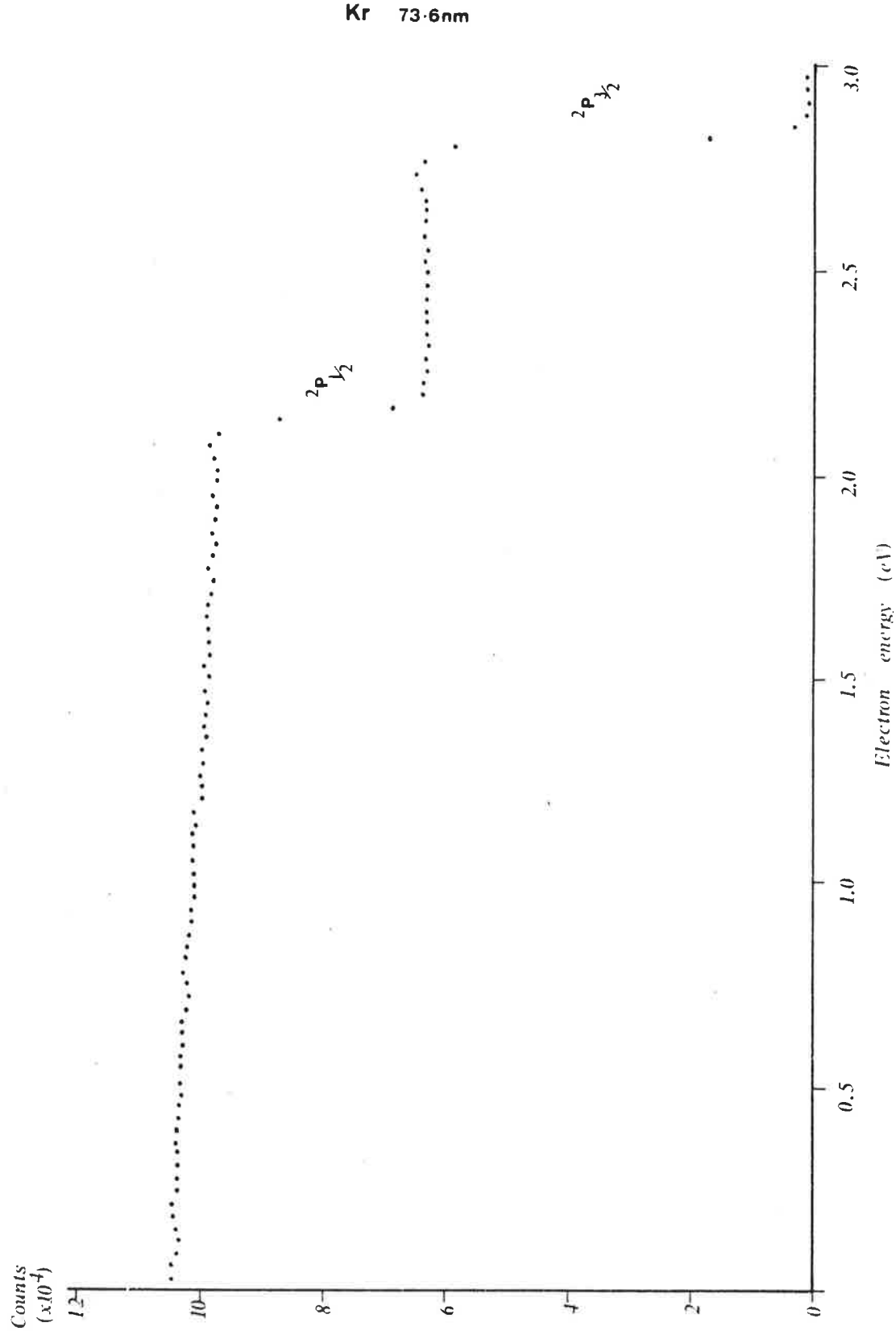

Fig. A8. Total photoelectron spectrum of Krypton at 73.6nm.

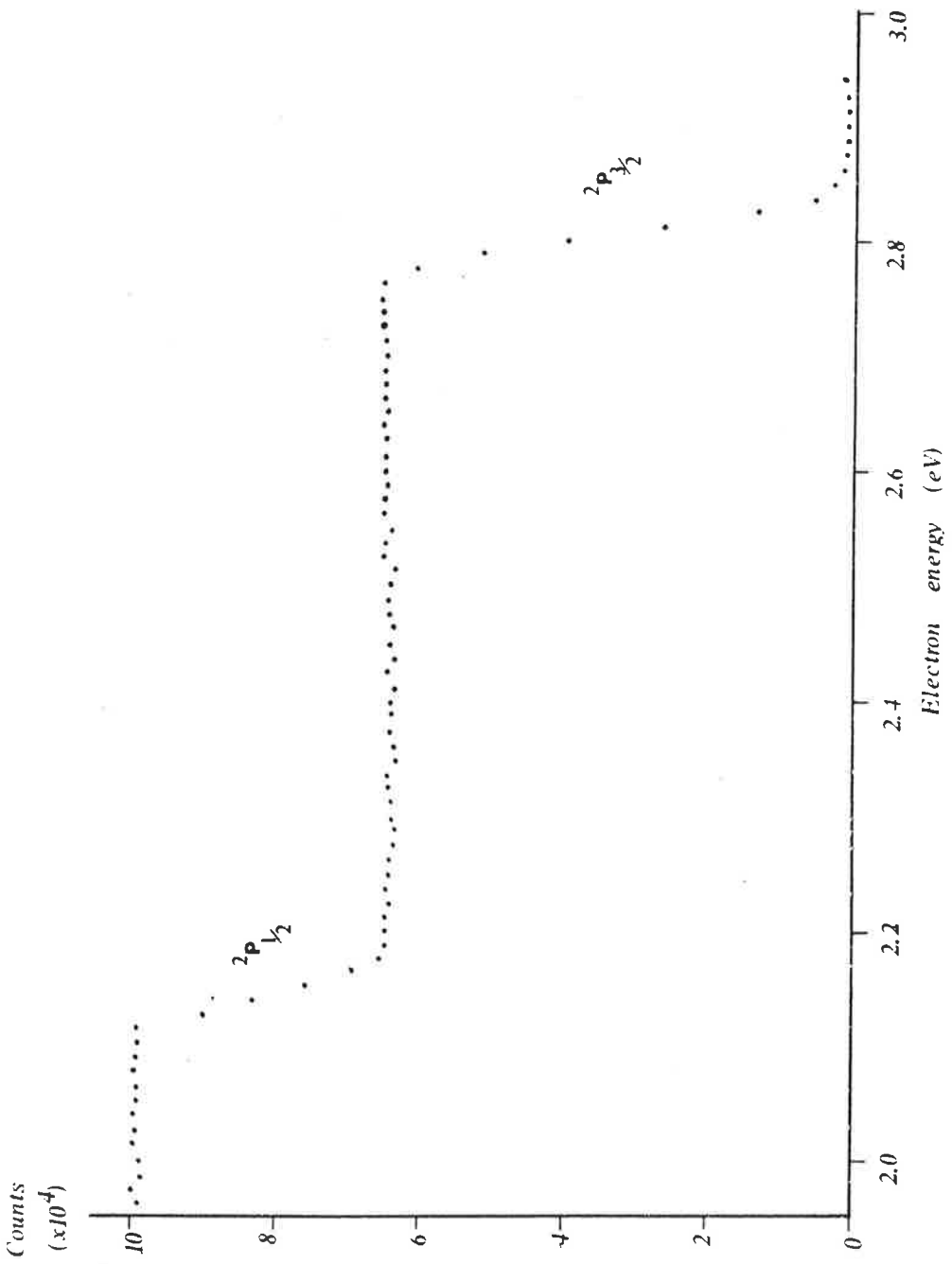

Fig. A9. Photoelectron spectrum of Krypton at 73.6nm scanned across the $^2P_{1/2}$ and $^2P_{3/2}$ states.

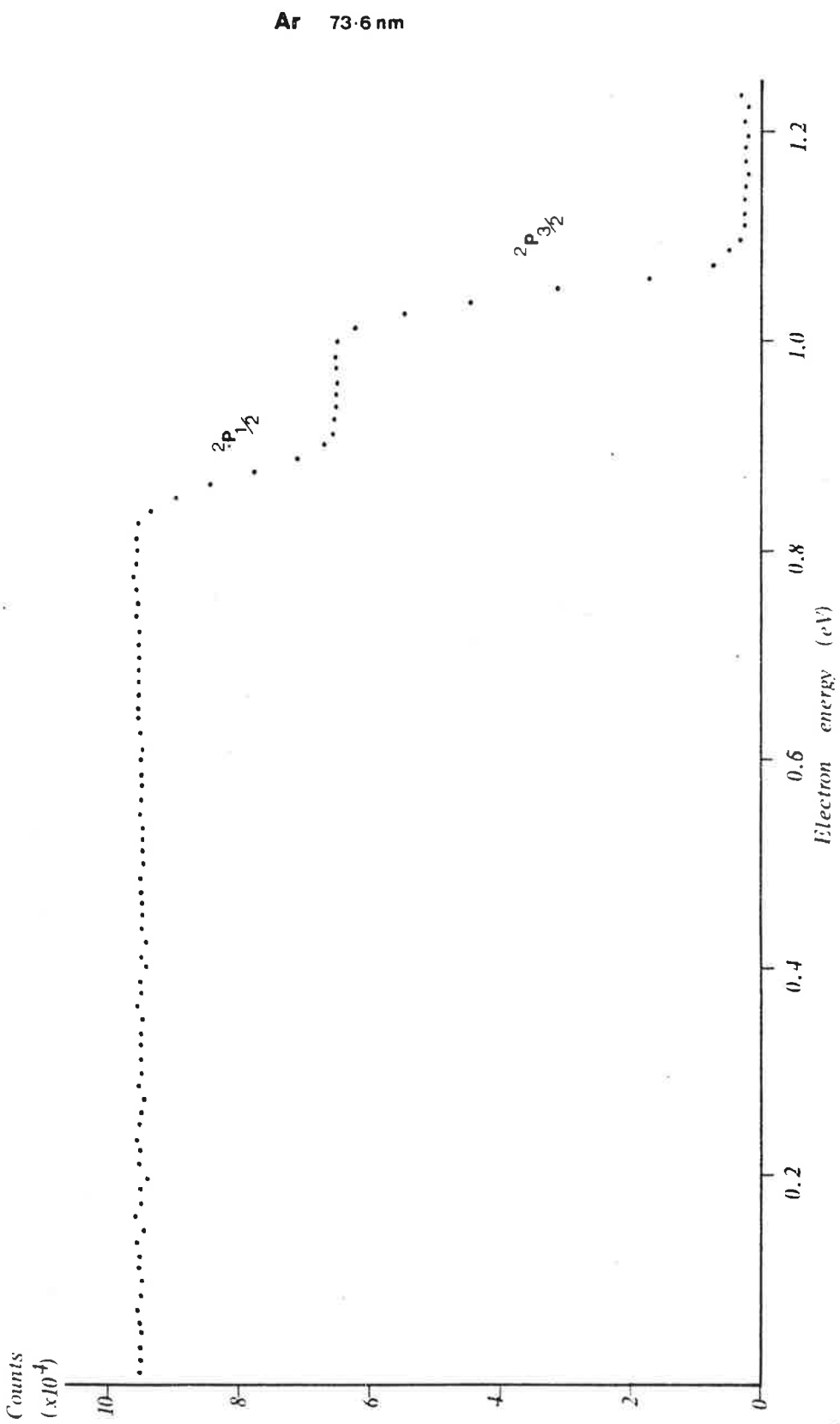

Fig. A10. Photoelectron spectrum of Argon at 73.6nm.

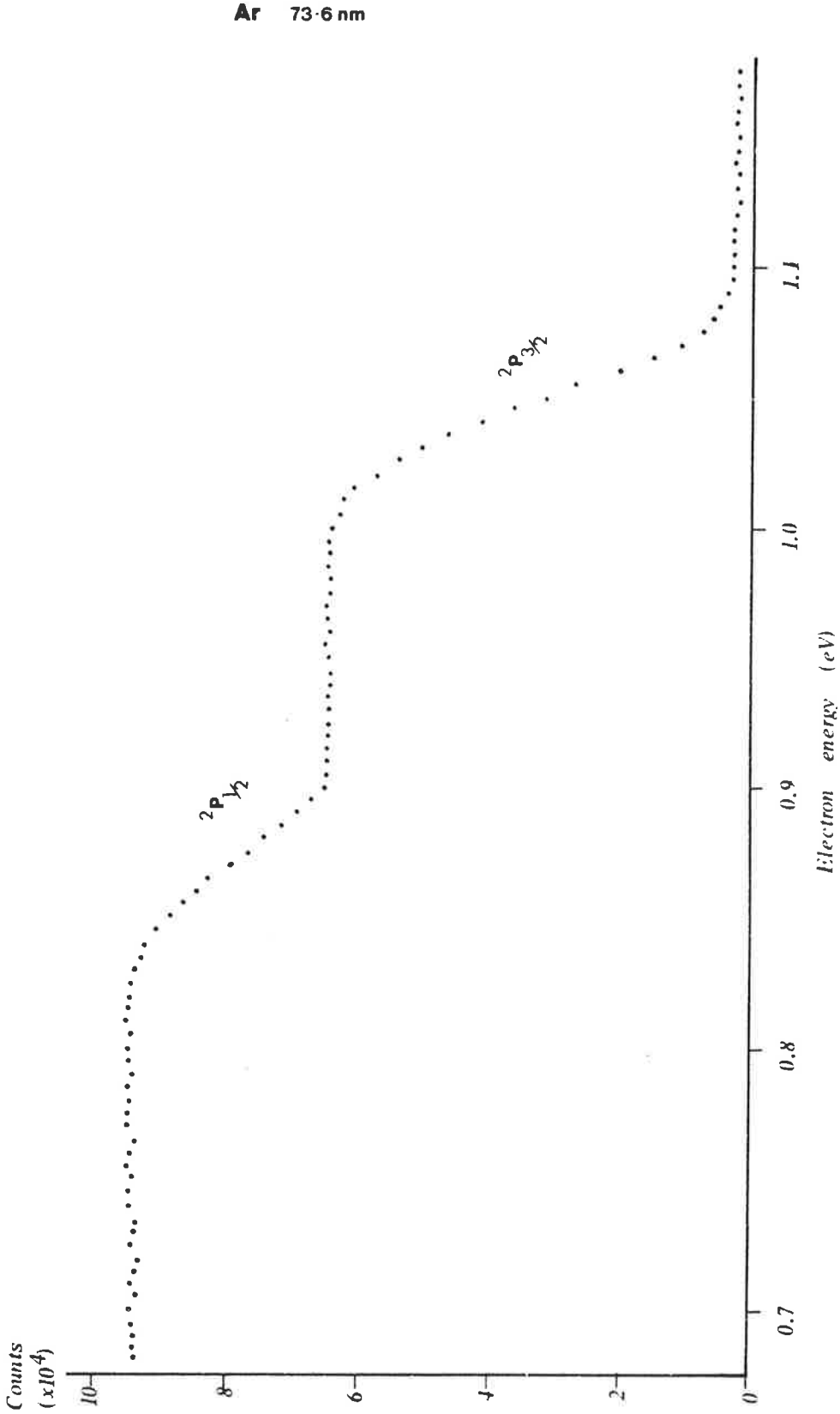

Fig. A11. Photoelectron spectrum of Argon at 73.6nm scanned across the $^2P_{1/2}$ and $^2P_{3/2}$ states.

Fig. No.	Gas	State	λ (nm)	E (eV)	I.P. (eV)	Gas Press (μ)	Light: Ent. slits (μ)	Light: Exit slits (μ)	Light: Resol (nm)	Light: Lamp Press Torr	Light: V_{PM}	Light: Lamp Power I(mA)	Light: CCO freq kHz	Timer	Time: No. of scans	Time: Total-timerx scans	Time: Time/ scan mins	Time: Tot. time hours	Retarding Pots.*: D/A SL	Retarding Pots.*: SL (V)	Retarding Pots.*: D/A ss	Retarding Pots.*: ss mV)	No. of chan	Max Count (k)
2.9a)	Xe	Total	58.4	21.23	7.78	0.35	1000	400	0.01	0.5	510	,60	9.3	$5x10^{-3}$	32	0.16	2	1	0040	0.000	40	100	100	140
2.9b)	"	Both	"	"	"	"	"	"	"	"	"	"	"	"	"	"	"	"	2930	7.225	08	40	"	"
2.9c)	"	$P^1/_2$	"	"	"	"	"	"	"	"	"	"	"	"	"	"	"	"	3080	7.600	01	2.5	"	"
2.9d)	"	P3/2	"	"	9.09	"	"	"	"	"	"	"	"	"	"	"	"	"	3590	8.875	"	"	"	80
3.1	N_2	Total	"	"	5.62	"	"	"	"	"	620	"	23	$2x10^{-2}$	20	0.4	1	0.3	0000	0.000	25	62.5	"	500
3.2	"	$B^2\Sigma u$	"	"	2.42	"	"	"	"	"	"	"	"	"	40	0.8	"	0.6	0280	0.700	08	20	"	90
3.3	"	$A^2\pi u$	"	"	4.50	"	"	"	"	"	"	"	"	"	50	1.2	"	0.9	1075	2.688	08	20	"	120
3.4	"	$X^2\Sigma g^-$	"	"	5.62	"	"	"	"	"	"	"	"	"	"	"	"	"	1960	4.900	04	10	"	50
3.5	O_2	Total	"	"	9.17	0.5	"	"	"	"	"	"	25	$2x10^{-2}$	40	0.8	1	0.6	0000	0.000	40	100	100	90
3.6	"	$X^2\pi g$	"	"	"	"	"	"	"	"	"	"	"	"	"	"	"	"	3000	7.500	08	20	"	40
3.8	"	A + a	"	"	4.18	"	"	"	"	"	"	"	"	"	80	1.6	"	1.2	1200	3.000	09	22.5	"	120
3.9	"	$b\Sigma g^-$	"	"	3.06	"	"	"	"	"	"	"	"	"	100	2.0	"	1.5	0840	2.100	06	15	"	240
3.10	"	$B^2\Sigma g^-$	"	"	0.93	"	"	"	"	"	"	"	"	"	80	1.6	"	1.2	0000	0.000	05	12.5	"	200
3.12	O_2	Jo	89.4	13.87	1.90	3	100	100	0.13	34	900	65%	6	$5x10^{-3}$	426	2.13	1	1.2	1200	3.000	09	22.5	100	6
3.13	"	X	89.2	13.90	1.84	"	"	"	"	"	"	"	5.4	$4x10^{-3}$	220	0.88	"	4	0000	+0.102	08	20	"	2.5
3.14	"	OR1	88.9	13.95	1.88	"	"	160	0.2	"	"	60%	8	$8x10^{-3}$	200	1.6	1.2	4	"	"	09	22.5	"	3
3.15a)	"	J1	88.6	14.00	1.93	0.6	"	"	"	40	"	"	11	"	1180	9.44	1.5	30	"	"	"	"	"	10
3.15b)	"	"	"	"	"	3	"	"	"	"	"	"	6	"	300	2.4	2.3	11	"	"	"	"	"	12
3.15d)	"	"	"	"	"	"	50	80	0.1	"	"	"	1.4	$2x10^{-3}$	520	1.04	2	17	"	"	"	"	"	6
3.15e)	"	"	"	"	"	"	100	100	0.13	30	"	"	7.8	$5x10^{-3}$	690	0.7	1.2	13	"	"	"	"	"	12
3.16	"	OR2	88.2	14.06	2.00	"	"	160	0.2	"	"	"	7.6	$8x10^{-3}$	800	6.4	1.2	16	"	"	"	"	"	12
3.17	"	J2	87.8	14.12	2.05	"	"	100	0.13	"	"	"	7.1	$5x10^{-3}$	1020	5.1	1	17	"	"	"	"	"	14
3.18	"	J3	87.1	14.23	2.16	"	"	"	"	"	"	,13	7	"	480	2.4	"	10	"	"	10	25	"	6
A1	Kr	Total	58.4	21.23	6.55	0.4	1000	400	0.01	0.45	510	,60	10	$5x10^{-3}$	16	0.08	2	0.5	0040	0.000	16	40	100	100
A2	"	Both	"	"	"	"	"	"	"	"	"	"	"	"	"	"	"	"	2560	6.300	01	2.5	"	100
A3	Ar	Total	"	"	5.28	0.5	"	"	"	"	"	"	"	"	"	"	"	"	0040	0.000	12	30	200	100
A4	"	Both	"	"	"	"	"	"	"	"	"	"	"	"	"	"	"	"	2080	5.100	01	2.5	"	100
A5	Xe	Total	"	"	3.41	0.3	"	"	"	"	"	"	"	"	20	0.1	0.5	0.2	0000	+0.100	10	25	"	110
A6	"	P1/2	"	"	"	"	"	"	"	"	"	"	"	"	"	"	"	"	1335	3.228	01	2.5	100	100
A7	"	P3/2	"	"	4.72	"	"	"	"	"	"	"	"	"	"	"	"	"	1850	4.625	01	2.5	"	60
A8	Kr	Total	73.6	16.85	2.85	0.45	250	350	"	"	540	,100	9	"	"	"	"	"	0040	0.000	06	15	200	100
A9	Kr	Both	"	"	"	"	"	"	"	"	"	"	"	"	"	"	"	"	0820	1.950	01	2.5	400	100
A10	Ar	Total	"	"	0.90	0.5	"	"	"	"	"	"	"	"	26	0.13	"	0.3	0040	0.000	05	12.5	100	100
A11	"	Both	"	"	"	"	"	"	"	"	"	"	"	"	"	"	"	"	0310	0.675	01	2.5	200	100

* D/A SL is the nubber on the retarding potential box which sets the initial voltage (LINDEMANS,1981)
SL(V) is the initial voltage
D/A ss is the number on the retarding potential box which sets the number of 2.5mV per channel
ss(mV) is the "step-size" i.e. the number of mV per channel

ANALYSER GRID VOLTAGES

For spectra 2.9a) - d), 3.12 - 3.14, 3.15e) - A11, $V_{CF} = V_F = 900V$, $V_a/V_r = 0.968$.
For the rest $V_{CF} = V_F = 650V$, $V_a^a/V_r^r = 0.91$

APPENDIX 3

Publications

The following paper has been written in conjunction with the work described in this thesis.

"An instrument for measuring branching ratios in photoionizing processes."

W.Lindemans, A.J.Blake , J.H.Carver, J.M.Hutton and L.Torr.

J.of Elec. Spec. and Rel. Phen.,1979,15, 287.

Journal of Electron Spectroscopy and Related Phenomena, 15 (1979) 287—294

AN INSTRUMENT FOR MEASURING BRANCHING RATIOS IN PHOTOIONIZING PROCESSES

W. LINDEMANS, A.J. BLAKE, J.H. CARVER, J.M. HUTTON and L. TOROP.
Physics Department, University of Adelaide, ADELAIDE AUSTRALIA 5001.

ABSTRACT

An instrument using photo-electron spectrometry has been developed to measure branching ratios and relative partial cross-sections for photoionizing processes in gases, with particular emphasis given to measuring variation of these parameters as a continuous function of wavelength. The instrument is described together with a consideration of sources of errors and a method of calibration.

INTRODUCTION

Measurements of partial cross-sections for photoionization processes which leave the ions of atoms and simple molecules in particular quantum states as a continuous function of wavelength have been reported by several authors (Ref. 1, 2 and 3). There is growing interest in accurate measurements of these partial cross-sections to provide data needed to model photoionization processes in the atmosphere and also as a method of studying basic atomic and molecular processes such as auto-ionization (Ref. 4, 5 and 6).

The technique of photo-electron spectrometry provides direct information about the probabilities of populating different states of the ions produced by the absorption of ultraviolet radiation (Ref. 1). This report describes an apparatus for measuring partial photoionization cross-sections continuously over a wavelength region where thresholds for many photoionization processes occur, and the total cross-section has structure associated with autoionization. The apparatus must include a tunable light source with sufficient wavelength resolution to distinguish autoionizing resonances in the cross-sections, and an electron energy analyser with an energy resolution of 100 meV or better to separate the vibrational levels of simple molecules. Since the intensity of the dispersed continuum light source used in this investigation is very low it was important to choose an electron energy analyser with a large electron collecting aperture, and to ensure that the analyser is highly stable over long data collecting periods. It was also necessary to develop a simple method of calibrating the relative electron collecting efficiency of the analyser as a function of electron energy, and to ensure that the sample of

photo-electrons collected by the analyser is independent of the angular distribution with which the electrons are released (Ref. 7).

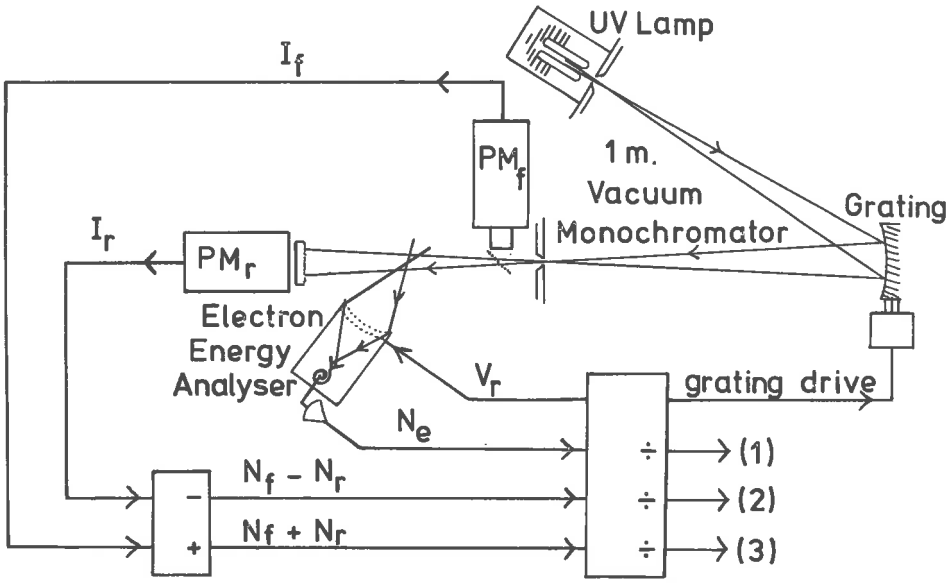

Fig. 1. Schematic diagram of experimental apparatus: (1) $N_e/(N_f - N_r)$, (2) $N_e/(N_f + N_r)$, (3) $(N_f - N_r)/(N_f + N_r)$

THE APPARATUS

Figure 1 gives a schematic view of the system used. A Hinteregger lamp filled with helium at a pressure of approximately 25 Torr and excited by a 5 kV pulsed discharge gives the characteristic Hopfield continuum (Ref. 8). Light from the discharge is dispersed by a one-metre normal incidence vacuum monochromator and the intermediate region between lamp and monochromator is differentially pumped to maintain the monochromator at a pressure less than 5×10^{-5} Torr.

Because very low light levels are obtained from such sources, a spherical grid retarding potential analyser is used to energy analyse the photo-electrons produced. Separate pumping of the analyser allows the detector pressure to remain below 5×10^{-4} Torr while the target gas pressure could be as high as 5×10^{-3} Torr.

Light monitors are placed equal distances in front of and behind the ionization region viewed by the analyser. Whereas a single light detector can be used to correct the electron signal for variations of light intensity with time, when the wavelength is scanned over a region where the cross-section of the target gas and absorption varies greatly, there will be significant errors in using this signal as a monitor of the light intensity in front of the electron analyser. Two detectors give information about the intensity of the light beam in the region viewed by the

analyser regardless of variations in the lamp intensity, gas pressure or absorption cross-section. The signals from the electron analyser and light monitors are each digitised and are processed in various ways described below.

As well as its large collecting aperture for a given resolution (Ref. 9) the spherical grid retarding potential analyser has the advantages of simplicity, stability, and ease of energy calibration. The integral form of the energy spectrum which it gives has the advantage of allowing simultaneous scanning of the wavelength and electron energy.

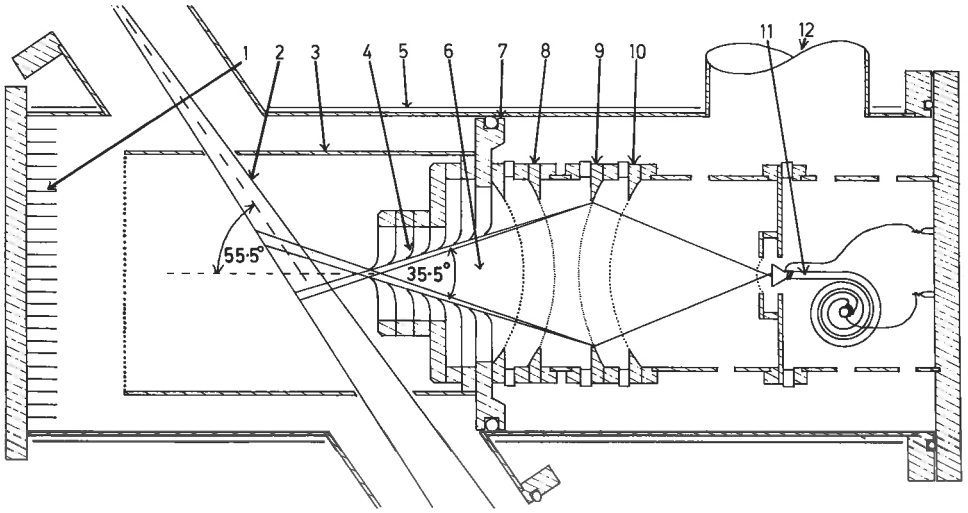

Fig. 2. Cross section of retarding grid electron energy analyser: (1) Electron & light trap, (2) Light beam, (3) Interaction chamber, (4) Electron baffle, (5) Magnetic shielding, (6) Field free region, (7) Gas partition flange, (8) Retarding grid, (9) Accelerating grid, (10) Focussing grid, (11) Channel electron multiplier, (12) Pumping port.

Figure 2 shows the electron analyser in section. Electrons are detected by a channel electron multiplier after traversing four wire grids which have a combined transparency of 45 per cent. The first grid is at the potential of the ionization region, while the second carries the retarding potential (V_r). The third grid gives the electrons a small acceleration, and a large focussing potential is applied between the third and fourth grids. Fine mesh with a wire spacing of 0.2 mm is used for the second and third grids to minimise the effects of field penetration. These effects contribute about 0.2 per cent to the energy resolution in the present analyser (Ref. 10).

The analyser chamber is completely surrounded with several layers of high permeability magnetic shielding which reduces the magnetic field inside

the analyser to less than 0.06 gauss. Residual magnetic fields are responsible for the low energy resolution limit of about 20 meV and effectively "retard" all incoming photo-electrons by a further 20 meV (Ref. 10). The entrance aperture of the analyser has been chosen to contribute about 0.1 per cent to the resolution. The net effect of these three limitations to the resolution is shown in Figure 3.

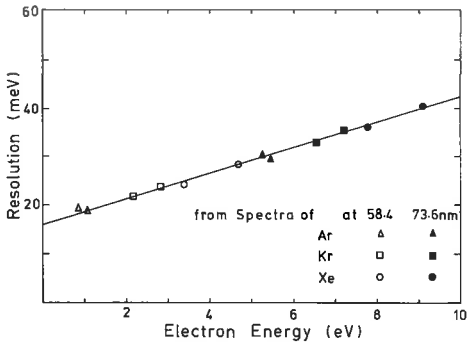

Fig. 3. Electron energy dependence of the resolution of the electron analyser. Resolution is defined as the F.W.H.M. of the differentiated spectrum

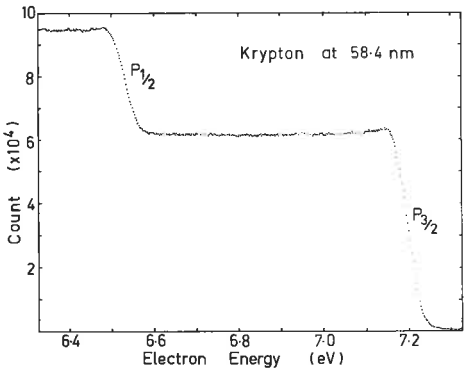

Fig. 4. Integral photo-electron spectrum for Krypton at 58.4 nm scanned across the $^2P_{1/2}$, $^2P_{3/2}$ steps, showing the characteristic spectrum of the analyser

The analyser has been gold plated on all its important surfaces, to minimise stray electric fields. However, dielectric surface contamination from vacuum oil deposits can cause serious loss of resolution to as much as 100 meV with offset errors of up to 60 meV and great instability. Contaminants are removed in a vapour bath, restoring the analyser's characteristics.

The spectrum of mono-energetic electrons from an ideal retarding potential analyser is a simple step. Careful adjustment of the potentials applied to the third and fourth grids produces a characteristic spectrum which is close to this ideal shape, and the present analyser gives a spectrum which is flat to within 3 per cent for all electron energies up to 10 eV. A typical integral spectrum is shown in Figure 4. The very low background count in this spectrum is mainly due to photo-electrons from the residual zenon impurity in krypton. An aluminium trap in front of the electron analyser efficiently reduces background count due to scattered photons and photo-electrons. The dark count rate of the channel electron multiplier is less than 0.05 Hz.

ANGULAR DISTRIBUTION OF THE PHOTO-ELECTRONS

The axis of the electron energy analyser has been aligned to the light beam at

an angle that makes the partial cross-section measurement independent of the angular distribution of the photo-electrons. It is well known (Ref. 11) that if unpolarized radiation is used the differential cross-section for electrons emitted in a dipole transition in a direction θ to the beam direction is given by

$$\frac{d\sigma}{d\omega} = \frac{\sigma_{total}}{4\pi} \left[1 - \frac{\beta}{2} P_2(\cos\theta) \right] \qquad (1)$$

where β is an assymetry parameter. For $\theta = 54^\circ 44'$ the relation between the differential cross-section and the total cross-section is independent of β. It can be shown (Ref. 12) that the number of electrons emitted from a point source into any circular cone is independent of β if the angle Φ between the axis of the analyser and the beam direction is $54^\circ 44'$. For the case of electrons emitted from a beam of finite dimensions the angular distribution is modified by a term which is approximately $(\sin\theta)^{-1}$, but the electron count is still independent of β in the limit of a small acceptance cone of the analyser, for $\Phi = 54^\circ 44'$. For the combination of finite beam source and finite entrance aperture the electron count rate is found by integrating (1) over the source volume and the cone of acceptance into the analyser. The expression which results has the form:

$$I(\Phi) = A(\Phi) + \beta B(\Phi) \qquad (2)$$

The value of Φ for which $B(\Phi) = 0$, making the electron count rate proportional to the cross-section σ_{total} depends on the geometry of the system and for the present apparatus is $55^\circ 33'$. In a comparison of the partial cross-sections of two processes which have different values of β an error will result if the analyser is not aligned to this direction. The largest possible error of 3.6 per cent per degree of misalignment, occurs when the values of β are respectively $+2$ and -1. Such errors can be expected in the vicinity of auto-ionizing resonances where rapid changes in β occur (Ref. 13). Sensitivity to partial polarization of the light beam is removed by placing the axis of the analyser in a plane which is at 45° to the Rowland plane of the monochromator.

EXPERIMENTAL METHODS

As indicated in Figure 1 the signals from two light monitors are available in addition to the electron count rate. Let the count rates from the detectors be N_f for the front light monitor, N_r for the rear light monitor, and N_e for the electron analyser. The photo-electron spectrum at a particular wavelength is found by recording N_e as a function of the retarding potential V_r. The quantity $N_f + N_r$ is proportional to the average light flux in the region viewed by the analyser, and the quantity $N_f - N_r$ is proportional to the light flux which is absorbed in the region viewed by the analyser. Hence, the electron count rate can be made independent of lamp intensity fluctuations by recording the quantity

$N_e(V_r)/(N_f + N_r)$, and it is independent of both lamp intensity and target gas pressure fluctuations if the quantity $N_e(V_r)/(N_f - N_r)$ is recorded.

The data handling system which has been developed for the apparatus also allows other useful combinations of the three count rates to be recorded as the wavelength is scanned. The quantity $(N_f - N_r)/(N_f + N_r)$ is proportional to the total absorption cross-section of the target gas to an excellent approximation, provided the transmission of the gas is greater than 70 per cent. Wavelength dependence of the total ionization cross-section can be determined by setting the analyser retarding potential to zero and recording $N_e(0)/(N_f + N_r)$. Similarly the ionization yield is proportional to $N_e(0)/(N_f - N_r)$.

These expressions are valid only if the efficiency with which the analyser detects an electron is independent of the energy of the electron. It is commonly the case that the efficiency for counting low energy electrons is energy dependent, and any such variations must be carefully measured so that the relative strengths of features in photo-electron spectra can be accurately compared. If the relative efficiency for counting electrons of energy E is $\varepsilon(E)$, then the quantity $N_e(0)/(N_f - N_r)$ is proportional to the photoionization yield multiplied by $\varepsilon(E)$. The form of $\varepsilon(E)$ can be found by measuring the apparent yield for an atomic gas for which the yield is equal to unity. The result obtained from observations of transitions to the $^2P_{3/2}$ state of the zenon ion is shown in Figure 5.

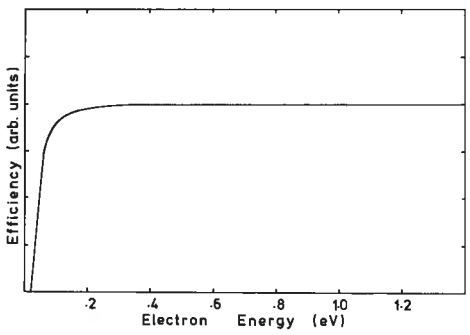

Fig. 5. Electron energy dependence of the collecting efficiency of the electron analyser obtained by recording $\frac{N_e(0)}{N_f - N_r}$ with zenon as the sample gas.

It is apparent that the analyser has an excellent efficiency characteristic which is constant within a few per cent for electron energies greater than 100 meV. The characteristic is found to be stable so that the measurements of partial photo-ionization cross-sections can be made for electron energies as low as 60 meV.

Examples of results which have been obtained with the apparatus are shown in Figures 6 to 8. Figure 6 shows the relative total absorption of oxygen in a

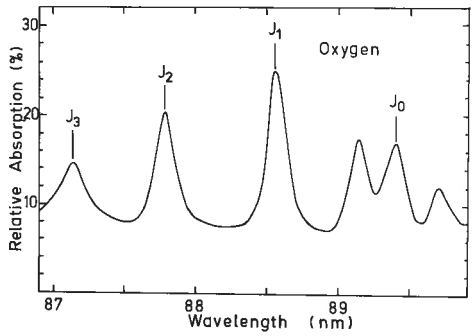

Fig. 6. Relative absorption by oxygen in a region oa autoionizing resonances obtained by recording $\frac{N_f - N_r}{N_f + N_r}$ and scanning wavelength.

region containing autoionizing resonances. Figure 7 shows oxygen integral photoelectron spectra recorded at a wavelength coinciding with an autoionizing resonance and at a nearby "off-resonance" wavelength. Figure 8 shows partial cross-sections for nine vibrational levels of the O_2^+ ground state as a function of wavelength across two of the autoionizing resonances.

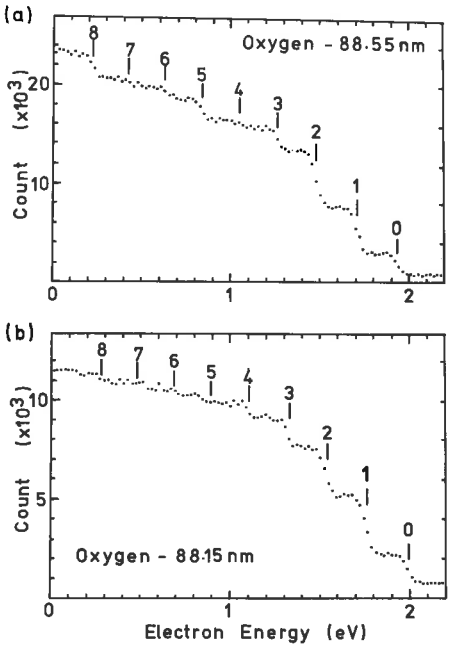

Fig. 7. Integral photo-electron spectra for oxygen: (a) on the J_1 autoionizing resonance, (b) between the J_1 and J_2 resonances.

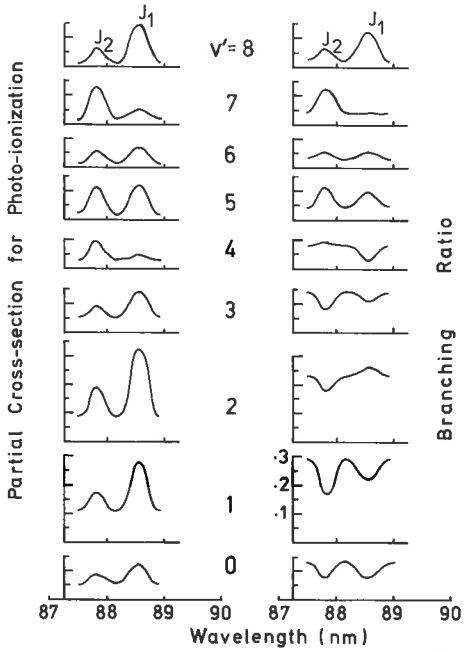

Fig. 8. Smoothed scans across the J_1 and J_2 resonances of oxygen at 0.2 nm resolution, showing the partial cross-sections and branching ratios for the nine vibrational levels.

CONCLUSION

The apparatus described in this paper has excellent characteristics for measurement of partial photoionization cross-sections as a continuous function of wavelength. The measurements are independent of the angular distribution of the photoelectrons, and can be made with a range of photon energies extending close to the threshold for the ionizing process under study. This technique is a valuable tool in the study of the autoionizing process, and other sources of structure in the photoionization cross-sections of atoms and simple molecules, and provides data which is needed for the modelling of atmospheric photoionization.

ACKNOWLEDGEMENTS

The authors acknowledge the technical assistance of J. A. Wright and S. C. Dowden. The work was supported by the Australian Research Grants Committee.

REFERENCES

1. A.J. Blake and J.H. Carver, J. Chem. Phys., 47(1967)1038-1044.
2. P.R. Woodruff and G.V. Marr, Proc. Roy. Soc. Lond. A 358(1977)87-103.
3. C.E. Brion, Radiation Research, 64(1975)37-52.
4. J.A.R. Samson, J.L. Gardner and A.F. Starace, Phys. Rev. A, 12(1975)1459-1463.
5. J.L. Bahr, A.J. Blake, J.H. Carver, J.L. Gardner and Vijay Kumar, J. Quant Spectrosc. Radiat. Transfer., 11(1971)1839-1852.
6. R.S. Stolarski and N.P. Johnson, J. Atmos. Terrestrial Phys. 34(1972)1691-1701.
7. J.A.R. Samson and J.L. Gardner, J. Opt. Soc. Am. 62(1972)856-864.
8. R.E. Huffman, J.C. Larrabee and D. Chambers, Appl. Optics, 4(1965)1145-1150.
9. D.W.O. Heddle, J. Phys. E: Sci. Instrum, 4(1971)589-592.
10. D.A. Hutchital and J.D. Rigden, J. Appl. Phys, 43(1972)2291-2302.
11. J. Cooper and R.N. Zare, J. Chem. Phys. 48(1968)942-943.
12. D. Gigney and W. Lindemans, in preparation.
13. D. Dill, Phys. Rev. A, 7(1973)1976-1987.

BIBLIOGRAPHY

Asundi, R.K. and Ramachandrarao, Ch.V.S., 1969. Chem. Phys. Letts, 4, 89.

Bahr, J.L., Blake, A.J., Carver, J.H. and Kumar, V., 1969. J.Q.S.R.T., 9, 139.

Bahr, J.L. Blake, A.J., Carver, J.H., Gardner, J.L. and Kumar, V., 1971 a) J.Q.S.R.T., 11, 1839.

Bahr, J.L., Blake, A.J., Carver, J.H., Gardner, J.L. and Kumar, V., 1971 b) J.Q.S.R.T., 11, 1953.

Bahr, J.L., Blake, A.J., Carver J.H., Gardner, J.L. and Kumar, V., 1972, J.Q.S.R.T., 12, 59.

Bahr, J.L., 1973. Contemporary Physics, 14, 329.

Baker, A.D. and Betteridge, D., 1972. "Photoelectron Spectroscopy". (Pergamon Press, Oxford).

Bardsley, J.N., 1968. Chem. Phys. Letts, 2, 329.

Berkowitz, J., Ehrhardt, H. and Tekaat, T., 1967. Z. Phys., 200, 69.

Berkowitz, J. and Chupka, W., 1969. J. Chem. Phys., 51, 2341.

Bevington, P., 1969. "Data Reduction and Error Analysis for Physical Sciences" (McGraw-Hill).

Beutler, H., 1935. Z. Phys., 86, 710.

Blake, A.J. and Carver, J.H., 1967. J. Chem. Phys., 47, 1038.

Blake, A.J., Bahr, J.L., Carver, J.H. and Kumar, V., 1970. Phil. Trans. Roy. Soc. Lond., A268, 159.

Born, M.and Oppenheimer, R., 1927. Ann. Physik, 84, 457.

Burke, P.G. and Taylor, K.T., from Torop, L., 1975. Daresbury synchrotron Radiation Lecture Note, Series no. 3 DL/SRF/R5.

Collin, J.E. and Natalis, P., 1968. Int. J. Mass Spec. and Ion Phys., 1, 483.

Collin, J.E. and Natalis, P., 1969. Int. J. Mass Spec. and Ion Phys, 2, 231.

Cooley, J.W., 1961. Maths of Computation, 15, 363.

Cooper, J. and Zare, R.N., 1968. J. Chem. Phys., 48, 942.

Coxon, J.A., 1971. J.Q.S.R.T., 11, 443.

Dehmer, P.M. and Chupka, W.A., 1975. J. Chem. Phys., 62, 4525.

Dill, D., Chang, E.S. and Fano, U., 1973. 8th Int. Conf. on Phys. of Elec. and Atomic Collisions, Extended Abstracts, Pt II, p536.

Doolittle, P.H. and Schoen, R.I., 1965. Phys. Rev. Letts, 14, 348.

Dromey, R.G., Morrison, J.D. and Peel, J.B., 1973. Chem. Phys. Letts, 23, 30.

Dunham, J.L., 1932. Phys. Rev., 41, 713, 721.

Eastman, D.E. and Nathan, M.I., 1975. Phys. Today, April, 44.

Edqvist, O., Lindholm, E., Selin, L.E. and Asbrink, L., 1970. Physica Scripta, 1, 25.

Eland, J.H.D., 1974. "Photoelectron Spectroscopy - An Introduction to U.V. Photoelectron Spectroscopy in the Gas Phase" (Butterworths).

Fadley, C.S., Miner, C.E. and Hollander, J.M., 1969. App. Phys. Letts, 15, 223.

Fano, U., 1935. Nuovo Cimento, 12, 156.

Fano, U., 1961. Phys. Rev., 124, 1866.

Fano, U., and Cooper, J.W., 1965. Phys. Rev., 137, A1364.

Feschbach, H., 1967. Ann. Phys. (N.Y.), 43, 410.

Frost, D.C., McDowell, C.A. and Vroom, D.A., 1965. Phys. Rev. Letts., 15, 612.

Frost, D.C., 1974. J. Elec. Spec. and Rel. Phen., 5, 99.

Gellender, M.E. and Baker, A.D., 1974. J. Elec. Spec and Rel. Phen, 4, 249.

Gardner, J.L., 1970. Ph.D. Thesis, University of Adelaide.

Gardner, J.L. and Samson, J.A.R., 1973. J. Elec. Spec. and Rel. Phen., 2, 267.

Gardner, J.L. and Samson, J.A.R., 1974 a). J. Chem. Phys., 61, 3311.

Gardner, J.L. and Samson, J.A.R., 1974 b). J. Chem. Phys., 61, 5472.

Gardner, J.L. and Samson, J.A.R., 1975. J. Elec. Spec. and Rel. Phen., 6, 53.

Gardner, J.L. and Samson, J.A.R., 1976. J. Elec. Spec. and Rel. Phen., 8, 469.

Gilmore, F.R., 1965. J.Q.S.R.T., 5, 369.

Heddle, D.W.O., 1971. J. Phys. E., 4, 589.

Huffman, R.E., Larrabee, J.C. and Chamber, D., 1965. Appl. Opt., 4, 1145.

Hulbert, H.M. and Hirschfelder, J.O., 1941. J.Chem. Phys., 9, 61.

Hurley, A.C., 1962. J. Chem. Phys., 36, 1117.

Hutchital, D.A. and Rigden, J.D., 1972. J. Appl. Phys., 43, 2291.

Jarmain, W.R., 1960. Can J. Phys., 38, 217.

Kaytayama, D.H., Huffman, R.E. and Tanaka, Y., 1973. 28th Symp. on Molec. Structure and Spec.

Kinsinger, J.A. and Taylor, J.W., 1973. Int. J. Mass Spec. and Ion Phys., 11, 461.

Kleimenov, V.I., Chizhov, Yu. V. and Vilesov, F.I., 1971. Opt. Spec., 535, 702.

Klein, O., 1932. 2. fur Phys., 76, 226.

Krupenie, P.H., 1972. J. Physical and Chemical Ref. Data, 1, 423.

Lindemans, W., Blake, A.J., Carver, J.H., Hutton, J.M. and Torop, L., 1979. J. Elec. Spec. and Rel. Phen., 15, 287.

Lindemans, W., 1981. Ph.D. Thesis, University of Adelaide.

Lippincott, E.R., 1953. J. Chem. Phys., 21, 2070.

Marquardt, D.W., 1963. J. Soc. Ind. Appl. Maths, 11, 431.

Massey, H.S.W., Burhop, E.H.S. and Gilbody, B., 1969. "Electronic and Ionic Impact Phenomena" (Oxford; Clarendon Press).

Mies, F.H., 1968. Phys. Rev., 175, 164.

Morse, P.M., 1929. Phys. Rev., 34, 57.

Natalis, P., 1976. J. Phys. Chem., 80, 2829.

Natalis, P., Collin, J.E., Delwiche, J., Caprace, G. and Hubin, M.J., 1979. J. Elec. Spec. and Rel. Phen., 17, 205.

Pauling, L., and Wilson, E.B., 1935. "Introduction to Quantum Mechanics" (McGraw-Hill, N.Y.).

Price, W.C., 1968. Molec. Spec., 4, 221.

Rees, A.L.G., 1947. Proc. Phys. Soc. (Lond), 59, 998.

Richards, W.G. and Barrow, R.F., 1964. Proc. Phys. Soc. (Lond.), 83, 1045.

Rydberg, R., 1931. Z. fur Phys., 73, 376.

Rydberg, R., 1933. Z. fur Phys., 80, 514.

Samson, J.A.R., and Cairns, R.B., 1968. Phys. Rev., 173, 80.

Schiff, L.I., 1968. "Quantum Mechanics" (Int. Student Edition, McGraw-Hill).

Sevier, K.D., 1972. "Low Energy Electron Spectrometry" (Wiley-Interscience).

Siegbahn, K., Nordling, G., Fahlman, A., Nordberg, R., Hamrin, K., Hedman, J., Johansson, G., Bergmark, J., Lindgreen, I., and Lindberg B., 1969. "ESCA applied to Free Molecules" (North Holland, Amsterdam).

Singh, N.L. and Jain, D.C., 1962. Proc. Phys. Soc., 79, 274.

Smith, A.L., 1970 a). Phil. Trans. Roy. Soc. Lond., A268, 169.

Smith, A.L., 1970 b). J.Q.S.R.T., 10, 1129.

Spindler, R., 1965. J.Q.S.R.T., 5, 165.

Steele, D., Lippincott, E. and Vanderslice, J., 1962. Rev. Mod. Phys., 34, 239.

Tanaka, K. and Tanaka, I., 1973. J. Chem. Phys., 59, 5042.

Tellinghuisen, J., 1972. J. Molec. Spec., 44, 194.

Turner, D.W. and Al-Jobury, M.I., 1962. J. Chem. Phys., 37, 3007.

Turner, D.W. and May, D.P., 1966. J. Chem. Phys., 45, 471.

Turner, D.W., Baker, C., Baker, A.D. and Brundle, C.R., 1970. "Molecular Photoelectron Spectroscopy" (Wiley-Interscience, London).

Vanderslice, J.T., Mason, E.A., Maisch, W. G. and Lippincott, E., 1959. J. Molec. Spec., 3, 17.

Vilesov, F.I., Kurbatov, B.L. and Terenin, A.N., 1961. Sov. Phys. Doklady, 6, 883.

Wallace, L., 1962. Astrophys. J. Supp., 7, 165.

Weissman, S., Vanderslice, J.T. and Battino, R., 1963. J. Chem. Phys., 39, 2226.

Zare, R.N. and Cashion, J.K., 1963. UCRL Report no 10881.

Zare, R.N., 1964. J. Chem. Phys., 40, 1934.

Zeleznik, F.J., 1965. J. Chem. Phys., 42, 2836.